Moisture availability in the Tangra Yumco region during the Late Quaternary and the implications for the precipitation regime on the southern Tibetan Plateau

---

DISSERTATION

(kumulativ)

zur Erlangung des akademischen Grades

doctor rerum naturalium (Dr. rer. nat.)

vorgelegt dem Rat der Chemisch-Geowissenschaftlichen Fakultät der

Friedrich-Schiller-Universität Jena

von Marieke Ahlborn (M.Sc.)

geboren am 08.02.1982 in Braunschweig

Gutachter

1. Prof. Dr. Roland Mäusbacher, Friedrich-Schiller-Universität Jena

2. PD Dr. Peter Frenzel, Friedrich-Schiller-Universität Jena

Tag der Verteidigung: Mittwoch, 25. November 2015

Table of Contents

Abstract

It is generally accepted that the Asian summer monsoon systems, particularly the Indian summer monsoon and the East Asian summer monsoon, as well as the westerlies affect the precipitation regime on the Tibetan Plateau. The Tibetan Plateau serves as “water tower” for the adjacent lowlands as the rivers originating on the plateau deliver water to over 1.4 billion people in the Asian lowlands. As these rivers are fed by the monsoonal precipitation to a significant extent, the predictability of monsoonal precipitation on different time-scales is crucial. This obvious importance inspired extensive climatic research on the Tibetan Plateau to further understand monsoonal dynamics.

The spatial and temporal variability of the monsoon has, however, been under strong discussion in recent years. The question arose whether the spatial and temporal monsoonal dynamics show a generally homogenous or heterogeneous pattern, i.e., has the monsoonal variability been spatially and temporally synchronous or not. Moreover, results of climate models launched the discussion about the annual cycle of precipitation on the Tibetan Plateau and the impact of local water recycling and pre-monsoon precipitation.

However, a systematic study of the spatial and temporal monsoonal variability has been lacking until now. To contribute to the ongoing discussion and to better understand the monsoonal variability the research project “*Reconstruction of the Hydrological Cycle in the Southern Transect of the Tibetan Plateau Utilizing Sediment Records”*

within the framework of the DFG priority program 1372 "*TiP* – Tibetan Plateau: Formation–Climate–Ecosystems" was initiated. The overall aim of this subproject is to systematically investigate the spatial and temporal variability of monsoonal dynamics by targeting three lakes along an east-west-transect on the southern Tibetan Plateau including Nam Co, Tangra Yumco, and Taro Co, and to furthermore assess if a currently existing east-west-gradient in available moisture has had an impact on the temporal variability of the monsoon. This thesis comprises three independent studies, examining the central lake Tangra Yumco and its catchment.

The first study of this thesis was conducted on a small lake named TT Lake within the Tangra Yumco catchment in order to assess modes of sediment deposition, sedimentary dynamics, and trigger mechanisms in the catchment. The results show that sedimentation in TT Lake is controlled by two modes of sediment deposition, particularly background sedimentation and event-related deposition. These event-related deposits (ERDs) have been attributed to hydrologic events.

In the second study of this thesis optically stimulated luminescence (OSL) dating was applied to recently exposed lacustrine sediments in the Tangra Yumco catchment. These results were compared to recalculated cosmogenic nuclide data and other previously published data to set up a Holocene lake level reconstruction. Results show that the lake level began to rise prior to 10.5 ka, reached a highstand thereafter, and dropped from that level at 8.5 ka. Lake levels subsequently continued to decline but this trend was interrupted by a short-term lake level rise at 2.1 ka. The lake level is steadily rising since 0.3 ka.

The third study examined an 11.5 m long sediment core from the northern part of Tangra Yumco. Implications from the TT Lake allowed to

demarcate seventeen ERDs that could probably also be attributed to hydrological events. Results furthermore show that the record covers 17.4 cal ka BP. Aeolian sediment transport prevailed prior to 17.1 cal ka BP and temperatures rose thereafter. A significant increase in moisture availability is shown at 16.0 cal ka BP, conditions were moister and warmer at 13.6-12.4 cal ka BP, and colder and drier at 12.4-11.4 cal ka BP. A rapid increase in moisture availability occurred at the transition to the Holocene at 11.4 cal ka BP and moistest conditions were recorded at 10.1-9.4 cal ka BP. As OSL and cosmogenic nuclide data could not resolve the onset of the lake level highstand, data from the sedimentary record were used to refine and likely the onset of the highstand co-occurred with moistest conditions at 10.1-9.4 cal ka BP. After this highstand, the moisture availability gradually declined showing only minor variations.

The east-west transect was extended by comparing the aforementioned results to published data from Tso Moriri, located in the northwestern Himalaya, and Naleng Co on the south-eastern Tibetan Plateau (investigations on Taro Co are currently in progress). The comparison of all records on the southern Tibetan Plateau shows a homogenous pattern indicating that moisture availability evolved synchronously on the southern Tibetan Plateau. Another comparison with records from the lakes Pumoyum Co (southern Tibetan Plateau) and Lake Qinghai (northeastern Tibetan Plateau) suggests a large-scale synchronous pattern on the entire Tibetan Plateau. Variations in moisture availability on the southern Tibetan Plateau were then compared to monsoonal intensity records from the Bay of Bengal and the Arabian Sea. The comparison revealed that the records from the southern Tibetan Plateau are primarily governed by monsoon-related

precipitations but minor deviations may be related to local peculiarities in the annual precipitation cycle. A nowadays observed east-west-gradient in moisture availability does not result in temporal shifts of climatic change.

Zusammenfassung

Das Niederschlagsregime auf dem Tibet-Plateau, auch Hochland von Tibet genannt, ist hauptsächlich geprägt durch die asiatischen Sommermonsune, bestehend aus dem Indischen und Ostasiatischen Monsun, sowie der Westwinde. Besonders die Monsunniederschläge liefern einen erheblichen Teil der Feuchtigkeit für die zahlreichen Flüsse, die auf dem Tibet-Plateau entspringen und über 1,4 Milliarden Menschen in Asien mit Frischwasser versorgen. Daher gilt das Tibet-Plateau auch als Wasserturm Asiens und eine Verbesserung der Vorhersagbarkeit der Monsunniederschläge ist zwingend notwendig. Um zu einem besseren Verständnis der Monsundynamik beizutragen, wurde das Tibet-Plateau daher zum Ziel intensiver Forschung.

Die räumliche und zeitliche Variabilität der Feuchteverfügbarkeit auf dem Tibet-Plateau seit dem Spätglazial wurde in den vergangen Jahren kontrovers diskutiert. Es stellte sich besonders die Frage, ob die räumlichen und zeitlichen Veränderungen der Monsundynamik ein homogenes oder heterogenes Muster zeigen. Zu dieser Diskussion kommt erschwerend hinzu, dass Klimamodelle für den Zeitraum vom mittleren Holozän bis heute und Reanalyse-Daten für die Jahre 2001-2011 eine deutliche saisonale Variabilität und einen signifikanten Einfluss von Recycling- und Prä-Monsun-Niederschlägen zeigen.

Systematische Studien zur Erfassung der räumlichen und zeitlichen Variabilität fehlen bisher. Um zur gegenwärtigen Diskussion über ein homogenes oder heterogenes Muster der Monsundynamik beizutragen,

wurde das Teilprojekt "*Reconstruction of the Hydrological Cycle in the Southern Transect of the Tibetan Plateau Utilizing Sediment Records"* im Rahmen des DFG Schwerpunktprogramms 1372 "*TiP* – Tibetan Plateau: Formation–Climate–Ecosystems" initiiert. Zu diesem Zweck wurde ein Ost-West-Transekt aus drei Seen, namentlich Nam Co, Tangra Yumco und Taro Co, auf dem südlichen Tibet-Plateau aufgespannt. Untersuchungen sollen zeigen, wie sich die räumliche und zeitliche Monsunvariabilität seit dem Spätglazial verhält und ob sich ein rezent existierender Ost-West-Gradient der Feuchteverfügbarkeit auf die zeitliche Variabilität auswirkt. Diese Dissertation wird den mittleren See des Transekts, den Tangra Yumco, und sein Einzugsgebiet detailliert untersuchen und zur Diskussion um die räumliche und zeitliche Monsunvariabilität beitragen.

Die erste Studie dieser Dissertation wurde an einem kleinen See namens TT Lake innerhalb des Tangra Yumco-Einzugsgebietes durchgeführt. Mit einem Multi-Proxy-Ansatz wurden zum einen die Prozesse im Einzugsgebiet des TT Lakes und zum anderen die verschiedenen vorherrschenden Sedimentationsprozesse erfasst. Die Ergebnisse zeigen, dass die Sedimentation im Wesentlichen durch zwei Faktoren gesteuert ist: die Hintergrundsedimentation und eine ereignis-gesteuerte Sedimentation. Letztere können Starkregenereignissen, die klimaunabhängig sind, zugeordnet werden.

In der zweiten Studie dieser Dissertation wurde optisch stimulierte Lumineszenz (OSL) angewendet, um zurzeit exponierte lakustrine Sedimente im Tangra Yumco-Einzugsgebiet zu datieren. Die Zusammenführung dieser Ergebnisse mit neu berechneten kosmogenen Nuklid-Altern sowie weiteren publizierten Daten von Seeterrassendatierungen resultierte in einer absoluten holozänen

Seespiegelrekonstruktion, die in dieser Form einzigartig auf dem südlichen Tibet-Plateau ist. Ein steigender Seespiegel wurde zunächst um 10.5 ka verzeichnet, worauf ein weiterer Anstieg des Seespiegels zu einem holozänen Hochstand folgte. Nach Erreichen dieses Hochstandes fiel der Seespiegel ab 8.5 ka, um danach kontinuierlich weiter zu fallen. Unterbrochen wurde dieser Seespiegelabfall nur von einem kurzzeitigen Anstieg um 2.1 ka. Seit einem Tiefstand um 0.3 ka steigt der Seespiegel wieder. Der rekonstruierte Seespiegelhochstand zwischen 10.5 und 8.5 ka ist ungefähr zeitgleich mit Hochständen in anderen Seesystemen auf dem Tibet-Plateau.

In der dritten Studie wird ein 11.5 m langer Sedimentkern aus dem nördlichen Teil des Tangra Yumco untersucht, der, basierend auf Radiokarbondatierungen, eine Zeitspanne von 17.4 cal ka BP bis heute abdeckt. Sedimentologische Erkenntnisse vom TT Lake erlaubten am Tangra Yumco eine Ausweisung von siebzehn ereignis-gesteuerten Sedimentlagen. Die Untersuchungen des Kerns zeigen, dass äolischer Sedimenttransport als Trockenheitsanzeiger nur vor 17.1 cal ka BP zu verzeichnen war. Im Gegenzug dazu zeigt sich um 16.0 cal ka BP ein signifikanter Anstieg an Feuchteverfügbarkeit. Um 13.6-12.4 cal ka BP sind die klimatischen Bedingungen weiterhin feucht und warm, im Anschluss, um 12.4-11.4 cal ka BP, hingegen kalt und trocken. Am Übergang zum Holozän stieg die Feuchtigkeit erneut rapide an und die klimatischen Bedingungen zeigen die höchste verfügbare Feuchtigkeit um 10.1-9.4 cal ka BP. Da OSL- und kosmogene Nuklid-Alter den Beginn des Seespiegelhochstandes nicht auflösen können, ermöglichen die neuen Erkenntnisse aus Untersuchungen des Sedimentkerns eine genauere Erfassung des Beginns des Hochstandes, der vermutlich mit den feuchtesten klimatischen Bedingungen um 10.1-9.4 cal ka BP

zusammenfällt. Nach diesem Hochstand nimmt die Feuchteverfügbarkeit graduell ab und zeigt nur noch geringe Variationen.

Das Ost-West-Transekt wurde durch die Seen Tso Moriri (nordwestlicher Himalaya) nach Westen und Naleng Co (südöstliches Tibet-Plateau) nach Osten verlängert. Der Vergleich der Archive auf dem südlichen Tibet-Plateau zeigt, dass sich die Feuchteverfügbarkeit synchron und grundsätzlich homogen entwickelt. Ein weiterer Vergleich mit Archiven vom Pumoyum Co (südliches Tibet-Plateau) und Lake Qinghai (nordöstliches Tibet-Plateau) zeigt auch großräumig ein synchrones Muster der Feuchtverfügbarkeit. Die Archive vom südlichen Tibet-Plateau wurden dann mit Monsunintensitätsraufzeichnungen aus dem Golf von Bengalen und dem Arabischen Meer verglichen, um den kontrovers diskutierten Einfluss des Monsuns auf das Niederschlagsregime des Tibet-Plateaus zu zeigen. Der Vergleich zeigt, dass monsunähnliche Niederschläge den größten Beitrag zum hydrologischen Budget leisten. Ein heutzutage existierender Ost-West-Gradient der Feuchteverfügbarkeit hat keine Auswirkungen auf die zeitliche Entwicklung der Feuchteverfügbarkeit.

CHAPTER 1 — Introduction

1.1 Moisture availability on the Tibetan Plateau

It is generally accepted that the precipitation regime on the Tibetan Plateau is affected by the Asian summer monsoon system *(e.g., Gasse et al. 1991, Lehmkuhl and Haselein 2000, Holmes et al. 2009, Liu et al. 2009, An et al. 2012b, Maussion et al. 2014*; Figure 1.1*)*. This system is characterized by a seasonal reversal of the wind direction combined with changes in the precipitation pattern *(e.g., Ramage 1971, Goswami 2005)*. These processes are driven by seasonal changes in the latitude-dependent insolation *(Dallmeyer et al. 2012)*. Different heat capacities of the ocean water and the continental landmass result in a thermal contrast between ocean and landmasses generating a large-scale pressure gradient *(Krishnamurti 1971b, Krishnamurti 1971a, Webster et al. 1998)*, which induces seasonally reversing wind circulations following the insolation *(Dallmeyer et al. 2012)*. The Indian monsoon (Figure 1.1) is characterized by a meridional pressure and temperature gradient *(Webster et al. 1998, Dallmeyer et al. 2012)* and is mainly linked to a northward migration of an east-west oriented low pressure belt also known as Intertropical Convergence Zone or ITCZ *(Gadgil et al. 2004)*. Moisture bearing air from the Indian Ocean is transported northwards to the Tibetan Plateau by the Indian summer monsoon. In contrast, the East Asian monsoon (Figure 1.1) is determined by a zonal pressure and temperature gradient *(Webster et al. 1998)* and the seasonality is reflected by the northwards excursion of a planetary subtropical front that

forms due to this zonal thermal contrast *(Ding 2007)*. In winter, the ITCZ migrates to the southern hemisphere, while a cold high pressure zone develops over Asia causing dry and cold conditions over the Tibetan Plateau (Figure 1.1).

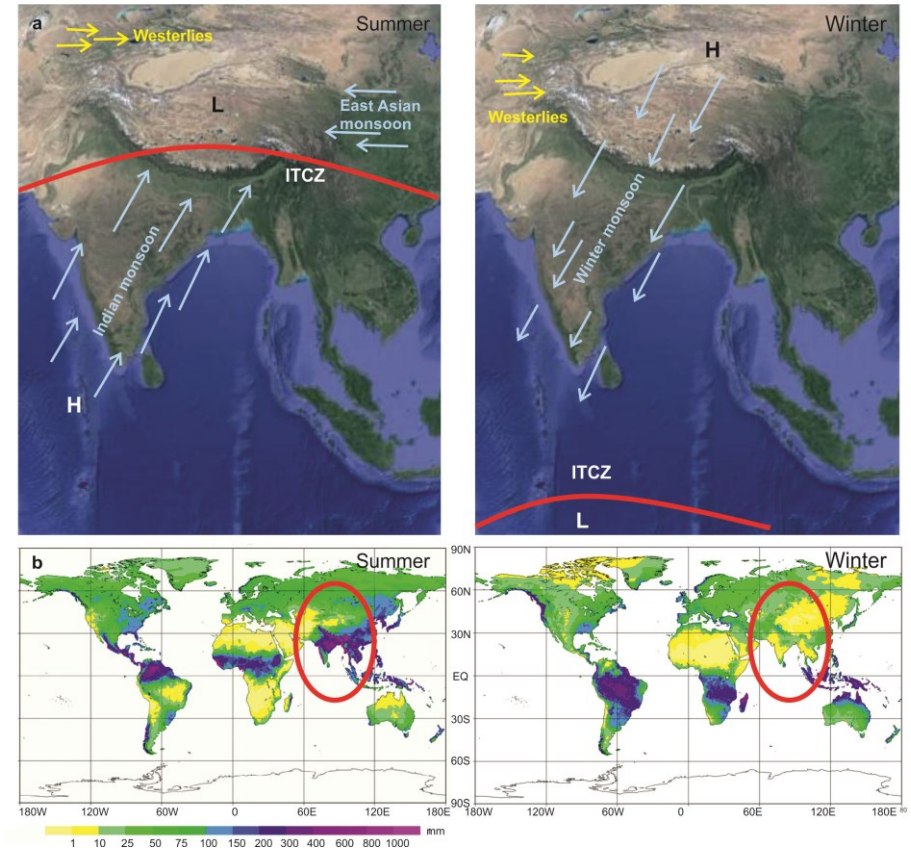

Figure 1.1: Monsoon on the Tibetan Plateau. (a) Schematic summer (July; left) and winter (January; right) conditions with high (H) and low (L) pressure areas, changing position of the Intertropical Convergence Zone (ITCZ; red line) and prevailing winds (arrows). Images based on Google Earth. (b) Mean precipitation [mm] on the Tibetan Plateau (red circles) in summer (July; left) with enhanced precipitation due to monsoon influence and in winter (January; right) with reduced precipitation. *(Schneider et al. 2014, modified)*.

The Tibetan Plateau, as all mountain ranges, is often called a “water tower” as it provides important sources of freshwater that are supplied by rivers such as Ganges, Yangtze, Yellow River, Indus, Brahmaputra, Salween, and Mekong (Figure 1.2) to the adjacent Asian lowlands

(Liniger et al. 1998, Viviroli et al. 2007). The discharge of these rivers basically depends on seasonal precipitation, i.e., monsoonal rainfall *(Wang et al. 2006, Jian et al. 2009)* and snowmelt *(Immerzeel et al. 2010)* providing water to more than 1.4 billion people *(Immerzeel et al. 2010)*. The water consumption is divers and includes agricultural irrigation, freshwater supply, and hydropower generation *(Mukhopadhyay and Khan 2014)*. The Yellow River, being the second largest river in China *(Miao et al. 2011)*, provides water for 162 million people *(Immerzeel and Bierkens 2012)* but experienced a significant reduction in river discharge in the past decades *(Yang et al. 1998)* carrying only 28.7% of the discharge of the 1950s *(Wang et al. 2006)*. Generally, climate change *(Vörösmarty et al. 2000, Immerzeel et al. 2010, Miao et al. 2011)* and enhanced human impact *(Miao et al. 2011)*, namely growths in water demand due to increasing population *(Vörösmarty et al. 2000)* have been recognized as the main drivers of current or prospective water scarcity *(Wang et al. 2006, Immerzeel and Bierkens 2012)*. Water scarcity, by definition, is a shortage in the freshwater availability relative to the demand *(Taylor 2009, Gain and Giupponi 2015)*. Many Asian riverine basins are likely to be affected by water scarcity in future *(Viviroli et al. 2007, Gain and Giupponi 2015)*. Between 1970-2008, the reduction in the Yellow River water discharge was attributable 17% to climate change and 83% to human impact *(Miao et al. 2011)*. 70% of the annual runoff of the Indus River are attributable to monsoonal rainfall *(Liniger et al. 1998)* and a recent assessment of risk factors for water scarcity in river basins of Asia concludes that it bears a very high risk for future water scarcity *(Immerzeel and Bierkens 2012)*. The river supplies densely populated areas *(Immerzeel and Bierkens 2012)* providing much of Pakistan's irrigation water and hydropower

generation *(Ahmad 1974, Liniger et al. 1998, Meadows and Meadows 1999)*. Ganges, Yangtze, and Yellow River (Figure 1.2), which also depend on monsoonal rainfall, have an intermediate risk for water scarcity but also supply densely populated areas, whereas for Brahmaputra, Salween, and Mekong the vulnerability to water scarcity is relatively limited *(Immerzeel and Bierkens 2012)*. Freshwater scarcity not only affects food and drinking water security as well as public health but can also hamper economic progress and foster civil disturbances *(Taylor 2009)*. For example, the economic damage of a reduction in monsoonal rainfall by 19% in India in 2002 was estimated to billions of dollars *(Gadgil et al. 2004)*. In contrast, the rivers Ganges and Brahmaputra regularly cause severe floods in Bangladesh as their increase or decrease in discharge is controlled by the intraseasonal monsoon variability *(Jian et al. 2009)*.

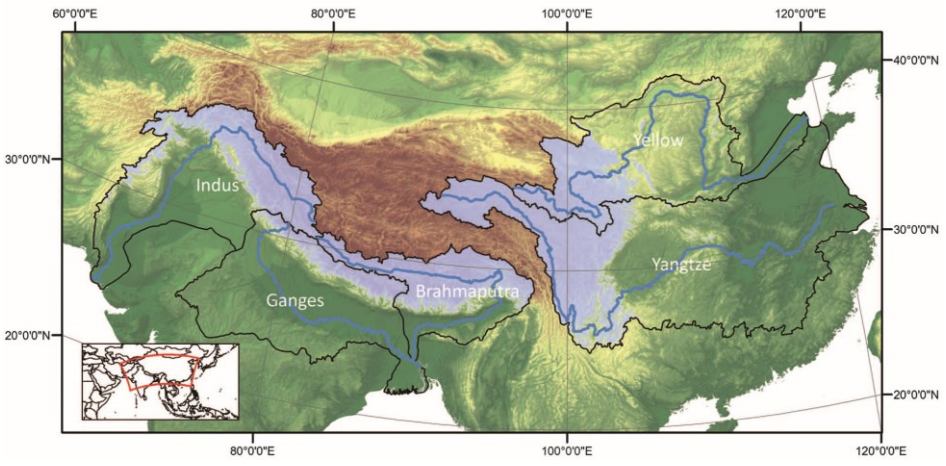

Figure 1.2: Rivers originating on the Tibetan Plateau. Basins and riverine courses of Indus River, Ganges, Yangtze, Brahmaputra, and Yellow River. Blue shaded areas are above 2000 m asl *(*Figure source: *Immerzeel et al. 2010)*.

Reliable predictions about the prospective water supply from river discharge are of critical importance for local and regional authorities to

ensure agricultural sustainability, constant freshwater supply, and disaster prevention *(Morrill et al. 2003, Jian et al. 2009, Mischke et al. 2010a)*: They are closely coupled to a profound understanding of monsoonal dynamics, its driving mechanisms, and its response to climate change since most rivers' discharge depends on monsoonal rainfall. The thorough investigation and reconstruction of past monsoonal variations may contribute to a better understanding of monsoonal dynamics and may provide an analogue for future scenarios. The Tibetan Plateau is particularly suitable for investigation of past monsoonal variability due to several reasons: (1) as described above, the Tibetan Plateau affects the climate of Asia significantly by triggering and maintaining the Asian monsoon system *(Broccoli and Manabe 1992, An et al. 2001, Morrill et al. 2006)*; (2) the modern extent of the monsoon partly crosses the Tibetan Plateau making it particularly vulnerable for monsoonal variations *(Morrill et al. 2006)*; and (3) relative to the densely populated regions of the adjacent Asian lowlands, the human impact on the Tibetan Plateau is limited simplifying the climate proxy interpretation *(Morrill et al. 2006)*. Therefore, numerous studies have been conducted on the Tibetan Plateau in the past decades to assess past monsoonal variations *(e.g., Gasse et al. 1991, Overpeck et al. 1996, Gupta et al. 2003, Shen et al. 2005, Morrill et al. 2006, Li et al. 2009, Doberschütz et al. 2014, Günther et al. 2015, Kasper et al. 2015)*.

The spatial and temporal variability of monsoonal dynamics has thoroughly and controversially been discussed during the recent years *(e.g., An et al. 2000, Yu and Kelts 2002, Morrill et al. 2003, He et al. 2004, Feng et al. 2006, Herzschuh 2006, Zhou et al. 2007, Chen et al. 2008, Mischke et al. 2008, Dong et al. 2010, Mischke and Zhang 2010)*. A heterogeneous and non-uniform or at least partly heterogeneous

summer monsoon development was proposed by *An et al. (2000), Yu and Kelts (2002), Morrill et al. (2003), He et al. (2004), Herzschuh (2006), Mischke et al. (2008),* and *Mischke et al. (2010a)*. The arguments were manifold and the question arose whether non-representative catchment-specific peculiarities or underestimated but complex climatic and atmospheric conditions caused this spatial heterogeneity *(He et al. 2004, Mischke et al. 2010a)*. Catchment-specific peculiarities such as water sources like ice, snow, and ground water as well as the complex interplay between precipitation, evaporation, and temperature complicate the interpretability of data *(Mischke and Zhang 2010)*. However, not solely causal reasons but also methodical uncertainties like uncertain chronologies *(Mischke et al. 2013)* or a poor understanding of the interpreted proxies *(Mischke et al. 2010b, Opitz et al. 2015)* lead to inconsistencies between the records. A generally homogeneous monsoon development (within each monsoon domain), on the contrary, was proposed by *Feng et al. (2006), Zhou et al. (2007), Chen et al. (2008), Dong et al. (2010),* and *Mischke and Zhang (2010)*.

In these above mentioned studies changes in moisture availability were equated to monsoonal dynamics. However, these studies reveal annual to centennial changes in moisture availability lacking a subseasonal resolution. Thus, these studies cannot assess seasonal climate phenomena such as the summer monsoon *(Dallmeyer et al. 2012)* but rather long-term changes in moisture availability. Most studies assumed a dominance of summer rainfall *(e.g., Morrill et al. 2006, Daut et al. 2010, Dietze et al. 2013, Miehe et al. 2014)* but the seasonal pattern of the precipitation is more complex *(Maussion et al. 2014)*. Recently published reanalysis and modelled data suggest that the precipitation regimes on the Tibetan Plateau are influenced by additional

precipitation processes besides the monsoon *(Dallmeyer et al. 2012, Maussion et al. 2014)*. Recycling and pre-monsoon (spring) precipitation contribute to changes in the precipitation pattern on the Tibetan Plateau meaning that these changes cannot solely be attributed to monsoonal dynamics but to the sum of monsoon and pre-monsoon precipitation *(Dallmeyer et al. 2012, Maussion et al. 2014)*. The controlling mechanism of pre-monsoon precipitation are, similar to the summer monsoon, changes in insolation *(Dallmeyer et al. 2012)*. The seasonal precipitation pattern is, however, spatially very different *(Dallmeyer et al. 2012, Maussion et al. 2014)*. During the years AD 2000–2011, pre-monsoon precipitation contributed a substantial amount to the annual precipitation on the western, southern, and northern Tibetan Plateau, whereas the contribution of pre-monsoon precipitation on the central Tibetan Plateau is negligible *(Maussion et al. 2014)*. *Dallmeyer et al. (2012)* observed differences in the seasonal precipitation pattern in the Indian and East Asian monsoon domain. As the Indian summer monsoon has a meridional orientation and the East Asian monsoon a zonal orientation of the pressure and temperature gradients they react differently to the zonally uniform changes in summer insolation *(Dallmeyer et al. 2012)*.

The discussions about the spatial and temporal variability of moisture availability and the annual cycle of precipitation reveal significant gaps of knowledge concerning the processes and dynamics of moisture availability on the Tibetan Plateau and highlight the necessity of ongoing research.

1.2 The east-west-transect on the southern Tibetan Plateau – a subproject within the DFG priority program 1372 "*TiP* – Tibetan Plateau: Formation–Climate–Ecosystems"

Until now, an interregional linking of results of spatial and temporal variations of climate change on the Tibetan Plateau was based on a reassessment of previously published data from individual sites *(e.g., Herzschuh 2006, Mischke and Zhang 2010)*. In subprojects within the DFG priority program 1372 "*TiP* – Tibetan Plateau: Formation–Climate–Ecosystems" (http://www.tip.uni-tuebingen.de/index.php/de/) lacustrine archives have been examined along east-west-transects established on the northern and southern Tibetan Plateau using comparable methods to systematically assess spatial and temporal variations in moisture availability. Subprojects within the *TiP* program generally focus on forcing mechanisms on the Tibetan Plateau and their effects on the environment on three time scales: plateau formation during the past tens of millions of years, climate development during the past ten to hundreds of thousands of years, and human impact during the past ca. 8000 years (http://www.tip.uni-tuebingen.de/index.php/de/). The southern east-west-transect, to which this thesis contributes, represents the subproject "Reconstruction of the Hydrological Cycle in the Southern Transect of the Tibetan Plateau Utilizing Sediment Records" funded with the grant number MA1308/23-2. This bilateral research project is jointly financed by the National Natural Science Foundation of China (Grant No. 41271225) and supported by the Institute of Tibetan Plateau Research (Beijing, China) as a part of the Chinese Academy of Sciences (CAS). The overall objective of this joint research approach has been to combine the outcome from the northern and the southern east-west-transects with the aim of a better understanding of monsoonal dynamics,

their spatial and temporal variations, and the resulting environmental processes.

The east-west-transect established on the southern Tibetan Plateau consists of three lakes called Nam Co, Tangra Yumco, and Taro Co. The objectives were twofold: (1) to investigate, if the modern gradual decrease of moisture availability from east to west *(Maussion et al. 2014)* had an impact on the temporal variability of the moisture pattern; (2) to explore the spatial and temporal variability of moisture availability on the southern Tibetan Plateau and thereby contribute to a better understanding of monsoonal dynamics.

The easternmost lake of the introduced east-west transect Nam Co was thoroughly investigated in a first phase of the *TiP* initiative *(*e.g., *Mügler et al. 2008, Zhu et al. 2008, Daut et al. 2010, Mügler et al. 2010, Günther et al. 2011, Kasper et al. 2012, Kasper et al. 2013, Doberschütz et al. 2014, Kasper 2014, Günther et al. 2015, Kasper et al. 2015, Wang et al. 2015)*. The reconstruction of variations in moisture availability and temperature of the past 24 cal ka BP showed that after a cold and dry Last Glacial Maximum the lake level initially rose at 20 cal ka BP *(Kasper et al. 2015)*. A moister and warmer phase prevailed at 14-13 cal ka BP (Bølling/Allerød chronozone) followed by cold and dry condition coinciding with the Younger Dryas chronozone *(Kasper et al. 2015)*. Conditions were moistest at 9.4 cal ka BP and moisture availability gradually decreased thereafter *(Doberschütz et al. 2014, Kasper et al. 2015)*. *Günther et al. (2011)* presented a record of evapotranspiration and relative humidity for the past 1000 years based on δD values of sedimentary *n*-alkanes that agrees with climatic events known from the northern Hemisphere such as the Medieval Warm Period and the Little Ice Age. A recently published study by *Wang et al. (2015)* thoroughly

investigated the modern mechanisms controlling the lake surface sediments and revealed the prevailing processes. Investigations on the westernmost lake Taro Co are currently in progress. Preliminary and unpublished multi-proxy results show a gradual decrease in moisture availability and increasing aridification since about 7.4 cal ka BP. A palynological record covering the past 10.3 cal ka BP generally supports these preliminary results showing steadily increasing aridity after 7.4 cal ka BP *(Ma et al. 2014)*. The central lake Tangra Yumco and its catchment is the research object of this thesis.

The counterparts to the east-west-transect on the southern Tibetan Plateau are the lakes Donggi Cona and Heihai Lake spanning an east-west-transect on the northern Tibetan Plateau (Figure 1.3). Donggi Cona was thoroughly investigated but results were not straightforward *(e.g., Mischke et al. 2010a, Dietze et al. 2012, IJmker et al. 2012, Opitz et al. 2012, Dietze et al. 2013)*. Analyses of exposed lake terraces consisting of fluvial–alluvial to littoral lacustrine facies *(Dietze et al. 2013)* and a multi-proxy data set from a sedimentary record *(Opitz et al. 2012)* document a high lake level and moist conditions in the early Holocene. In contrast, ostracod analyses reveal unstable conditions in the early Holocene, moistest conditions after 6.8 cal ka BP, and indicate that sediments interpreted as sediments from Donggi Cona by *Dietze et al. (2013)* rather represent small ponds, not lacustrine sediments *(Mischke et al. 2010a, Mischke et al. 2015)*. The lake levels of the other lake from the northern transect, Lake Heihai, were lowest in the Late Glacial and earliest Holocene and highest in the early to mid-Holocene *(G. Lockot, personal communication)*. A short dry spell occurred at around 3 cal ka BP and lake levels were rising thereafter *(G. Lockot, personal communication)*.

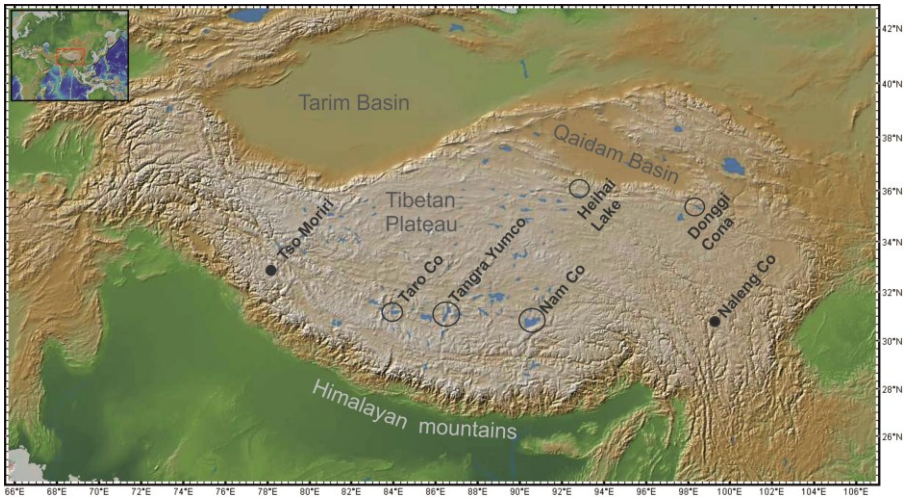

Figure 1.3: Tibetan Plateau with study sites mentioned in the text. Southern east-west-transect including Taro Co, Tangra Yumco, and Nam Co (circles). Heihai Lake and Donggi Cona form a similar east-west-transect on the northern plateau (circles). Additionally, Tso Moriri and Naleng Co are shown which extend the southern east-west-transect (http://www.geomapapp.org).

1.3 Objectives and outline of thesis

As a part of the above-mentioned bilateral *TiP* subproject, this thesis focuses on the central lake of the east-west-transect on the southern Tibetan Plateau, Tangra Yumco, and its catchment (Figure 1.3). Tangra Yumco (30°45'-31°22'N, 86°23'–89°49'E; Figure 1.4) is located at an elevation of 4545 m asl *(Rades et al. 2013)* in a north-south-trending graben structure *(Miehe et al. 2014)*. It is a brackish lake with a salinity of 8.3‰ and a water depth of 230 m covering 818 km² *(Long et al. 2012)* while its catchment covers 8219 km^2 *(Long et al. 2012)*. A small lake named TT Lake (31.10°N, 86.57°E, 4750 m asl; Figure 1.4) is located ~1.5 km west and ~205 m above the recent western shoreline of lake Tangra Yumco but within its catchment.

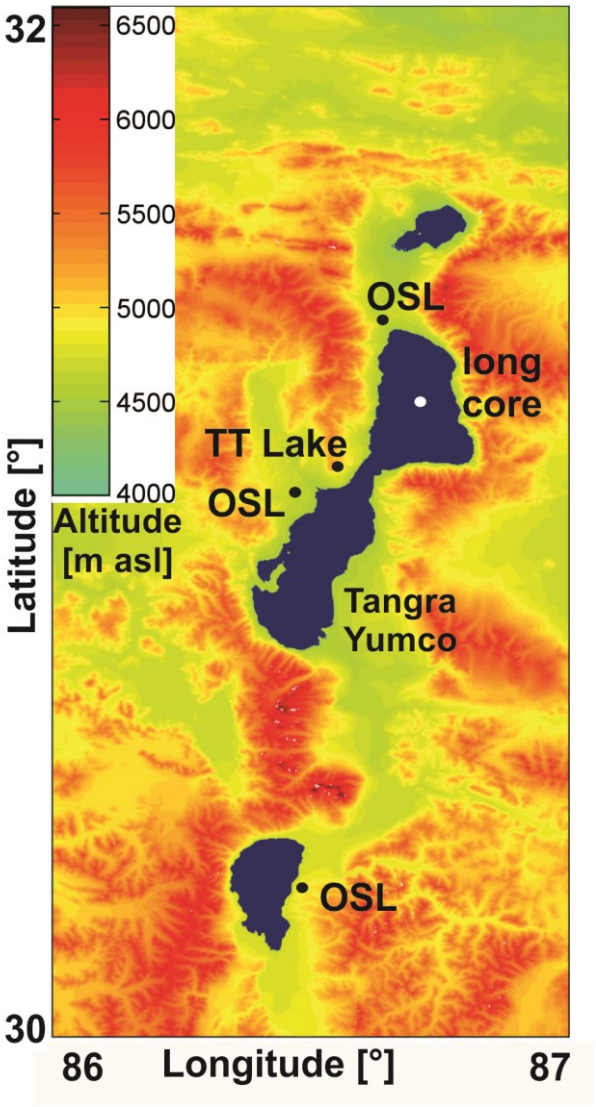

Figure 1.4: Sampling and coring locations in the Tangra Yumco area. Several gravity cores were investigated from the TT Lake *(chapter 2)*, a Holocene lake level history is based on OSL ages from three locations *(chapter 3)*, and a long core (white dot) from Tangra Yumco was studied to reveal past moisture availability *(chapter 4)*.

The overall aim of this thesis is to contribute to a better understanding of the variability of variations in moisture availability on the southern Tibetan Plateau. To extent the east-west-transect, Tangra Yumco and its catchment processes were thoroughly examined in three individual studies presented in this thesis. An initial study on gravity cores from the small TT Lake was conducted to reveal the sedimentary dynamics as a response to catchment processes prevailing in the catchment of Tangra Yumco (Figure 1.4). In a second study the Holocene lake level history of the Tangra Yumco lake system was reconstructed by dating currently exposed lacustrine sediments (Figure 1.4). A third study investigated a long sediment core from Tangra Yumco to receive a high-resolution record of changes of moisture availability since the Late Glacial and evaluated the results from all three studies (Figure 1.4). More precisely the objectives of my thesis are:

(1) the assessment of catchment processes and sedimentary dynamics of the small TT Lake that is located within the Tangra Yumco catchment and their connection to climate settings *(chapter 2)*;

(2) the quantitative reconstruction of lake level variations by optically stimulated luminescence dating (OSL) on currently exposed lacustrine sediments to reveal the rate and the scale of lake level changes *(chapter 3)*;

(3) the continuous and high-resolution reconstruction of past variations of moisture availability by applying a multi-proxy approach on a sediment core from Tangra Yumco *(chapter 4)*;

(4) the synthesis of results from OSL and sediment core analyses yielding in a continuous, high-resolution and quantitative approach suitable to assess magnitude, timing, and environmental impact of variability of moisture availability on lake levels of

Tangra Yumco *(chapter 4)*;

(5) the comparison of results from Tangra Yumco to Nam Co to deduce spatial and temporal variability on the east-west-transect on the southern Tibetan Plateau (*chapter 4*);

(6) the assessment of the monsoonal impact on the southern Tibetan Plateau by a comparison to monsoon intensity records *(chapter 4)*;

(7) a first preliminary comparison of the southern and the northern east-west-transect to reveal possible synchronicities or asynchronicities of the variability of moisture availability *(chapter 5)*.

This thesis consists of five chapters. *Chapter 2* contains a peer-reviewed article published in *The Holocene* dealing with the TT Lake. The content of *chapter 3* presents the Holocene lake level history of the Tangra Yumco lake system based on OSL data and is accepted by *The Holocene*, while the content of *chapter 4* discusses the moisture availability at Tangra Yumco and the southern Tibetan Plateau and was submitted to *Quaternary Science Reviews*. Finally, the gained insights and implications for the development of the Tibetan climate are synthesized and discussed in *chapter 5* containing also proposals for future research.

CHAPTER 2 — Sediment dynamics and hydrologic events affecting small lacustrine systems on the southern-central Tibetan Plateau — the example of TT Lake

Ahlborn M, T Haberzettl, J Wang, M Alivernini, F Schlütz, A Schwarz, Y Su, P Frenzel, G Daut, L Zhu, and R Mäusbacher (2015): Sediment dynamics and hydrologic events affecting small lacustrine systems on the southern-central Tibetan Plateau — the example of TT Lake. *The Holocene* 25: 508-522.

Licensor: SAGE Publications Ltd
1 Oliver's Yard
55 City Road
London, UK

Research paper

The Holocene
2015, Vol. 25(3) 508–522
© The Author(s) 2014
Reprints and permissions:
sagepub.co.uk/journalsPermissions.nav
DOI: 10.1177/0959683614561885
hol.sagepub.com
SAGE

Sediment dynamics and hydrologic events affecting small lacustrine systems on the southern-central Tibetan Plateau – the example of TT Lake

Marieke Ahlborn,[1] Torsten Haberzettl,[1] Junbo Wang,[2] Mauro Alivernini,[3] Frank Schlütz,[4] Anja Schwarz,[5] Youliang Su,[6] Peter Frenzel,[3] Gerhard Daut,[1] Liping Zhu[2] and Roland Mäusbacher[1]

Abstract

A sedimentological, geochemical, micropaleontological, and palynological study of a lacustrine sediment record from the small TT Lake (southern-central Tibetan Plateau) shows that the background sedimentation was frequently interrupted by event-related deposits. These event-related deposits are interpreted as the result of hydrologic events that are triggered by above-average precipitation events. In total, 11 events were recorded in the TT Lake sequence. Two types can be differentiated: fluvial runoff events caused by precipitation that carried sediment in suspension into the lake and a sediment mass transport caused by torrential precipitation. The hydrologic events appear to be decoupled from long-term climate and environmental variations, but there is evidence that anthropogenic impact, in terms of pastoralism, might have favored the runoff events. The multi-proxy approach proved to be valuable and allowed for a detailed study of sedimentary processes within the lake and its watershed in order to assess their triggering processes and dynamics. The findings show the complexity of these sedimentary processes and their controlling factors, and the study aims to improve their understanding. This study is the first effort to investigate event-related deposits and sedimentary processes on the Tibetan Plateau and its triggering processes and dynamics by utilizing lacustrine sediment records.

Keywords

event layer, human impact, lake sediments, multi-proxy approach, precipitation, sediment transport processes, Tibetan Plateau

Received 23 June 2014; revised manuscript accepted 30 October 2014

Introduction

Numerous large lakes on the Tibetan Plateau were targeted for paleoenvironmental investigations in recent years (Kasper et al., 2013; Mischke et al., 2010; Morrill et al., 2006; Nishimura et al., 2014; Shen et al., 2005; Yang et al., 2014; Zhao et al., 2010). However, the complexity and the dynamics of processes affecting the catchment of large lakes are difficult to assess because usually deep lake sediments were obtained in distal areas which are chosen to recover a preferably continuous sediment record. Distal parts of the lakes are generally controlled by long-term variations and not by single events in the catchment. This is also indicated by the predominantly homogeneous sediments recovered from large lakes (Doberschütz et al., 2014; Kasper et al., 2012; Li et al., 2008; Wang et al., 2002; Zhao et al., 2010) further supporting that event-related catchment processes rarely influence distal sedimentary processes. To investigate and understand the complex driving mechanisms of sedimentary processes on the Tibetan Plateau, small lakes appear to be more suitable. The proximity of the coring location to the shore and inflows allows a sensitive reaction of the system to catchment processes and the recording of rapid changes and disturbances that would not be documented in sediment records of large lakes.

Lakes can act as traps for event-related deposits (ERDs), resulting in records with detrital layers intercalated in pelagic background sediments (Gilli et al., 2013; Kämpf et al., 2012; Mangili et al., 2005). Sedimentary records can thus provide a valuable archive for reconstruction of mechanism, magnitude, and frequency of event-related sedimentation in the past (Mangili et al., 2005). Trigger mechanisms for event-related sedimentation are generally ascribed to hydrologic, particularly

[1]Physical Geography, Institute of Geography, Friedrich Schiller University Jena, Germany
[2]Key Laboratory of Tibetan Environment Changes and Land Surface Processes, Institute of Tibetan Plateau Research, Chinese Academy of Sciences, China
[3]Institute of Geosciences, Friedrich Schiller University Jena, Germany
[4]Lower Saxony Institute for Historical Coastal Research, Wilhelmshaven, Germany
[5]Institut für Geosysteme und Bioindikation, Technische Universität Braunschweig, Germany
[6]Key Laboratory of Cenozoic Geology and Environment, Institute of Geology and Geophysics, Chinese Academy of Sciences, China

Corresponding author:
Marieke Ahlborn, Physical Geography, Institute of Geography, Friedrich Schiller University Jena, Löbdergraben 32, D-07743 Jena, Germany.
Email: marieke.ahlborn@uni-jena.de

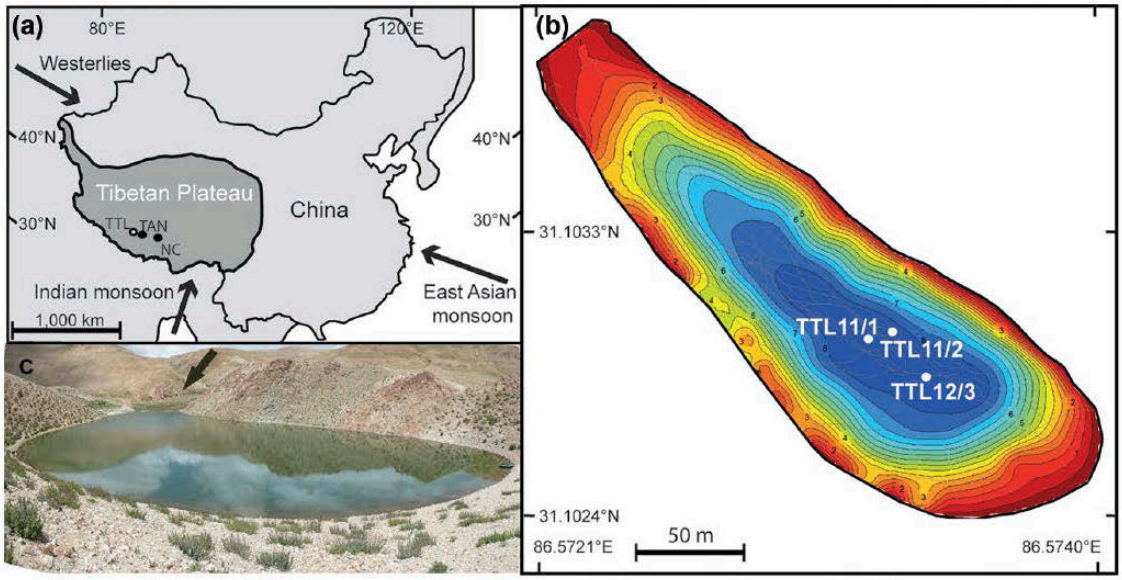

Figure 1. Study site: (a) China and the Tibetan Plateau with TT Lake (TTL), Tangra Yumco (TAN), and Nam Co (NC) – indicated (arrows) are the main moisture delivering systems; (b) bathymetric map (http://www.drdepth.se) of TT Lake with coring locations of sediment cores TTL11/1, TTL11/2, and TTL12/3, inflow at the north-western shore; (c) photo of TT Lake (view to WNW) showing the slopes in the north and south and the wetlands with the inflow in the west (arrow; Photo: Steffen Mischke).

meteorological events (Brown et al., 2000; Irmler et al., 2006; Nesje et al., 2001; Osleger et al., 2009; Schlolaut et al., 2014; Schneider et al., 2010; Sletten et al., 2003) or seismic activities (Beck, 2009; Karlin et al., 2004; Leroy et al., 2002; Petersen et al., 2014; Strasser et al., 2013). Studies mainly focus on the generation of an event calendar either for meteorological or seismic events. Despite the fact that past meteorological or seismic instrumental data are very limited, gaining knowledge about frequency, magnitude, and trigger mechanisms is important to provide a risk assessment for the future. However, studies examining event-related sedimentary processes in lacustrine systems in detail are rare (Irmler et al., 2006), and this is especially the case for the Tibetan Plateau. The only study available was presented recently by Jiang et al. (2014) who conducted a sedimentological approach on exposed lacustrine sediments from the eastern Tibetan Plateau in order to understand their link to paleoseismic events.

The study presented here is the first lacustrine sediment record from the Tibetan Plateau containing evidence for event-related sedimentary processes. This study focuses on the understanding of these processes in a small lake called TT Lake. A multi-proxy approach was applied to conceive the complexity of sedimentary processes. Sedimentological techniques reveal sedimentary processes controlling sediment deposition, whereas micropaleontologic and geochemical methods were applied to detect the reaction of the lacustrine system. Palynology was used to assess the supra-regional and local vegetational changes. This integrated approach aims to contribute to a better understanding of event-related sedimentation on the Tibetan Plateau.

Site description

TT Lake (31.10°N, 86.57°E, 4750 m.a.s.l.) is located on the southern-central Tibetan Plateau, ~1.5 km west and ~205 m above the recent western shoreline of lake Tangra Yumco but within its catchment (Figure 1). Tangra Yumco is a tectonic basin with a catchment area of 8219 km^2 (Long et al., 2012), bound by N-S trending normal faults forming a graben-like structure (Reicherter, 2012). Well-preserved terraces of former lake level highstands reach up to ~200 m above its recent lake level (Kong et al., 2011; Rades et al., 2013). Moisture mainly arrives by the Indian monsoon during summer months with a mean annual precipitation of 200–250 mm (Miehe et al., 2014), whereas the westerly winds prevail during winter. Re-analysis data, covering the years 1979–2010, reveal a mean annual precipitation of ~310 mm, while the mean precipitation from November to April is ~40 mm and from May to October ~270 mm (Chen et al., 2011). The mean annual temperature in January is −11.4°C and 10.9°C in July (Miehe et al., 2014).

The 9 m deep TT Lake covers ~14,500 m^2 (Figure 1). The geological strata in the ~4.6 km^2 large catchment consist of granitoids, conglomerates, sandstones, and limestones. TT Lake is surrounded by steep slopes with elevated plains in the north and south and a 3-m-high barrier in the east (Figure 1). The lake is fed by a small stream (September 2011 and June 2012) entering the lake from the north-west (Figure 1). This stream is surrounded by wetlands extending as a flat plain at the inflow at the north-western shore of the lake (Figure 1). A spring, several meters below and east of the lake, suggests a subterrestrial outflow into the Tangra Yumco catchment, so that the TT Lake can be considered as an open lake system. Vegetation around TT Lake is mainly limited to these wetlands and is sparse in the remaining area. The lake bottom is partly covered by filamentous algae. Anthropogenic impact is restricted to grazing and watering of domesticated animals such as yaks in the catchment.

Material and methods

Field methods

Coring locations were selected and a bathymetric map (Figure 1; http://www.drdepth.se) was established based on results of a hydro-acoustic survey with a standard fish finder. Three sediment gravity cores (Figures 1 and 2, Table 1) with a 63 mm diameter and lengths of 49.2 cm (TTL11/1), 64.0 cm (TTL11/2), and 89.0 cm (TTL12/3) were obtained in 2011 and 2012 from water depths of 8.2–8.8 m using a modified ETH gravity coring device (Kelts et al., 1986). Additionally, 15 surface sediment samples were obtained in different water depths (September 2011) using a UWITEC box-corer for deeper water and a hand-net for very shallow water. The uppermost centimeter of the surface sediment was scraped and put into plastic bags. Physico-chemical water

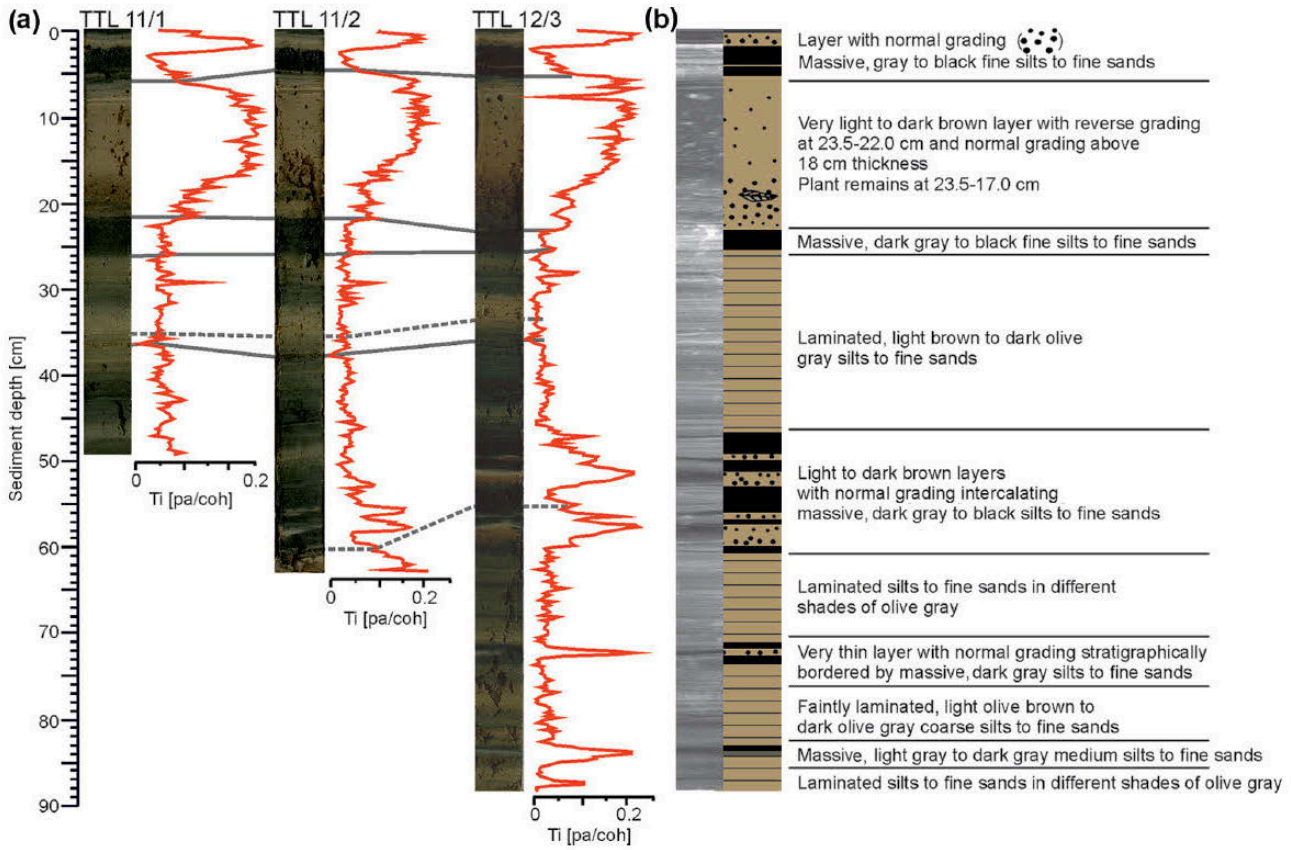

Figure 2. Correlation and core description: (a) Core correlation of sediment cores TTL11/1, TTL11/2, and TTL12/3 based on Ti values and lithology (solid lines), transfer of ages from core TTL11/2 to cores TTL11/1 and TTL12/3 (dashed line) and (b) schematic image of core TTL12/3 with lithological description (right) and x-ray image (left).

Table 1. Information for cores obtained from TT Lake.

Core information							
Core ID	Latitude (°N)	Longitude (°E)	Water depth (m)	Distance to inflow (m)	Length (cm)	Coring method	Year of coring (AD)
TTL11/1	31.103107	86.573214	8.2	129	49.2	Modified ETH gravity corer[a]	2011
TTL11/2	31.103147	86.573341	8.8	134	64.0	Modified ETH gravity corer[a]	2011
TTL12/3	31.102887	86.573370	8.4	157	89.0	Modified ETH gravity corer[a]	2012

[a]Kelts et al. (1986).

parameters were measured on a depth profile in 2 m steps at the deepest part of the lake in June 2012 utilizing a multi-parameter instrument (Multi 340i WTW). Alkalinity was titrated with a Macherey-Nagel rapid test.

Non-destructive laboratory methods

The cores were stored under dark and cold (+4°C) conditions until further processing. An initial core description was conducted including high-resolution imaging, sediment description, and a bulk magnetic susceptibility scan (κ) in 2 mm resolution (Bartington MS 2E). The split cores were subjected to XRF scanning and x-ray imaging (ITRAX Corescanner) (Croudace et al., 2006). XRF analyses were performed in 2 mm steps with an exposure time of 10 s using a molybdenum target tube set to 55 kV and 40 mA. The element peak area (pa) values were normalized to coherent counts (coh). Only elements constantly >100 pa were used for interpretation (Kasper et al., 2012). The cores TTL11/1, TTL11/2, and TTL12/3 were correlated based on lithological pattern and Ti values (pa/coh). Since core TTL12/3 is the longest record retrieved, it serves as a standard for all other cores (Figure 2, Table 1).

Destructive laboratory methods

Double-L-channels from core TTL12/3 were continuously subsampled in 1 cm intervals for granulometric, geochemical, and mineralogical analyses. For granulometric analyses, samples were pretreated with HCl 10% and H_2O_2 10% to dissolve carbonates and organic matter. Sodium pyrophosphate ($Na_4P_2O_7 \cdot 10\ H_2O$, 0.1 mol L^{-1}) was added and samples were shaken for 2 h. The grain size distribution was measured (LS 13320 Beckmann Coulter) in seven cycles of 60 s. The first reproducible measurement was taken for interpretation. Statistical calculations were carried out using a modified version of Gradistat 4.2 by Blott and Pye (2001).

Mineralogical composition of eight layers (20, 32, 37, 52, 53, 58, 59, and 73 cm sediment depth) and eight bulk sediment samples (25, 26, 27, 28, 40, 49, 64, and 80 cm sediment depth), each integrating 1 cm sediment depth of core TTL12/3 was analyzed by XRD (AXS-Bruker D8-Discover) using a CuKα x-ray source. Sediment samples from 53.5, 66.5, and 86.0 cm were analyzed with a scanning electron microscope (SEM; Leica S440i).

Water content was defined by scaling before and after freeze-drying of the samples. In total, 66 freeze-dried and ground (<40 μm) sediment samples of core TTL12/3 (below 24 cm sediment depth) were used for analysis of total carbon (TC), total organic carbon (TOC), total sulfur (TS), and total nitrogen (TN) utilizing a CNS-analyzer (Vario El Cube). The error was estimated based on two triplicate measurements and sulfanilic acid served as standard. Total inorganic carbon (TIC) was calculated as the difference of TC and TOC. Based on the XRD results, TIC was multiplied with 8.33 to get in the calcite content of the sediment.

For palynological analysis, 10 subsamples of 2 cm^3 integrating 1 cm sediment depth were obtained in 8 cm intervals from 88 to 24 cm, and an additional sample was taken in 4 cm sediment depth. Samples were processed after Faegri and Iversen (1989). A known number of *Lycopodium* spores (batch #710961 corresponds to 13,911 ± 1541 spores) was added to each sample (Maher, 1981). Pollen sums of 360–450 pollen grains of terrestrial plants including Cyperaceae were counted per sample to receive a statistically relevant number of grains. All percentages refer to these pollen sums. Pollen and non-pollen palynomorphs (NPP) were identified using relevant literature (Beug, 2004; Van Geel et al., 2003; Wang et al., 1995) and a private collection of over 5500 type slides. Selected taxa are plotted on the pollen diagram.

A total of 10 subsamples were taken for diatom analysis following the pattern as described for palynological analysis and additionally at 82, 49, and 27 cm sediment depth. For preparation, 0.3 g wet sediment was treated with 30% H_2O_2 and 30% HCl for 15–20 min at 70°C in a water bath. After cooling, the suspension was filled up with water and allowed to stand overnight. The supernatant was pipetted off and the residue was dissolved and boiled in 20 mL H_2SO_4 added with 2 mL $KMnO_4$ for 20 min. The solution was cleared by adding drops of oxalic acid. Washing and sedimentation were repeated until the suspension became neutral. Divinylbenzene microspheres were added into the diatom suspension, and different concentrated drops therefrom were placed on cover-glasses, dried, and embedded in Naphrax®. At least 400 valves were counted in each sample using an Axio Imager.M2 (Zeiss) research microscope equipped with a Plan-Apochromatic oil immersion objective (×100/NA1.4). Diatom species were mainly identified based on Lange-Bertalot and Moser (1994), Reichardt (1999), Lange-Bertalot (2001), Krammer (2002); Krammer (2003), Scheffler and Morabito (2003), Krammer and Lange-Bertalot (2008), Levkov (2009), Houk et al. (2010), and Hofmann et al. (2013).

For ostracod analysis, 88 samples (TTL12/3) with 1 cm resolution and 15 surface sediment samples were washed, weighed, and sieved (200 μm and 63 μm meshes). Ostracods were taxonomically classified relying on Wrozyna et al. (2009), and at least 300 valves were counted from each sample to be statistically relevant. Other biological components like seeds, plant remains, bivalves, and head capsules of chironomid larvae were recorded semi-quantitatively.

Dating

Seven bulk sediment samples, each integrating 1 cm sediment depth, from cores TTL11/2 and TTL12/3 were submitted for ^{14}C AMS dating (Beta Analytic Inc., USA). Three ages from core TTL11/2 were transferred to core TTL12/3 based on the lithology and Ti data. The conventional radiocarbon ages were calibrated (2σ) with Calib 7.0 based on the IntCal13 data set (Reimer et al., 2013).

Plant remains from a section with normal grading at 18–22 cm sediment depth were sieved using 1 mm and 500 μm meshes and submitted to the same laboratory for radiocarbon dating. The conventional radiocarbon ages given in pMC were calibrated (2σ) using CaliBomb (Hua et al., 2013). The NHZ3 calibration data set was applied for calibration.

For paleomagnetic analyses, a u-channel from sediment core TTL11/1 was AF demagnetized using 5 mT intervals from 0–75 mT and measured for the natural remanent magnetization (NRM) in 1 cm intervals utilizing a 2G Enterprises DC-4K liquid 109 helium free magnetometers (Model 755-1.65 UC) with a water cooled compressor. Inclination and declination data were computed with Principle Component Analyses (Kirschvink, 1980) implemented in an Excel macro (Mazaud, 2005) using the characteristic remanent magnetization (ChRM: mostly 20–50 mT) also providing maximum angular deviation (MAD) values. For comparison with the CALS3k.4 geomagnetic field model (Korte and Constable, 2011) and data from Nam Co (Kasper et al., 2012) inclination data of core TTL11/1 were plotted on ages obtained from a linear interpolation of ages transferred from sediment core TTL11/2 based on lithological features and magnetic susceptibility.

Results

Water parameter

In June 2012, TT Lake had a secchi depth of 2.85 m. In the water column, the pH values were between 8.5 and 8.7, temperatures ranged from 10.3–12.3°C (June 2012), and the alkalinity was 2.2–2.6 mmol L^{-1} (Figure 3). The specific conductivity was relatively constant at 328–332 μS cm^{-1} (Figure 3). Applying a conversion factor of 0.725 after Hölting (1992), a salinity of ~0.2 g L^{-1} can be deduced. The water is dominated by Ca and SO_4 ions.

Geophysical, geochemical, and mineralogical properties

The macroscopic description of the 88.4 cm long sediment core TTL12/3 revealed predominantly stratified, grayish-brown to black sandy mud (Figure 2). Three major lithostratigraphical units can be subdivided in core TTL12/3: (1) fine silty to fine sandy, light brown to dark olive gray sediments with laminae of millimeter-scale; (2) dark gray almost black, massive, fine silty to fine sandy sediments; (3) discrete, sharp-bounded sediment sections with internal grading from fine sand to very fine silt (Figure 2). Sections with normal grading (fining upward) are markedly thicker than the lamination and are distinguishable at 73.1–72.3, 60.0–57.2, 57.0–56.3, 53.3–51.2, 50.5–49.6, and 2.2–0 cm sediment depth. The section at 23.5–5.4 cm has a reverse graded (coarsening upward) part at 23.5–22.0 cm and normal grading at 22.0–5.4 cm. This section contains macroflora remains at its bottom, has an erosional basal contact, and occurs in all three cores (Figure 2). This layer is 15 cm thick in core TTL11/1, 17 cm in TTL11/2, and 18 cm in TTL12/3 (Figure 2).

The water content varies between 45% and 74% and increases gradually toward the top, while water content is <60% in sections with internal grading and between 59% and 74% in remaining parts (Figure 4). Magnetic susceptibility (κ) varies between −10 and $90 \cdot 10^{-6}$ SI and shows values up to $300 \cdot 10^{-6}$ SI in sediment sections with internal grading (Figure 4).

Median grain sizes range from 3–81 μm and are highest around 20 cm sediment depth (Figure 4). The optically determined internal grading at 60.0–57.2 cm, 53.3–51.2 cm, 23.5–5.4 cm, and 2.2–0 cm is confirmed by grain size analysis (resolution of grain size

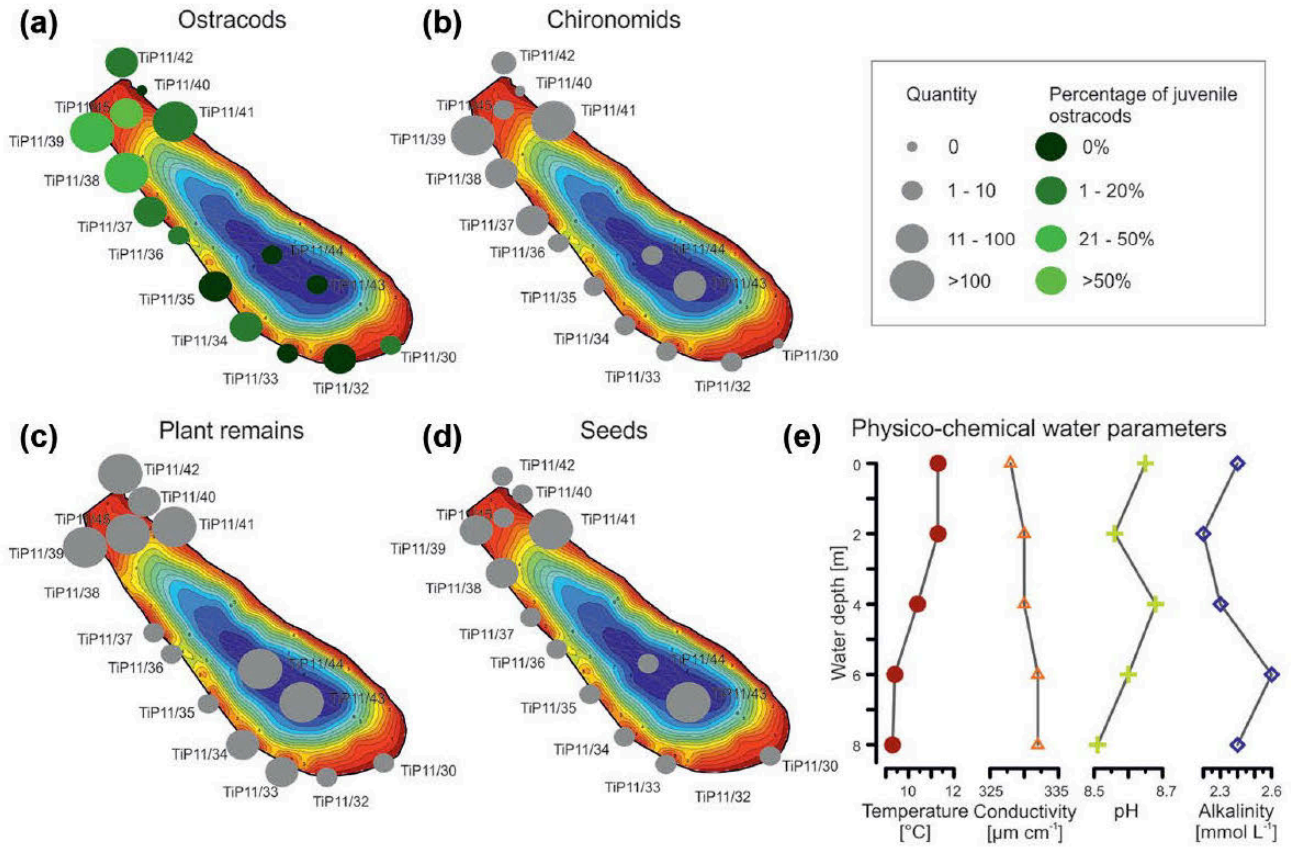

Figure 3. Modern biological data and physico-chemical water parameter: (a) Quantity of ostracods including percentages of juvenile individuals, (b) quantity of head capsule of chironomid larvae, (c) quantity of plant remains, (d) quantity of seeds (all four parameter show a dominance at the inflow), and (e) physico-chemical water parameters measured in June 2012.

analysis is 1 cm, remaining sections are too thin to reveal internal grading by grain size analysis). In the section at 23.5–5.4 cm, the median grain size decreases from 81 µm at the bottom to 4 µm further up (Figure 4b). Additionally, normal grading is observed in a gray layer at 84.8–83.4 cm. Sediments can be mainly assigned to very fine sand to (very) coarse silt and are generally (very) poorly sorted. The major fraction of sediments is silt accounting for 65.3%, followed by the sand fraction with 20.6%, and the clay fraction with 14.1% (Figure 4b). The sand fraction resembles the median grain size with a correlation coefficient of $R_{\text{median-sand}}=0.93$, whereas the silt and clay fraction are negatively correlated with $R_{\text{median-silt}}=-0.74$ and $R_{\text{median-clay}}=-0.72$.

Mineralogical analyses revealed that sediments mainly consist of quartz, feldspar, and clay minerals. The carbonate phase is composed of calcite. The sediment composition is homogeneous over time, and sections with internal grading have the same mineralogical composition.

K, Ca, Ti, Fe, Rb, Mn, and Sr were measured with counts >100 and are thus used for interpretation. K, Ti, Fe, and Rb reveal similar patterns and also reproduce κ showing significant peaks in sediment sections with internal grading and additionally at 87.6–87.4, 47.2, and 28.4–28.2 cm sediment depth (Figure 4). K, Ti, Fe, and Rb are negatively correlated to Ca and Sr with a correlation coefficient of $R_{\text{Ca-Ti}}=-0.75$. Mn shows only minor variations, but significantly increased values in sediment sections with internal grading and at 35.0–23.5 cm sediment depth. X-ray images show higher densities in internally graded sections and at 87.5, 81.5–79.5, 47.5, and 28.5 cm and fine lamination in remaining parts of the core (Figure 2).

TOC is characterized by values between 5% and 12% (relative error 0.2%), with generally lower values above 47.2 cm (Figure 4). TN is mostly in phase with the TOC pattern with a correlation coefficient of $R_{\text{TN-TOC}}=0.76$ and values between 0.52% and 0.94% (relative error 2.2%). Carbonate content ranges from 9% to 52%. TOC, TN, and carbonate content show lowest values in sediment sections with internal grading, and TOC values are reduced in these sections by 2–5% (Figure 4). C/N ratios vary between 9 and 18.

Palynology

In total, 105 pollen palynomorphs and NPP were identified. The proportion of tree and shrub pollen in the spectra is <5% with a high portion of pollen from long distance transport (Figure 5a). Findings of the Juniper-type, Myricaria, and Hippophae might refer to shrubs in the wider area of the TT Lake. The spectra are dominated by pollen of herbs, perennials, and grasses mostly by *Artemisia*, Poaceae, Cyperaceae, and Chenopodiaceae. Spores of coprophilous fungi occur with varying percentages (Figure 5a).

Micropaleontology

In total, 69 diatom species were detected in 16 samples. The diatom concentration values are between $14.69 \cdot 10^7$ and $104.88 \cdot 10^7$ valves per gram (Figure 5b). Higher diatom concentrations with $96.00–104.88 \cdot 10^7$ valves per gram were calculated in the middle part of the record at 55–48 cm sediment depth. Below 27 cm sediment depth, the diatom assemblages were dominated by planktonic species, especially *Cyclotella comensis* morphotype *minima* Scheffler (Scheffler and Morabito, 2003). Furthermore, *Staurosirella pinnata* (Ehrenberg) D.M.Williams & Round and *Fragilaria tenera* (W. Smith) Lange-Bertalot occurred frequently. *Staurosirella pinnata* could be detected having an average relative abundance of 13.1% in the core. It occurred with a relative abundance of 59.8% only at 4 cm sediment depth. The benthic diatom *Fragilaria tenera* appeared only in the sediment depths 49–48 cm (53.5% and 89.3%), 24 cm (70.7%), and 4 cm (28.6%)

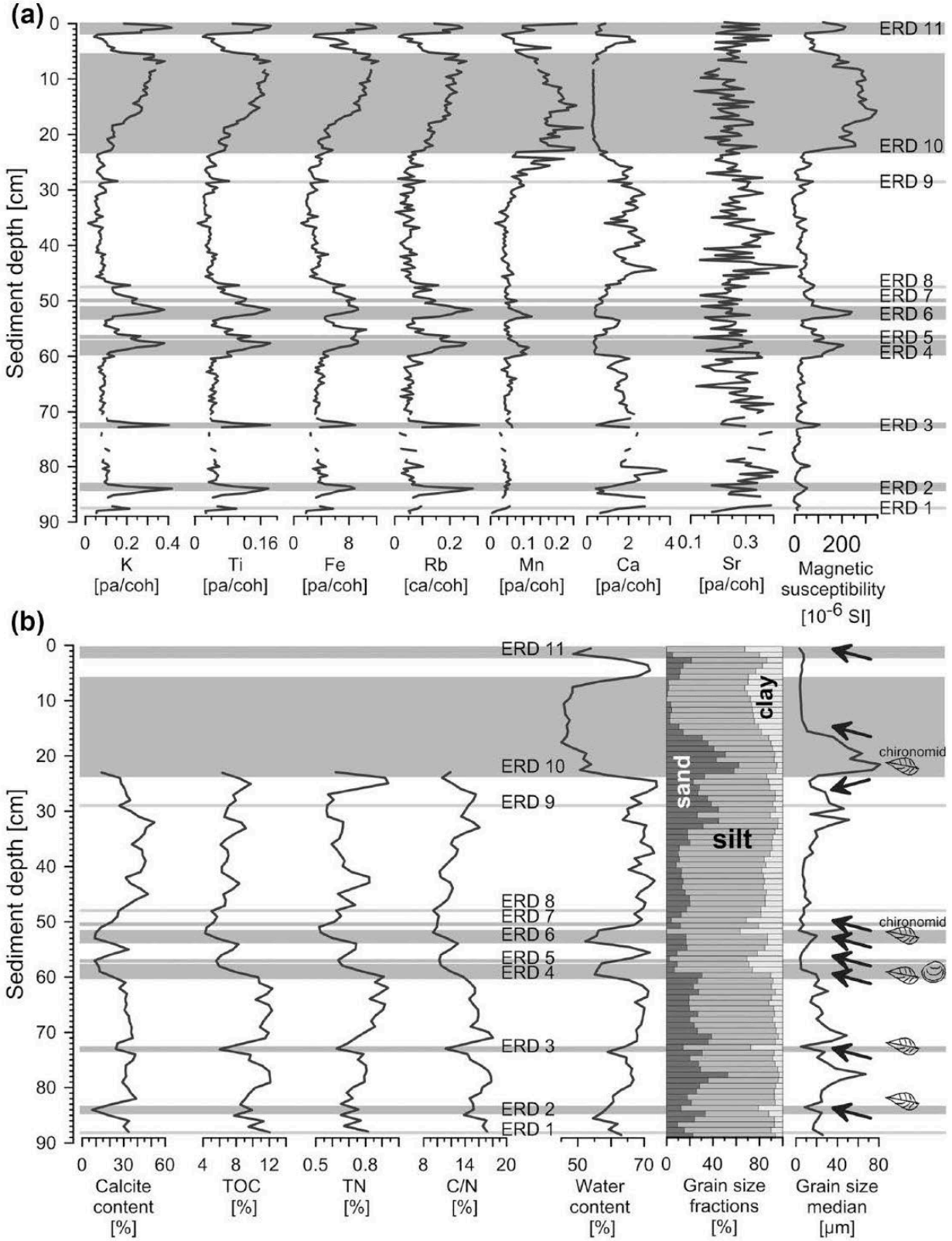

Figure 4. Multi-proxy data set with event-related deposits (ERDs) I–I I (gray bars). (a) XRF and magnetic susceptibility data. Gaps in the data are because of holes in the sediment. (b) Geochemical data ($CaCO_3$, TOC, TN, C/N), water content, and grain size data. Arrows indicate normal or reverse grading. Occurrence of plant remains (leaf), head capsules of chironomid larvae, and bivalve *Pisidium* sp. (mussel) are indicated by sketches (right).

with high relative abundances (Figure 5b). A semi-quantitative estimation with SEM analyses revealed a reduced diatom content in sections with internal grading.

Ostracods are completely missing in sediment core TTL12/3. Microscopic plant remains are very abundant in several sediment sections with internal grading and in 83 cm sediment depth (Figure 4). Head capsules of chironomid larvae (50 and 18 cm sediment depth) and the bivalve *Pisidium* sp. (57 cm sediment depth) were recorded within sediment sections with internal grading (Figure 4).

In total, four ostracod species were found in the modern sediment surface samples of the TT Lake: *Tonnacypris gyirongensis* (first described by Yang in 1982), *Limnocythere inopinata* (first described by Baird in 1843), *Fabaeformiscandona gyirongensis*

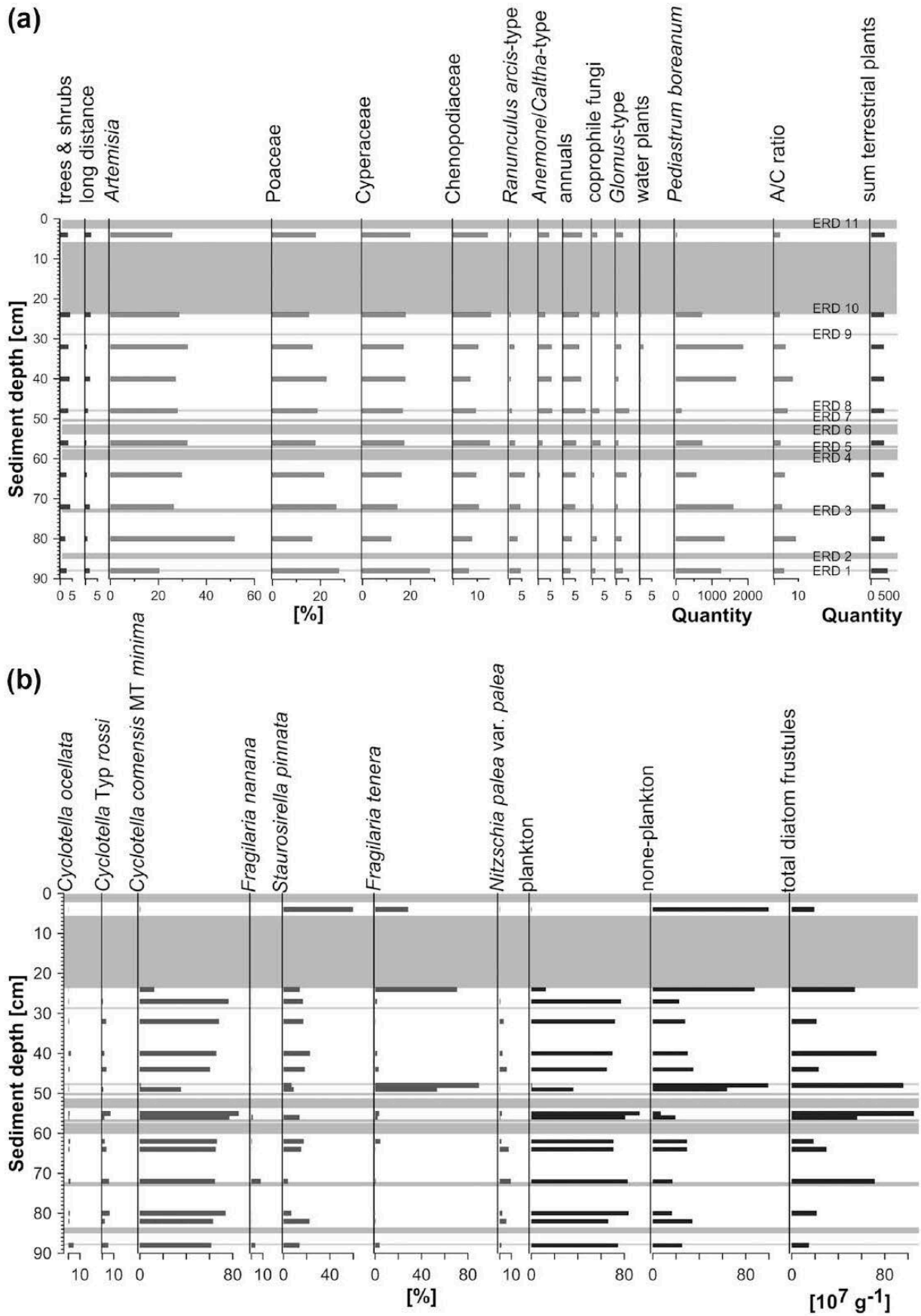

Figure 5. Pollen, spores, and diatom data with event-related deposits (ERDs) 1–11 (gray bars). (a) Pollen and spores data. Pollen indicate a significant shift to stronger grazing pressure correlating with ERDs 4–8 and coprophilous fungi co-occur with ERDs (gray bars). (b) Diatom data: Noticeable is the occurrence of *Fragilaria tenera* at 49, 48, 24, and 4 cm sediment depth and the occurrence of *Fragilaria pinnata* var. *pinnata* at 4 cm. The tychoplanktic species *Fragilaria pinnata* var. *pinnata* is a pioneer species and can indicate disturbances in the ecosystem. It occurs in significant abundances only once, after ERD 10.

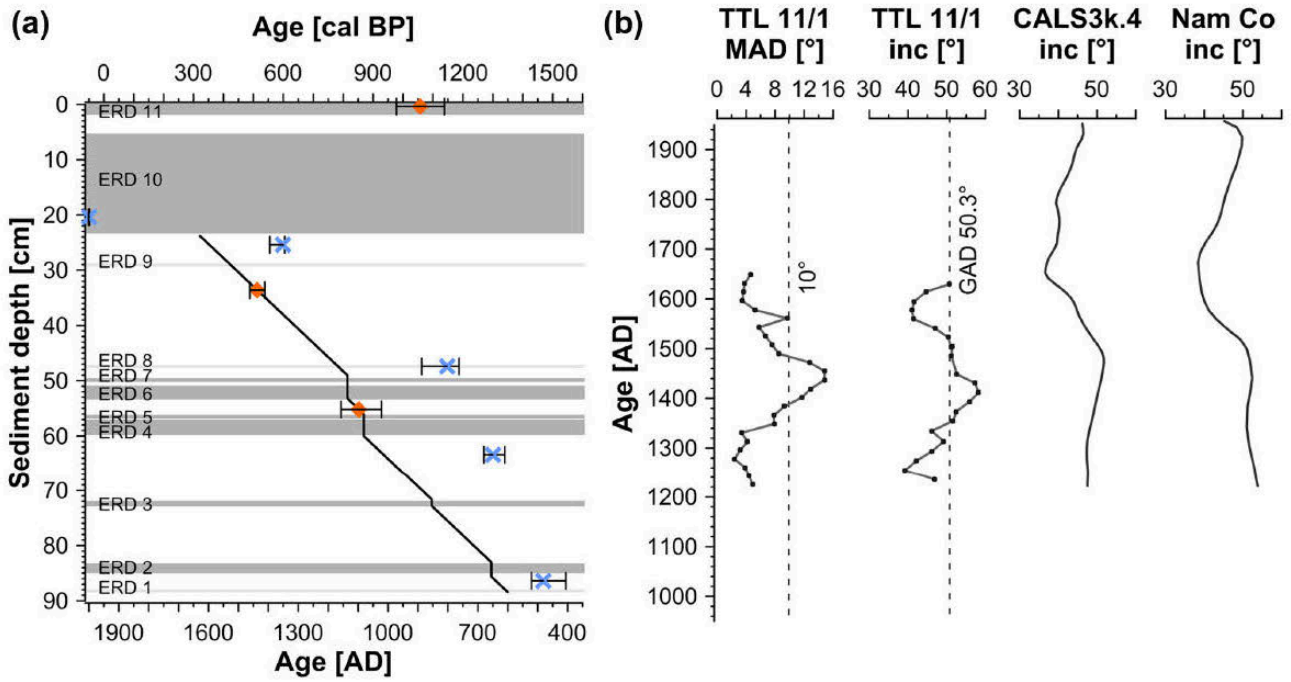

Figure 6. Chronology: (a) Age–depth relationship based on radiocarbon ages of sediment core TTL11/2 (orange rhombus) and ages of core TTL12/3 (blue cross). Age determination from event-related deposit (ERD) 10 integrates from 22 to 18 cm. ERDs marked by gray bars. (b) Maximum angular deviation (MAD) and inclination data from TTL11/1. CALS3k.4 model (Korte and Constable, 2011) and data from Nam Co (Kasper et al., 2012) for comparison.

(first described by Huang in 1982), and *Leucocythere dorsotuberosa* (first described by Huang in 1982). The most abundant and the only species found living is *Tonnacypris gyirongensis* which dominates the taphocoenosis to almost 100%. The other species are extremely rare and probably reworked from older sediments. *Tonnacypris gyirongensis* is most abundant close to the inflow and especially rare in the deep water (>8 m). Only one surface sediment sample completely lacks ostracods (Figure 3). Most valves are disarticulated and the majority of valves are from adult stages (Figure 3). This is expressed by low juvenile/adult ratios, while juvenile valves are completely missing in the deep water (>8 m). Head capsules of chironomid larvae and plant remains including seeds are concentrated in the samples near the inflow (Figure 3). Most seeds belong to the terrestrial family Chenopodiaceae.

Chronology

Linear interpolation of radiocarbon ages obtained from sediment cores TTL12/3 and TTL11/2 show an offset of 100–300 years from TTL12/3 to TTL11/2 (Figure 6, Table 2). An age from 0.4 cm sediment depth of core TTL11/2 of AD 890 is inverse to the underlying ages. The calibrated age of the dated plant remains from 18 to 22 cm sediment depth has a 2σ range of AD 1997–2000 (Figure 6, Table 2).

Paleomagnetic data

The high NRM intensities are in the range of $3.1 \cdot 10^{-3}$ to $3.2 \cdot 10^{-2}$ A m^{-1}. MAD values are mostly <10° (Figure 6). ChRM fluctuate around the geocentric axial dipole (GAD) model of 50.3°. Unfortunately, declination was influenced by coring artifacts and hence is not shown.

Interpretation and discussion

Modern processes

Physico-chemical water parameters indicate a well-mixed freshwater lake without stratification at least at the time of measurement (Figure 3). The recent ostracod association can be considered as monospecific because of the clear dominance of *Tonnacypris gyirongensis*, the only ostracod species found living, which is characteristic of freshwater springs, ponds, and estuaries at Tangra Yumco (Lailah Gifty Akita, personal communication). Most living individuals occur in the shallow water close to the mouth of the small stream feeding the lake. The high percentage of well-preserved adult *Tonnacypris gyirongensis* often with soft parts points to an autochthonous association without high post-mortem disturbance through storms or biological activity (Boomer et al., 2003). The low abundance of adults and missing juvenile ostracods in the deepest parts of the basin suggest shell dissolution in this area (Figure 3). Juvenile shells are smaller and much thinner than adult ones and therefore prone to faster dissolution. Even though the picked ostracod valves from the deepest surface samples show no clear signs of dissolution and the carbonate content in the core is partly as high as 50%, shell dissolution remains the only possible explanation for the lack of ostracods in the core. Potentially seasonal pH changes causing temporary dissolution of shells might be a possible explanation. The monospecific ostracod fauna indicates a freshwater body with highly fluctuating physico-chemical parameters and probably periodic oxygen deficiency impeding a continuous colonization of the deeper water.

The large number of terrestrial Chenopodiaceae seeds in sediment samples of the north-western part of TT Lake indicates transport and input of terrigenous plant material by the small stream entering the lake at the north-western shore (Figures 1 and 3). Consequently, and in agreement with living ostracod distribution, input of clastic material is probably also controlled by the stream, and therefore, fluvial input from the north-west dominates the sedimentary processes in the lake (Figure 1). The benthic biological production of the TT Lake is concentrated in the stream inflow area.

Chronology

The most probable explanation for the topmost inverse age determination is that the sample contained reworked material. The offset in age estimations from core TTL11/2 to TTL12/3 is difficult

Table 2. AMS radiocarbon age determinations.

Radiocarbon data

Core	Core depth (cm)	Transferred depth of core TTL12/3 (cm)	Lab. ID (Beta Analytics Inc.)	Dating material	Conventional ^{14}C age	Calibrated min. age 2σ (AD)	Calibrated max. age 2σ (AD)	Calibrated median age 2σ (AD)
TTL11/2	1		322428	Bulk sediment	1150 ± 30 BP	800	970	890[a]
TTL11/2	36	33.6	322429	Bulk sediment	460 ± 30 BP	1415	1465	1440[b]
TTL11/2	61	55.2	322430	Bulk sediment	940 ± 30 BP	1025	1160	1100[b]
TTL12/3	22–18		375715	Plant remains	110.2 ± 0.3 pMC	1997	2000	
TTL12/3	26		343273	Bulk sediment	650 ± 30 BP	1345	1395	1350
TTL12/3	48		343274	Bulk sediment	1220 ± 30 BP	760	885	800
TTL12/3	64		340282	Bulk sediment	1380 ± 30 BP	610	680	650
TTL12/3	87		340283	Bulk sediment	1590 ± 30 BP	405	540	480

[a]Within event-related deposit (ERD 11).
[b]Used for age–depth relationship.

to explain (Figure 6). Younger ages are more reliable because they are less likely to be affected by a reservoir effect and hence are considered to represent a maximum age. Linear interpolation of the two age determinations of core TTL11/2 were used to establish an age–depth relationship below 23.5 cm sediment depth showing that the record covers ~1000 years from approximately AD 600–1600 (Figure 6). Since the plant remains from 22–18 cm sediment depth have a modern age of AD 1997–2000, it can be assumed that the record contains a hiatus of ~400 years above 23.5 cm sediment depth (Figure 6, Table 2).

Since this is a very conservative approach, this hypothesis was tested using magnetostratigraphy. Inclination data calculated for TTL11/1 for AD 1400–1600 (Figure 6) are in good agreement with the CALS3k.4 model (Korte and Constable, 2011) and data from Nam Co (Kasper et al., 2012) confirming the chosen age–depth modeling approach. Although MAD values exceed 10° around AD 1400, inclination data of sediment core TTL11/1 still agree perfectly with the CALS3k.4 model and the Nam Co data (Figure 6). Data of the topmost 22 cm were not used for comparison because of a sediment section with internal grading showing ill-defined directions. The match of the inclination data from sediment core TTL11/1 with the CALS3k.4 model and the Nam Co data indicates that the radiocarbon age–depth relationship is a good first order approach.

Modes of sediment deposition

Presuming that the sediments have identical provenance throughout the record, as suggested by the homogeneous mineralogical composition, it is implied that sections with internal grading must be driven by essentially different sedimentary processes than surrounding sediments. Based on geochemical, geophysical, and mineralogical properties (Figures 2 and 4), two modes of sediment deposition can be identified. The primary mode, characterized by relatively low and constant Ti and κ, consists of partly laminated clastic sediments containing diatom frustules and high amounts of organic matter (Figures 2 and 4). Generally, the low Ti and κ content point to low allochthonous clastic input and little surface runoff (Haberzettl et al., 2005; Kasper et al., 2012; Mackereth, 1966; Niemann et al., 2009; Osleger et al., 2009). The lamination of the sediment in this mode indicates undisturbed sediments. This primary mode represents the continuous background sedimentation resulting from an interaction of continuous terrigenous input induced by fluvial processes and autochthonous productivity (Osleger et al., 2009).

The second mode is characterized by discrete and partially normally graded sediment sections associated with increased Ti and κ values, reduced water content, higher density, and distinctively lower diatom content compared with the background sedimentation (Figures 2 and 4). As TOC was measured below 24 cm sediment depth only, reduced TOC in sediment sections with internal grading were observed at least below 24 cm sediment depth. Decreased TOC might be ascribed to dilution of organic matter by terrigenous clastic sediments (Osleger et al., 2009) but could also result from the input of sediments with low organic content from the catchment (Brown et al., 2000). The increased proportion of clastic material also explains the higher density in these sections. Lower diatom concentrations, as shown by a semi-quantitative SEM analysis, indicate a lake-external origin of the sediments. Reduced water content of sediment sections with internal grading might be caused by rapid deposition (Bøe et al., 2006; Sletten et al., 2003). Based on these features, second mode sediments are defined as ERDs resulting from an interruption of the background sedimentation by abrupt and short-lasting input of increased amounts of terrigenous clastic material (Bierman et al., 1997; Bøe et al., 2006; Brown et al., 2000; Osleger et al., 2009; Sletten et al., 2003). Eleven ERD were identified, at 87.6–87.4 cm (ERD 1), 84.8–83.4 cm (ERD 2), 73.1–72.3 cm (ERD 3), 60.0–57.2 cm (ERD 4), 57.0–56.3 cm (ERD 5), 53.3–51.2 cm (ERD 6), 50.5–49.6 cm (ERD 7), 47.2 cm (ERD 8), 28.4–28.2 cm (ERD 9), 23.5–5.4 cm (ERD 10), and 2.2–0 cm (ERD 11), whose properties distinctly contrast from the background sediments (Figure 4).

Based on lithology and granulometric data, two types of ERDs can further be distinguished, likely representing different depositional processes. The macroscopically visible ERDs 2–7 and 11 have generally similar characteristics (discrete, sharp-bounded, normally graded, high Ti and κ, low TOC, low water content, no macroflora remains), suggesting that they were deposited by similar processes (Figures 4 and 7a). Comparable sediments were described earlier by Brown et al. (2000), Sletten et al. (2003), Bøe et al. (2006), and Irmler et al. (2006) and were associated with enhanced surface sediment erosion during individual hydrologic events (Bøe et al., 2006). None of these ERDs has a basal erosional contact probably indicating that the effluent had a low density and moved as overflow into TT Lake possibly similar to a hypopycnal or homopycnal flow (Irmler et al., 2006; Mulder and Alexander, 2001; Mulder and Chapron, 2001).

Sections with elevated Ti and κ values and increased density at 87.5, 47.5, and 28.5 cm show no internal grading and no rise in the mean grain size, suggesting the occurrence of hydrologic events with a minor impact on the watershed. These minor events are represented by ERDs 1, 8, and 9 (Figures 4 and 7a). Obviously, the event magnitude must exceed a threshold to generate a visible ERD (Czymzik et al., 2010). These thresholds determine whether a hydrological event produces an associated ERD depending on factors like current velocity, entry point into the lake, lake size,

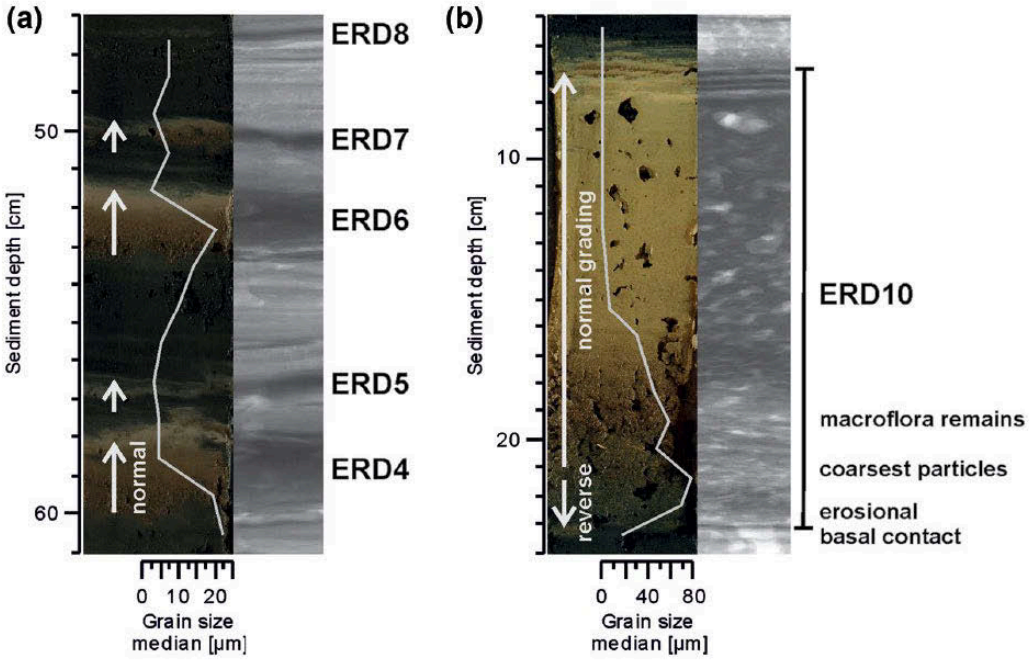

Figure 7. Detailed images of ERDs 4–8 and 10. (a) Core photo (left) and x-ray (right) of ERDs 4–8 with median grain size data (left). All ERDs show normal grading (upward arrows). ERD 8 represents an ERD with minor impact on the watershed and is not visible in the core photo but x-ray image indicates increased density. (b) Core photo (left) and x-ray (right) of ERD 10 with median grain size data (left). This ERD is unique in terms of grading (reverse at the base, normal above, indicated by upward and downward arrows), thickness, macroflora remains at the base, and particle size (coarsest in the core). Please note the different scaling of the axes in (a) and (b).

basin morphology, and weathering rates (Czymzik et al., 2010; Sturm and Matter, 1978). The magnitude of these events might not have exceeded the threshold and was not effective enough to produce a visible ERD. But since the Ti values contrast strongly from the background sedimentation (Figure 4), they are considered to be the result of an abrupt event and not continuous background sedimentation. Considering this, it can be assumed that the number of hydrologic events is higher than the related number of ERDs because not all hydrologic events are represented by an ERD or significantly high Ti values in the sediment record (Kämpf et al., 2012). Furthermore, there is a general trend that hydrologic events of greater magnitude produce a thicker ERD (Kämpf et al., 2012), suggesting that ERD 4 and ERD 6 were the most pronounced events.

Several climatic settings can trigger hydrologic events in small lacustrine systems, for example, precipitation, rapid snow melt, or warm rain on a snow cover (Bøe et al., 2006; Osleger et al., 2009). Winter months are generally dry at TT Lake (Miehe et al., 2014), and the snow cover is very sparse as documented by satellite images (Google™ earth, Figure 8). Re-analysis data, covering the years 1979–2010, reveal a mean precipitation of ~40 mm from November to April (Chen et al., 2011) also pointing to a sparse snow cover. Re-analysis data and satellite images indicate that there is nowadays no significant snow melt affecting the TT Lake watershed; therefore, ERDs 1–9 and 11 are most likely the result of precipitation events during summer months. Specifically, it is assumed that during precipitation events, terrigenous sediments from the watershed were eroded by runoff and transported as overflow into the lake. The absolute amount of precipitation that triggered these hydrological events cannot be assessed, but it must have been above average either in intensity or in duration. Since benthic biological production is mainly restricted to the inflow area, a recorded head capsule of a chironomid larva in ERD 7 might indicate that sediments forming the ERD were transported to the lake by the stream and entered the lake from there (Figures 3 and 4). As indicated by the distribution of Chenopodiaceae seeds, background sedimentation as well as event-related sedimentation is probably predominantly controlled by the inflow at the north-western shore and other transport directions seem to be negligible.

ERD 10 is unique in terms of grading (reverse at the base, normal above), thickness, macroflora remains at the base, and particle size (coarsest in the core), pointing to a different transport process than ERDs 1–9 and 11 (Figures 2, 4 and 7b). Since ERD 10 is at least 15 cm thick, over 200 m^3 of sediment were accumulated only in the deepest part of the lake (>8 m) showing that a massive volume of sediment was deposited during a single event. The macroflora remains indicate an allochthonous origin of ERD 10 and probably reflect the removal of the vegetation cover by a sediment mass movement (Sletten et al., 2003). Satellite images (Google™ earth, Figure 8) show that a mass transport, possibly comparable to a debris flow, occurred in the TT Lake catchment between AD 2004 and 2011 and reached the lake from the north, proving that mass transport is a modern phenomenon in the TT Lake catchment. The age determination of plant remains from ERD 10 revealed an age range of AD 1997–2000 (Figure 6, Table 2). The sediment mass transport could have easily transported dead plant material from the catchment and thus could possibly be younger than the age measured. Since only one sediment mass transport is recorded in the TT Lake record during the most recent time, there is a high probability that the sediment mass transport from the satellite images and ERD 10 represent the same event (Figure 8). The erosional basal contact of ERD 10 (Figure 7) indicates that the mass transport moved as underflow probably similar to a hyperpycnal flow into the lake basin (Irmler et al., 2006; Mulder and Alexander, 2001; St-Onge and Lajeunesse, 2007). An underflow results from the relatively higher density of the effluent compared with the ambient water (Mulder and Alexander, 2001). The reverse grading at the base of ERD 10 (Figure 7b) might point to a hyperpycnal flow since it develops a reverse graded unit at the base stacked up by a normal graded unit (Mulder et al., 2001; St-Onge and Lajeunesse, 2007). However, ERD 10 is dated to AD 1997–2000 and the age beneath is ~AD 1600, and consequently, the sediment mass transport eroded and reworked a sediment package equivalent to a time interval of 400 years and caused a considerable hiatus. The reverse graded

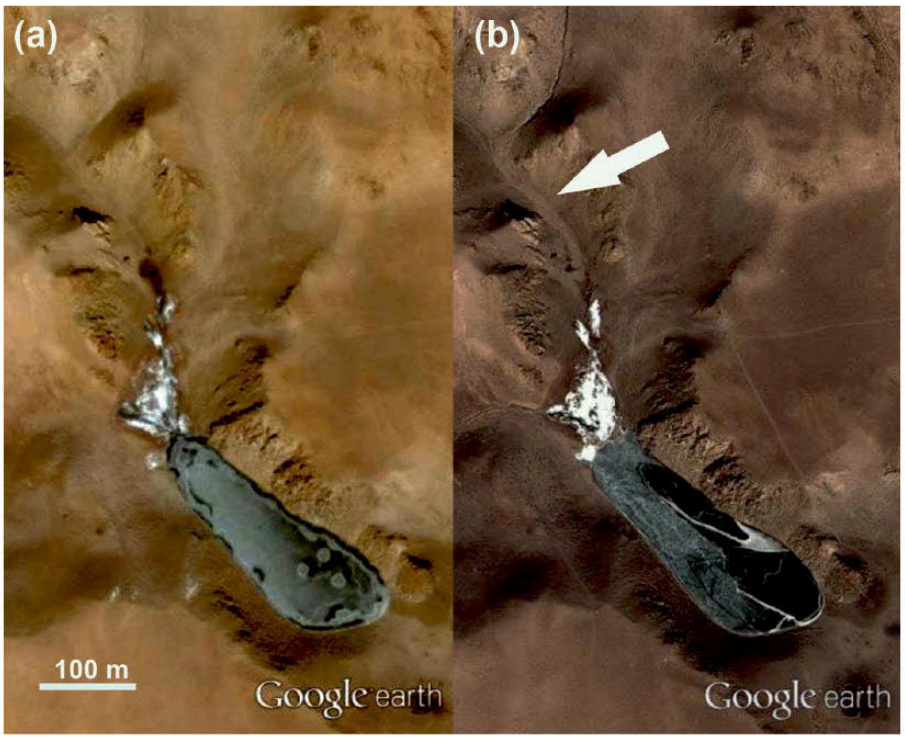

Figure 8. Satellite images (Google™ earth) of frozen TT Lake and watershed with very sparse snow cover in winter. (a) 10 November 2004 and (b) 13 December 2011, sediment mass transport indicated by white arrow.

base of ERD 10 (Figure 7b) could thus also be because of reworked, finer material.

A trigger of the mass transport is difficult to define. Under seismic activity, a decreasing frictional strength and liquefaction can instantly cause slope failures and sediment mass transport (Sletten et al., 2003). On the contrary, under seismic stability, a mass transport may be initiated by the reduction of normal stress and shear strength of the sediment as a result of pore water pressure rise (Anderson and Sitar, 1995; Sandersen, 1997) that causes soil failures. The pore water pressure can rapidly rise as a consequence of high precipitation, fast snow melt, or their combination (Sandersen, 1997). Because of the above discussed reasons, snow-induced processes can be excluded. TT Lake is situated in a tectonically active area, but no tear-off edge is recognizable in satellite images (Google™ earth) making a seismically induced slope failure an unlikely trigger for the recent mass transport (Figure 8). Consequently, a hydrologic event caused by precipitation possibly triggered soil failure and induced a sediment mass transport. Since the precipitation was capable of inducing a sediment mass transport, this event must have been of greater magnitude than for the other ERDs and of torrential intensity. Besides the amount of precipitation, various factors such as vegetation cover, hill slope inclination and morphology, weathering, material, amount of available debris in the watershed, and soil-moisture (Church and Miles, 1987; Jomelli et al., 2004; Moser and Hohensinn, 1983; Pavlova et al., 2014) affect the generation of sediment mass transports. Among these factors, antecedent soil-moisture seems to be determining whether or not a precipitation event can induce sediment mass transport (Johnson and Sitar, 1990), particularly meaning that not every torrential precipitation event can cause sediment mass transport (Sletten et al., 2003).

Link between proxies and hydrologic events

Eleven events (ERDs 1–11) of enhanced precipitation are documented in the TT Lake record (Figure 4). The tentative age model provides age control for events related to ERDs 1–9 (Figure 6). ERDs 1 and 2 are in quick succession, and related events probably occurred around AD 600 and the event linked to ERD 3 around AD 900. The event frequency is highest around AD 1100, where ERDs 4–8 were deposited. The event responsible for ERD 9 occurred around AD 1500. The event with the strongest effect on the lake and the watershed is represented by ERD 10 and probably occurred after AD 2000.

Spores of coprophilous fungi occur at 88 and 80 cm sediment depth (~AD 600), at 56 and 48 cm sediment depth corresponding to highest ERD frequency (~AD 1100), at 24 cm (~AD 1600), and 4 cm (modern age) sediment depth (Figure 5a). Coprophilous fungi are a group of fungi attributed to pastoralism, and their occurrence indicates anthropogenic activity in the TT Lake watershed. Since TT Lake is the only permanent freshwater source in the Tangra Yumco catchment, local people nowadays water and feed their cattle in the wetlands of TT Lake. This is reflected by the occurrence of coprophilous fungi at 4 cm sediment depth representing a time after AD 2000 which represent present day conditions. The lake was also used in this way in previous times, suggesting that the lake must have permanently contained freshwater. Most intense pastoralism is suggested by highest abundances of spores of coprophilous fungi occurring at 56 and 48 cm sediment depth (~AD 1100) and co-occurs with highest ERD frequency, implying a possible link between pastoralism and ERD generation (Figure 5a). An increasing pastoralism influence on the alpine vegetation at about 1000 years ago seems to be a quite common phenomenon in Asia (Schlütz and Lehmkuhl, 2009; Schlütz and Zech, 2004) and is also demonstrated by the changes in weed species (*Ranunculus acris*-type, *Anemone/Caltha*-type) including the spreading of annual weeds (e.g. *Koenigia islandica*-type, *Lasiocaryum*). Pastoralism was less intense but obvious at 88 and 80 cm sediment depth (~AD 600). ERD 1 and 2 occur in this period, whereas ERD 1 and additionally ERD 8 are directly coincident with increased abundances of coprophilous fungi spores. Pastoralism could possibly cause sparser vegetation or loosen the sediments increasing the erodibility of the sediments in the watershed. However, the occurrence of ERD 3 is not coinciding with increased abundances of coprophilous fungi. Consequently, it might be assumed that the generation of ERDs is probably favored

by pastoralism, but pastoralism is not considered to have triggered these events. Spores of coprophilous fungi are probably transported by draining water into the lake because they occur together with water transported pollen of tiny annual insect pollinated plants (e.g. *Lasiocaryum, Koenigia islandica*-type). These annuals grow on disturbed places with a very loose plant cover on easily erodible soils (Miehe et al., 2009).

The relatively stable diatom assemblage provides no evidence for significant changes in the environmental conditions during the period investigated (Figure 5b). Noticeable are the high abundance of *Fragilaria tenera* at 48, 24, and 4 cm and the dominance of *Staurosirella pinnata* in 4 cm sediment depth. The increased presence of *Fragilaria tenera* is not associated with hydrological events. Instead, coprophilous fungi were detected in the same depth. Hausmann et al. (2002) were able to demonstrate intensive grazing indicated by coprophilous fungal spores and a simultaneous change in the diatom assemblage because of eutrophication (Figure 5). Perhaps the change from *Cyclotella comensis* to *Fragilaria tenera* dominance could be based on nutrient enrichment in TT Lake. *Staurosirella pinnata*, classified as tychoplanktonic in Vos and De Wolf (1993) and Bunting et al. (1997), is considered to be a pioneer species and can indicate disturbances in the ecosystem. It occurs in significant abundances only once, after ERD 10 (Figure 5b). Since the mass transport that deposited ERD 10 moved as an underflow, it probably destroyed the benthic flora and *Staurosirella pinnata* acted as an initial colonist taking advantage from the lack of other species. Apart from ERD 10, the diatom association is not affected by hydrologic events.

Climatic implications

Except for the ERDs, Ti is relatively constant showing neither a certain long-term trend nor major variations. Relatively constant Ti values in the TT Lake record indicate a rather stable precipitation pattern except for hydrologic events (Figure 4). Tree and shrub pollen including long distance transported pollen show only minor variations and provide no evidence for climatic variations during the time investigated in the TT Lake record (Figure 5a). The same applies to local pollen representing herbs, perennial plants, and grasses. The local pollen association is relatively constant, and moisture-sensitive plants like *Artemisia* and Chenopodiaceae (Herzschuh, 2007; Zhao et al., 2012) show only minor variations, indicating rather stable moisture availability in the watershed. Both local and long distance pollen suggest stable supraregional climatic conditions. The diatom association is relatively stable and shows no indications for changes in the environmental conditions within TT Lake or the watershed (Figure 5b). Dry but stable climate conditions are also reported from lake Nam Co (Kasper et al., 2012) east of TT Lake for the period represented here. Hence, relatively stable long-term climate conditions with generally constant precipitation and stable environmental conditions can be inferred in the TT Lake area during the period investigated here. Since the pollen association from 4 cm sediment depth (>AD 2000) represents present day conditions, it can be assumed that vegetation cover from AD 600–1600 was very similar to modern conditions.

As prevailing climate and local environmental conditions were relatively stable, hydrologic events were apparently decoupled from long-term climate variations. Hydrologic events hence represent short-term and local meteorological phenomena that are not straightforwardly linked to or favored by the climate conditions, especially average long-term precipitation. Anthropogenic activity in the watershed in terms of pastoralism favors the occurrence of ERDs.

Several studies that investigated ERDs also indicate that their occurrence is decoupled from climate change (Brown et al., 2000; Irmler et al., 2006; Jomelli et al., 2004; Lauterbach et al., 2012; Schlolaut et al., 2014). Lauterbach et al. (2012) showed that runoff events in a lake of the Italian Alps are partly decoupled from variations of solar variability and regional lake level highstands (Magny, 2004) demonstrating that hydrologic events might also be controlled by other factors than climate. Also, Schlolaut et al. (2014) state that precipitation events over the past 40 ka in Japanese Lake Suigetsu were decoupled from the average long-term precipitation pattern. Brown et al. (2000) presented a 10,000-year record of extreme hydrologic events from Vermont (USA) showing that the frequency of hydrologic events is decoupled from climate change. Irmler et al. (2006) found that debris flow events in Lago di Braies (Northern Italy) are not favored by any climatic trend. Jomelli et al. (2004) examined debris flows and climatic change in the French Alps and stated that a link between debris flows and climatic change is problematic because too little is known about the trigger mechanism of debris flows. However, a coupling of hydrologic events and climate settings is proposed by other studies (Giguet-Covex et al., 2012; Jenny et al., 2014; Moreno et al., 2008; Vasskog et al., 2011). This is obviously not mandatory, and other controlling factors must be carefully regarded. There is no hint that a certain geographical setting such as lake size, catchment size and morphology, or altitude would promote a link to the climate. Jomelli et al. (2004) conclude that the link between hydrologic events and climate settings is difficult to establish in high altitudes. The review shows, however, that lakes on low altitudes are also lacking the link between hydrologic events and climate (Brown et al., 2000; Lauterbach et al., 2012; Schlolaut et al., 2014). So a correlation to altitude may be given under certain preconditions but is not generally responsible for a link between climate and hydrologic events.

In addition to climatic triggers, changing erosion rates in the watershed caused by, for instance, earthquakes (Schlolaut et al., 2014) or anthropogenic activity can raise the erodibility of the sediments and favors ERD generation. A link to anthropogenic impact is also visible in other records, and disentangling the influence of climate and anthropogenic impact is not always straightforward (Lauterbach et al., 2012). For the TT Lake record, a contribution of seismic activity on erodibility of sediments cannot be assessed.

Conclusion

The lacustrine record from the small TT Lake shows that the watershed is affected by hydrologic events that are represented as ERDs in the record. Whereas 10 ERDs are linked to precipitation events causing enhanced runoff that carries sediment in suspension into the lake, one ERD reflects sediment mass transport which was probably triggered by torrential precipitation. ERDs are partly macroscopically visible and partly detected by geochemical analyses showing the importance to apply different methods for the examination of sediment cores.

Hydrologic events were decoupled from large scale climate and environmental conditions. Possibly, the generation of ERDs was favored by anthropogenic activity in terms of pastoralism in the watershed. Pastoralism could have enhanced the availability of erodible material. The decoupling of the precipitation events from the climate, also observed in other studies, implies that the interplay of processes affecting a watershed of a lake is complex and processes causing ERDs should be thoroughly ascertained. More investigations are needed to understand the links between the occurrence of hydrologic events and large scale climate settings and other possible controlling factors, especially if such studies should provide a risk assessment for the future. Particularly, lacustrine sediment data from other small lakes with similar catchments on the Tibetan Plateau should be studied to better understand the impacts of hydrologic events on the lakes and their triggering mechanisms. This is especially important since hydrologic events occurring in the watershed of large lakes

would probably not form a visible ERD because of the lake size and could be easily misinterpreted as a phase with higher precipitation. The presented data here illustrate that the multi-proxy approach provides valuable insights and an improved understanding of processes and driving mechanisms of sedimentary dynamics in a small Tibetan lake and its watershed.

Acknowledgements

We gratefully acknowledge the help of Heidrun Garlipp, Kati Hartwig, Dana Höfer, Carmen Kirchner, Kim Jasmin Krahn, Stephanie Meschner, and Tina Trautmann with analyses and sample pretreatment. We thank Bastian Reinwarth for calculation of catchment and lake size, Jaques Labrie for providing a modified version of the GRADISTAT software, Steffen Mischke for providing a photo of TT Lake, and Lailah Gifty Akita, Nicole Börner, Karoline Henkel, Jianting Ju, and Qingfeng Ma for help during the field campaigns in 2011 and 2012. The forcing data set used in this study was developed by Data Assimilation and Modeling Center for Tibetan Multi-spheres, Institute of Tibetan Plateau Research, Chinese Academy of Sciences. We also thank two anonymous reviewers for their helpful comments that markedly improved the manuscript.

Funding

This work is part of the Sino-German collaboration within DFG priority program 1372 'TiP – Tibetan Plateau: Formation–Climate–Ecosystem' (grant no. MA1308/23-2) and jointly financed by the National Natural Science Foundation of China (grant no. 41271225).

References

Anderson SA and Sitar N (1995) Analysis of rainfall-induced debris flows. *Journal of Geotechnical Engineering* 121(7): 544–552.

Beck C (2009) Late Quaternary lacustrine paleo-seismic archives in north-western Alps: Examples of earthquake-origin assessment of sedimentary disturbances. *Earth-Science Reviews* 96(4): 327–344.

Beug H-J (2004) *Leitfaden der Pollenbestimmung für Mitteleuropa und angrenzende Gebiete*. München: Verlag Dr. Friedrich Pfeil.

Bierman P, Lini A, Zehfuss P et al. (1997) Postglacial ponds and alluvial fans: Recorders of Holocene landscape history. *GSA Today* 7(10): 1–8.

Blott SJ and Pye K (2001) GRADISTAT: A grain size distribution and statistics package for the analysis of unconsolidated sediments. *Earth Surface Processes and Landforms* 26(11): 1237–1248.

Bøe A-G, Dahl SO, Lie Ø et al. (2006) Holocene river floods in the upper Glomma catchment, southern Norway: A high-resolution multiproxy record from lacustrine sediments. *The Holocene* 16(3): 445–455.

Boomer I, Horne DJ and Slipper IJ (2003) The use of ostracods in paleoenvironmental studies, or what can you do with an ostracod shell? In: Park LE and Smith AJ (eds) *Bridging the Gap: Trends in the Ostracod Biological and Geological Sciences* (Paleontological Society Papers). Tuscaloosa, AL: The Paleontological Society pp. 153–179.

Brown SL, Bierman PR, Lini A et al. (2000) 10 000 yr record of extreme hydrologic events. *Geology* 28(4): 335–338.

Bunting JM, Duthie HC, Campbell DR et al. (1997) A palaeoecological record of recent environmental change at Big Creek Marsh, Long Point, Lake Erie. *Journal of Great Lakes Research* 23(3): 349–368.

Chen Y, Yang K, He J et al. (2011) Improving land surface temperature modeling for dry land of China. *Journal of Geophysical Research: Atmospheres* 116(D20), 1–15.

Church M and Miles MJ (1987) Meteorological antecedents to debris flow in southwestern British Columbia: Some case studies. *Reviews in Engineering Geology* 155: 63–79.

Croudace IW, Rindby A and Rothwell RG (2006) ITRAX: Description and evaluation of a new multi-function X-ray core scanner. In: Rothwell RG (ed.) *New Techniques in Sediment Core Analysis*. London: Geological Society of London (Special Publications 267), pp. 51–63.

Czymzik M, Dulski P, Plessen B et al. (2010) A 450 year record of spring-summer flood layers in annually laminated sediments from Lake Ammersee (southern Germany). *Water Resources Research* 46(11): 1–16.

Doberschütz S, Frenzel P, Haberzettl T et al. (2014) Monsoonal forcing of Holocene paleoenvironmental change on the central Tibetan Plateau inferred using a sediment record from Lake Nam Co (Xizang, China). *Journal of Paleolimnology* 51(2): 253–266.

Faegri KJ and Iversen J (1989) *Textbook of Pollen Analysis*. Chichester: John Wiley & Sons.

Giguet-Covex C, Arnaud F, Enters D et al. (2012) Frequency and intensity of high-altitude floods over the last 3.5 ka in northwestern French Alps (Lake Anterne). *Quaternary Research* 77(1): 12–22.

Gilli A, Anselmetti F, Glur L et al. (2013) Lake sediments as archives of recurrence rates and intensities of past flood events. In: Schneuwly-Bollschweiler M, Stoffel M and Rudolf-Miklau F (eds) *Dating Torrential Processes on Fans and Cones* (Advances in Global Change Research). Heidelberg: Springer, pp. 225–242.

Haberzettl T, Fey M, Lücke A et al. (2005) Climatically induced lake level changes during the last two millennia as reflected in sediments of Laguna Potrok Aike, southern Patagonia (Santa Cruz, Argentina). *Journal of Paleolimnology* 33(3): 283–302.

Hausmann S, Lotter AF, van Leeuwen JFN et al. (2002) Interactions of climate and land use documented in the varved sediments of Seebergsee in the Swiss Alps. *The Holocene* 12(3): 279–289.

Herzschuh U (2007) Reliability of pollen ratios for environmental reconstructions on the Tibetan Plateau. *Journal of Biogeography* 34(7): 1265–1273.

Hofmann G, Werum M and Lange-Bertalot H (2013) *Diatomeen im Süßwasser-Benthos von Mitteleuropa: Bestimmungsflora Kieselalgen für die ökologische Praxis: Über 700 der häufigsten Arten und ihre Ökologie*. Ruggell: A.R.G. Gantner.

Hölting B (1992) *Hydrogeologie. Einführung in die allgemeine und angewandte Hydrogeologie*. Stuttgard: Enke.

Houk V, Klee R and Tanaka H (2010) Atlas of freshwater centric diatoms with a brief key and descriptions. Part III: Stephanodiscaceae A, Cyclotella, Tertiarius, Discostella. *Fottea* 10: 1–498.

Hua Q, Barbetti M and Rakowski AZ (2013) Atmospheric radiocarbon for the period 1950–2010. *Radiocarbon* 55(4): 2059–2072.

Irmler R, Daut G and Mäusbacher R (2006) A debris flow calendar derived from sediments of lake Lago di Braies (N. Italy). *Geomorphology* 77(1–2): 69–78.

Jenny JP, Wilhelm B, Arnaud F et al. (2014) A 4D sedimentological approach to reconstructing the flood frequency and intensity of the Rhône River (Lake Bourget, NW European Alps). *Journal of Paleolimnology* 51(4): 469–483.

Jiang H, Mao X, Xu H et al. (2014) Provenance and earthquake signature of the last deglacial Xinmocun lacustrine sediments at Diexi, East Tibet. *Geomorphology* 204: 518–531.

Johnson KA and Sitar N (1990) Hydrologic conditions leading to debris-flow initiation. *Canadian Geotechnical Journal* 27(6): 789–801.

Jomelli V, Pech VP, Chochillon C et al. (2004) Geomorphic variations of debris flows and recent climatic change in the French Alps. *Climatic Change* 64(1–2): 77–102.

Kämpf L, Brauer A, Dulski P et al. (2012) Detrital layers marking flood events in recent sediments of Lago Maggiore (N. Italy) and their comparison with instrumental data. *Freshwater Biology* 57(10): 2076–2090.

Karlin RE, Holmes M, Abella SEB et al. (2004) Holocene landslides and a 3500-year record of Pacific Northwest earthquakes from sediments in Lake Washington. *Geological Society of America Bulletin* 116(1–2): 94–108.

Kasper T, Frenzel P, Haberzettl T et al. (2013) Interplay between redox conditions and hydrological changes in sediments from Lake Nam Co (Tibetan Plateau) during the past 4000 cal BP inferred from geochemical and micropaleontological analyses. *Palaeogeography, Palaeoclimatology, Palaeoecology* 392: 261–271.

Kasper T, Haberzettl T, Doberschütz S et al. (2012) Indian Ocean Summer Monsoon (IOSM)-dynamics within the past 4 ka recorded in the sediments of Lake Nam Co, central Tibetan Plateau (China). *Quaternary Science Reviews* 39: 73–85.

Kelts K, Briegel U, Ghilardi K et al. (1986) The limnogeology-ETH coring system. *Schweizerische Zeitschrift für Hydrologie* 48(1): 104–115.

Kirschvink JL (1980) The least-squares line and plane and the analysis of palaeomagnetic data. *Geophysical Journal International* 62(3): 699–718.

Kong P, Na C, Brown R et al. (2011) Cosmogenic ^{10}Be and ^{26}Al dating of paleolake shorelines in Tibet. *Journal of Asian Earth Sciences* 41(3): 263–273.

Korte M and Constable C (2011) Improving geomagnetic field reconstructions for 0–3 ka. *Physics of the Earth and Planetary Interiors* 188(3–4): 247–259.

Krammer K (2002) *Diatoms of Europe: Cymbella*, vol. 3. Ruggell: A.R.G. Gantner.

Krammer K (2003) *Diatoms of Europe: Cymbopleura, Delicata, Navicymbula, Gomphocymbellopsis, Afrocymbella*, vol. 5. Ruggell: A.R.G. Gantner.

Krammer K and Lange-Bertalot H (2008) *Süßwasserflora von Mitteleuropa: Bacillariophyceae, 2. Teil: Bacillariaceae, Epithemiaceae, Surirellaceae*. Stuttgart: Fischer.

Lange-Bertalot H (2001) *Diatoms of Europe: Navicula sensu stricto, 10 Genera Separated from Navicula sensu stricto, Frustulia*, vol. 2. Ruggell: A.R.G Gantner.

Lange-Bertalot H and Moser G (1994) Brachysira. Monographie der Gattung. *Bibliotheca Diatomologica* 29: 1–212.

Lauterbach S, Chapron E, Brauer A et al. (2012) A sedimentary record of Holocene surface runoff events and earthquake activity from Lake Iseo (Southern Alps, Italy). *The Holocene* 22(7): 749–760.

Leroy S, Kazancı N, İleri Ö et al. (2002) Abrupt environmental changes within a late Holocene lacustrine sequence south of the Marmara Sea (Lake Manyas, N-W Turkey): Possible links with seismic events. *Marine Geology* 190(1–2): 531–552.

Levkov Z (2009) *Diatoms of Europe: Amphora sensu lato*, vol. 5. Ruggell: A.R.G. Gantner.

Li M, Kang S, Zhu L et al. (2008) Mineralogy and geochemistry of the Holocene lacustrine sediments in Nam Co, Tibet. *Quaternary International* 187: 105–116.

Long H, Lai Z, Frenzel P et al. (2012) Holocene moist period recorded by the chronostratigraphy of a lake sedimentary sequence from Lake Tangra Yumco on the south Tibetan Plateau. *Quaternary Geochronology* 10: 136–142.

Mackereth FJH (1966) Some chemical observations on post-glacial lake sediments. *Philosophical Transactions of the Royal Society of London, Series B* 250(765): 165–213.

Magny M (2004) Holocene climate variability as reflected by mid-European lake-level fluctuations and its probable impact on prehistoric human settlements. *Quaternary International* 113(1): 65–79.

Maher LJ (1981) Statistics for microfossil concentration measurements employing samples spiked with marker grains. *Review of Palaeobotany and Palynology* 32(2–3): 153–191.

Mangili C, Brauer A, Moscariello A et al. (2005) Microfacies of detrital event layers deposited in Quaternary varved lake sediments of the Pianico-Sellere Basin (northern Italy). *Sedimentology* 52: 927–943.

Mazaud A (2005) User-friendly software for vector analysis of the magnetization of long sediment cores. *Geochemistry, Geophysics, Geosystems* 6(12): 1–5.

Miehe G, Miehe S, Kaiser K et al. (2009) How old is pastoralism in Tibet? An ecological approach to the making of a Tibetan landscape. *Palaeogeography, Palaeoclimatology, Palaeoecology* 276(1–4): 130–147.

Miehe S, Miehe G, Leeuwen JN et al. (2014) Persistence of *Artemisia* steppe in the Tangra Yumco Basin, west-central Tibet, China: Despite or in consequence of Holocene lake-level changes? *Journal of Paleolimnology* 51(2): 267–285.

Mischke S, Bößneck U, Diekmann B et al. (2010) Quantitative relationship between water-depth and sub-fossil ostracod assemblages in Lake Donggi Cona, Qinghai Province, China. *Journal of Paleolimnology* 43(3): 589–608.

Moreno A, Valero-Garcés BL, González-Sampériz P et al. (2008) Flood response to rainfall variability during the last 2000 years inferred from the Taravilla Lake record (Central Iberian Range, Spain). *Journal of Paleolimnology* 40(3): 943–961.

Morrill C, Overpeck JT, Cole JE et al. (2006) Holocene variations in the Asian monsoon inferred from the geochemistry of lake sediments in central Tibet. *Quaternary Research* 65: 232–243.

Moser M and Hohensinn F (1983) Geotechnical aspects of soil slips in Alpine regions. *Engineering Geology* 19(3): 185–211.

Mulder T and Alexander J (2001) The physical character of subaqueous sedimentary density flows and their deposits. *Sedimentology* 48(2): 269–299.

Mulder T and Chapron E (2001) Flood deposits in continental and marine environments: Character and significance. In: Slatt RM and Zavala C (eds) *Sediment Transfer from Shelf to Deep Water: Revisiting the Delivery System* (AAPG Studies in Geology). Tulsa, OK: SEPM, pp. 1–30.

Mulder T, Migeon S, Savoye B et al. (2001) Inversely graded turbidite sequences in the deep Mediterranean: A record of deposits from flood-generated turbidity currents? *Geo-Marine Letters* 21(2): 86–93.

Nesje A, Dahl SO, Matthews JA et al. (2001) A ~4500-yr record of river floods obtained from a sediment core in Lake Atnsjøen, eastern Norway. *Journal of Paleolimnology* 25(3): 329–342.

Niemann H, Haberzettl T and Behling H (2009) Holocene climate variability and vegetation dynamics inferred from the (11700 cal. yr BP) Laguna Rabadilla de Vaca sediment record, southeastern Ecuadorian Andes. *The Holocene* 19(2): 307–316.

Nishimura M, Matsunaka T, Morita Y et al. (2014) Paleoclimatic changes on the southern Tibetan Plateau over the past 19,000 years recorded in Lake Pumoyum Co, and their implications for the southwest monsoon evolution. *Palaeogeography, Palaeoclimatology, Palaeoecology* 396: 75–92.

Osleger DA, Heyvaert AC, Stoner JS et al. (2009) Lacustrine turbidites as indicators of Holocene storminess and climate: Lake Tahoe, California and Nevada. *Journal of Paleolimnology* 42(1): 103–122.

Pavlova I, Jomelli V, Brunstein D et al. (2014) Debris flow activity related to recent climate conditions in the French Alps: A regional investigation. *Geomorphology* 219: 248–259.

Petersen J, Wilhelm B, Revel M et al. (2014) Sediments of Lake Vens (SW European Alps, France) record large-magnitude

earthquake events. *Journal of Paleolimnology* 51(3): 343–355.

Rades EF, Hetzel R, Xu Q et al. (2013) Constraining Holocene lake-level highstands on the Tibetan Plateau by ^{10}Be exposure dating: A case study at Tangra Yumco, southern Tibet. *Quaternary Science Reviews* 82: 68–77.

Reichardt E (1999) *Iconographia Diatomologica: Zur Revision der Gattung Gomphonema*, vol. 8. Ruggell: A.R.G. Gantner.

Reicherter K (2012) Active tectonics in the northern Tangra Yum Co Basin (central Tibet, VR China). *Quaternary International* 279–280: 396–397.

Reimer PJ, Bard E, Bayliss A et al. (2013) IntCal13 and Marine13 radiocarbon age calibration curves 0–50,000 years cal BP. *Radiocarbon* 55(4): 1869–1887.

Sandersen F (1997) The influence of meteorological factors on the initiation of debris flows in Norway. *European Paleoclimate and Man* 12: 321–332.

Scheffler W and Morabito G (2003) Topical observations on centric diatoms (Bacillariophyceae, Centrales) of Lake Como (N. Italy). *Journal of Limnology* 62(1): 47–60.

Schlolaut G, Brauer A, Marshall MH et al. (2014) Event layers in the Japanese Lake Suigetsu 'SG06' sediment core: Description, interpretation and climatic implications. *Quaternary Science Reviews* 83: 157–170.

Schlütz F and Lehmkuhl F (2009) Holocene climatic change and the nomadic Anthropocene in Eastern Tibet: Palynological and geomorphological results from the Nianbaoyeze Mountains. *Quaternary Science Reviews* 28(15–16): 1449–1471.

Schlütz F and Zech W (2004) Palynological investigations on vegetation and climate change in the Late Quaternary of Lake Rukche area, Gorkha Himal, Central Nepal. *Vegetation History and Archaeobotany* 13(2): 81–90.

Schneider H, Höfer D, Irmler R et al. (2010) Correlation between climate, man and debris flow events – A palynological approach. *Geomorphology* 120(1–2): 48–55.

Shen J, Liu X, Wang S et al. (2005) Palaeoclimatic changes in the Qinghai Lake area during the last 18,000 years. *Quaternary International* 136(1): 131–140.

Sletten K, Blikra LH, Ballantyne CK et al. (2003) Holocene debris flows recognized in a lacustrine sedimentary succession: Sedimentology, chronostratigraphy and cause of triggering. *The Holocene* 13(6): 907–920.

St-Onge G and Lajeunesse P (2007) Flood-induced turbidites from northern Hudson Bay and western Hudson Strait: A two-pulse record of lake Agassiz final outburst flood? In: Lykousis V, Sakellariou D and Locat J (eds) *Submarine Mass Movements and Their Consequences*. Dordrecht: Springer, pp. 129–137.

Strasser M, Monecke K, Schnellmann M et al. (2013) Lake sediments as natural seismographs: A compiled record of Late Quaternary earthquakes in Central Switzerland and its implication for Alpine deformation. *Sedimentology* 60(1): 319–341.

Sturm M and Matter A (1978) Turbidites and varves in Lake Brienz (Switzerland): Deposition of clastic detritus by density currents. *Special Publication International Association of Sedimentologists* 2: 147–168.

Van Geel B, Buurman J, Brinkkemper O et al. (2003) Environmental reconstruction of a Roman Period settlement site in Uitgeest (The Netherlands), with special reference to coprophilous fungi. *Journal of Archaeological Science* 30(7): 873–883.

Vasskog K, Nesje A, Støren EN et al. (2011) A Holocene record of snow-avalanche and flood activity reconstructed from a lacustrine sedimentary sequence in Oldevatnet, western Norway. *The Holocene* 21(4): 597–614.

Vos PC and De Wolf H (1993) Diatoms as a tool for reconstructing sedimentary environments in coastal wetlands; methodological aspects. *Hydrobiologica* 269/270: 285–296.

Wang F, Chien N, Zhang Y et al. (1995) *Pollen Flora of China*. Beijing: Science Press.

Wang RL, Scarpitta SC, Zhang SC et al. (2002) Later Pleistocene/Holocene climate conditions of Qinghai–Xizhang Plateau (Tibet) based on carbon and oxygen stable isotopes of Zabuye Lake sediments. *Earth and Planetary Science Letters* 203(1): 461–477.

Wrozyna C, Frenzel P, Xie M et al. (2009) A taxonomical and ecological overview of Recent and Holocene ostracodes of the Nam Co region, southern Tibet. *Quaternary Sciences* 29: 665–677.

Yang Q, Jochum KP, Stoll B et al. (2014) Trace element variability in single ostracod valves as a proxy for hydrochemical change in Nam Co, central Tibet, during the Holocene. *Palaeogeography, Palaeoclimatology, Palaeoecology* 399: 225–235.

Zhao C, Yu Z, Zhao Y et al. (2010) Holocene millennial-scale climate variations documented by multiple lake-level proxies in sediment cores from Hurleg Lake, Northwest China. *Journal of Paleolimnology* 44(4): 995–1008.

Zhao Y, Liu H, Li F et al. (2012) Application and limitations of the Artemisia/Chenopodiaceae pollen ratio in arid and semiarid China. *The Holocene* 22(12): 1385–1392.

CHAPTER 3 — Holocene lake level history of the Tangra Yumco lake system, southern-central Tibetan Plateau

Ahlborn M, T Haberzettl, J Wang, S Fürstenberg, R Mäusbacher, J Mazzocco, J Pierson, L Zhu, and P Frenzel (2015): Holocene lake level history of the Tangra Yumco lake system, southern-central Tibetan Plateau. *The Holocene.*

Licensor: SAGE Publications Ltd
1 Oliver's Yard
55 City Road
London, UK

Research paper

The Holocene
1–12
© The Author(s) 2015
Reprints and permissions:
sagepub.co.uk/journalsPermissions.nav
DOI: 10.1177/0959683615596840
hol.sagepub.com
SAGE

Holocene lake level history of the Tangra Yumco lake system, southern-central Tibetan Plateau

Marieke Ahlborn,[1] Torsten Haberzettl,[1] Junbo Wang,[2] Sascha Fürstenberg,[3] Roland Mäusbacher,[1] Jeaneth Mazzocco,[4] James Pierson,[4] Liping Zhu[2] and Peter Frenzel[3]

Abstract

Massive carbonate banks representing ancient lacustrine deposits are exposed in the catchment of the lake Tangra Yumco (southern-central Tibetan Plateau) and nearby lake Xuru Co. Nine sediment samples were taken below and above these lacustrine deposits to determine periods of changing lake level using optically stimulated luminescence (OSL) applying a multiple-aliquot regeneration (MAR) protocol. According to facies and stratigraphy, samples below the carbonate banks indicate a rising and samples from above a falling lake level. The results indicate that the rising lake level of Tangra Yumco passed the sampling location at 10.5 and 2.1 ka while a falling lake level passed the sampling location at 0.9 ka. The rising lake level of Xuru Co passed the sampling location at 7.9 and 1.7 ka and a falling lake level at 0.5 ka showing a similar trend as at Tangra Yumco. Combining these results with recalculated cosmogenic nuclide ages and previously published feldspar luminescence data allows the establishment of a Holocene lake level reconstruction for Tangra Yumco, which is unique for the southern-central Tibetan Plateau. The lake level of Tangra Yumco crested a lake level highstand of 181–183 m above the recent lake level prior to 8.5 ka and has generally fallen after 8.5 ka, with a minor lake level rise at 2.1 ka. Lake level variations at Tangra Yumco occur simultaneously with other lakes on the Tibetan Plateau indicating that variations were controlled by monsoonal dynamics with a moist early Holocene and a successive reduction of available moisture thereafter. The average rate of the lake level rise between 10.5 and 8.5 ka is at least 0.05 m a^{-1} (compared with a modern value of 0.38 m a^{-1}), providing valuable insights in the monsoonal impact on lake level change on the southern-central Tibetan Plateau.

Keywords

Holocene, lake level changes, lake sediments, luminescence dating, monsoon, Tangra Yumco, Tanqung Co, Tibetan Plateau, Xuru Co

Received 27 March 2015; revised manuscript accepted 7 June 2015

Introduction

On the Tibetan Plateau (Figure 1a), lake level changes are assumed to reflect variations in intensity of the Indian summer monsoon (Dietze et al., 2013). Numerous studies of lacustrine sediments from the Tibetan Plateau assessed significant lake level changes in the late Quaternary that are related to monsoon variability (Dietze et al., 2012; Doberschütz et al., 2014; Kasper et al., 2012; Mischke et al., 2010; Shen et al., 2005; Zhao et al., 2007). Usually, these approaches reconstructed relative lake level changes inferred from climate proxy reconstructions that identify the timing of past moist and arid periods, but the absolute elevation of former lake levels mostly remains unknown. Understanding the pace and scale of lake level changes may provide insights into the magnitude, timing, and environmental impact of monsoonal variability on the Tibetan Plateau.

Absolute lake level changes have been assessed by dating relict beach ridges, lake terraces, and shallow lacustrine sediments from the Tibetan Plateau (Chen et al., 2013; Fan et al., 2010; Lee et al., 2009; Liu et al., 2013, 2015; Long et al., 2012; Rades et al., 2013). These studies use optically stimulated luminescence (OSL), cosmogenic radionuclides, and, more rarely, ^{14}C dating to determine the age of lake level highstands. OSL dating is a particularly suitable technique for constraining the age of sediments that lack organic carbon, exceed the range of ^{14}C dating, or are affected by hard water effects (Berger et al., 2002; Forman et al., 2006; Lee et al., 2009; Li et al., 2002). OSL dating is based on time-dependent dosimetric properties of quartz and feldspar (Aitken, 1998) and provides an estimate of the time since mineral grains, like quartz and K-feldspar, were last exposed to sunlight prior to ultimate burial.

Several studies were recently conducted in the catchment area of Tangra Yumco to investigate environmental changes on the southern-central Tibetan Plateau. Kong et al. (2011) and Rades

[1]Physical Geography, Institute of Geography, Friedrich Schiller University Jena, Germany
[2]Key Laboratory of Tibetan Environment Changes and Land Surface Processes, Institute of Tibetan Plateau Research, Chinese Academy of Sciences, China
[3]Institute of Geosciences, Friedrich Schiller University Jena, Germany
[4]Luminescence Dating Research Laboratory, Department of Earth and Environmental Sciences, University of Illinois at Chicago, USA

Corresponding author:
Marieke Ahlborn, Physical Geography, Institute of Geography, Friedrich Schiller University Jena, Löbdergraben 32, D-07743 Jena, Germany.
Email: mail@mariekeahlborn.de

Downloaded from hol.sagepub.com by guest on September 2, 2015

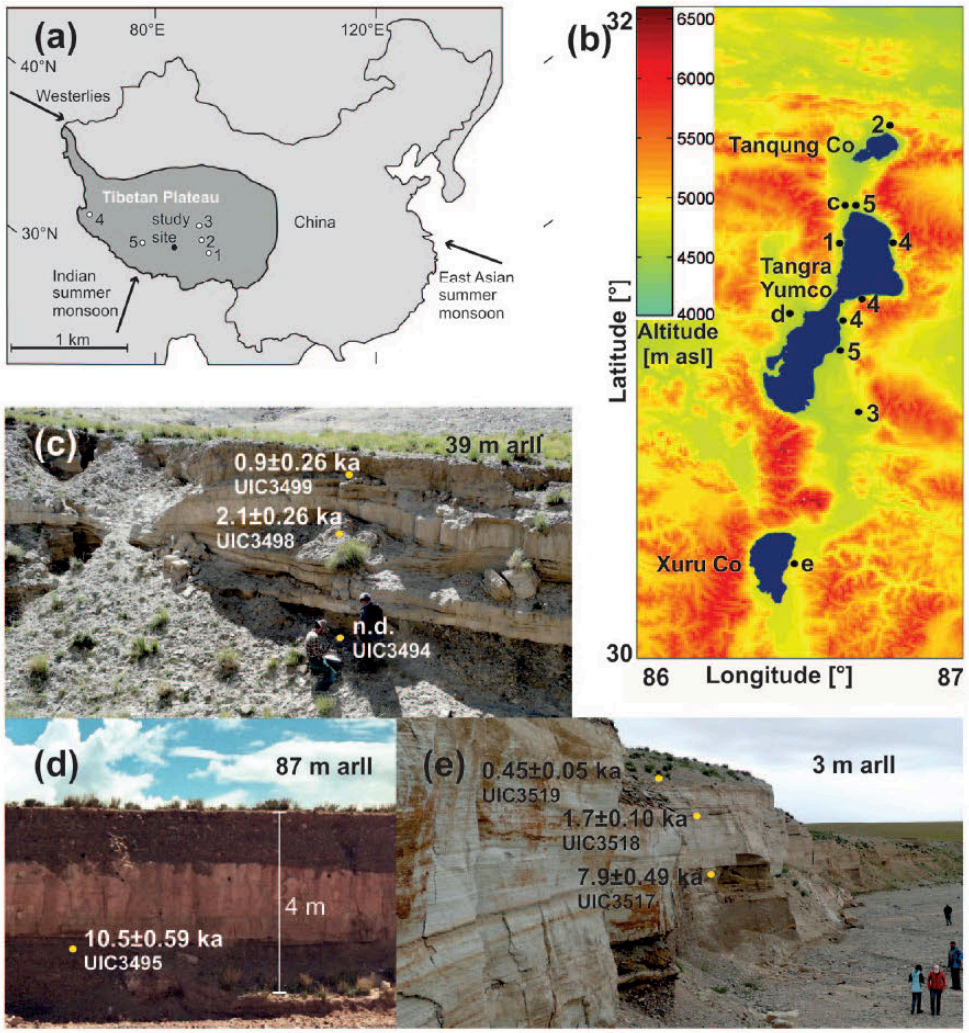

Figure 1. Study site and sample locations. (a) Map showing China (outlined) with the Tibetan Plateau (dark gray). Indicated are the main moisture delivering air currents (arrows), study site Tangra Yumco (black dot), and other archives discussed in the text: 1 – Nam Co (Doberschütz et al., 2014), 2 – Selin Co (Li et al., 2009), 3 – Linggo Co (Pan et al., 2012), 4 – Tso Kar (Demske et al., 2009), 5 – Ngangla Ring Tso (Hudson et al., 2015) and Baqan Tso (Huth et al., 2015). (b) Tangra Yumco (center), Tanqung Co (north), and Xuru Co (south) with recent lake level, study sites (c, d, e), and location of other studies discussed: 1 – Long et al. (2012), 2 – Kong et al. (2011), 3 – Miehe et al. (2014), 4 – Rades et al. (2013), 5 – Rades et al. (2015). (c) Outcrop between Tangra Yumco and Tanqung Co (photo: Steffen Mischke), where samples UIC3494, UIC3498, and UIC3499 were collected, with dating results; no dating results (n.d.) are available for sample UIC3494. (d) Outcrop, where sample UIC3495 was collected, with dating results, 87 m above recent lake level (m arll) of Tangra Yumco. (e) Outcrop near Xuru Co, where samples UIC3517–19 were collected, with dating results, at its base 3 m arll of Xuru Co (photo: Lailah Gifty Akita).

et al. (2013) used cosmogenic radionuclide dating to constrain the age of exposed paleoshorelines at Tangra Yumco and Tanqung Co (Figure 1b). Miehe et al. (2014) investigated a sediment record spanning the past 11 ka from Targo Xian peat bog located on a recessional lake terrace within the Tangra Yumco catchment. Rades et al. (2015) applied feldspar luminescence dating to date exposed paleoshorelines and calculated the pace of the lake level retreat, whereas Long et al. (2012) inferred a moist period by OSL dating of lacustrine sediments. Our study provides new chronologic control on lake level changes by OSL dating of currently exposed lacustrine sediments. For Tangra Yumco and adjacent Xuru Co, we combine these new OSL ages with previously published data, including recalculated cosmogenic nuclide ages (Crétaux et al., 2011; Long et al., 2012; Miehe et al., 2014; Rades et al., 2015), to reconstruct the Holocene lake level history of the Tangra Yumco lake system.

Site description

Tangra Yumco (30°45′–31°22′N, 86°23′–86°49′E; Figure 1) is a terminal lake located at 4545 m a.s.l. (Rades et al., 2013) on the southern-central Tibetan Plateau at the northern slope of the Gangdis Mountains. The lake is part of an active north–south trending graben system (Armijo et al., 1986). Extensive lake level changes are indicated by well-preserved paleoshorelines that extend up to 185 m above recent lake level (arll; Kong et al., 2011; Long et al., 2012; Rades et al., 2013). These landforms reflect the largest lake level changes observed on the Tibetan Plateau (Kong et al., 2011; Rades et al., 2015). Precipitation in this area is dominated by the Indian summer monsoon (Miehe et al., 2014). Weather data extrapolated from the nearest meteorological station indicate a mean annual precipitation of 200–250 mm (Miehe et al., 2014). The mean temperature in January is −11.4°C and in July 10.9°C (Miehe et al., 2014). The surface area of Tangra Yumco is 818 km^2 within a catchment area of 8219 km^2 (Long et al., 2012). The lake has a maximum depth of 230 m (Haberzettl et al., 2015), and a salinity of 8.3‰ (measured in 2009–2012). Two large rivers enter the currently terminal lake from the west and the southeast. Lake level changes are predominantly controlled by precipitation (i.e. monsoon) and temperature, whereas melt water from glaciers only has a minor impact (Rades et al., 2013). Therefore, rising lake levels are considered to

Downloaded from hol.sagepub.com by guest on September 2, 2015

Table 1. OSL samples of exposed lacustrine sediments from the Tangra Yumco catchment.

OSL samples								
Lab ID	Longitude	Latitude	Altitude (m)	Elevation above recent lake level (m)	Burial depth (m)	Depth beneath carbonate layer (m)	Sediment type	Facies
UIC3497	E 86.63032°	N 31.27068°	4585	40	1.2	0.1	Sand	Very shallow lake
UIC3494	E 86.63845°	N 31.37958°	4584	39	3.9	0.5	Fine sand	Fluvio-lacustrine
UIC3498	E 86.63845°	N 31.37958°	4584	39	2.2	0.3	Medium sand	Shallow lake
UIC3499	E 86.63845°	N 31.37958°	4584	39	0.6	+0.42	Medium sand	Shallow fluvio-lacustrine
UIC3495	E 86.47078°	N 31.04124°	4632	87	3.2	0.05	Sand	Shallow lake
UIC3496	E 86.48677°	N 31.09063°	4577	32	11.0	0.2 (intercalated)	Medium sand	Fluvio-lacustrine
UIC3517	E 86.47455°	N 30.29105°	4722	3	5.5	0.05	Fine sand	Fluvio-lacustrine
UIC3518	E 86.47455°	N 30.29105°	4722	3	3.5	Intercalated	Medium sand	Shallow lake, <10 m
UIC3519	E 86.47455°	N 30.29105°	4722	3	3.0	+0.05	Sandy marl	Shallow lake

OSL: optically stimulated luminescence.

represent conditions with higher moisture availability, whereas falling lake levels result from reduced moisture availability. The anthropogenic impact in the Tangra Yumco area is restricted to pasture of domestic cattle and rare irrigated agriculture (Miehe et al., 2014). However, ancient stone tools, buildings and field remnants, and irrigation channels indicate widespread human inhabitance in the past (Miehe et al., 2014).

Xuru Co (30°18′N, 86°25′E), the other investigated lake, is located about 41 km south of Tangra Yumco at an elevation of 4719 m a.s.l. or 174 m arll of Tangra Yumco (Figure 1b). A lake level at 198 m arll of Tangra Yumco (=24 m arll of Xuru Co) would merge Xuru Co and Tangra Yumco. Xuru Co covers an area of 152 km^2, is 211 m deep, and has a salinity of 3.2‰ as measured in 2012. The catchment covers 1913 km^2.

The smaller lake Tanqung Co (31°31′N, 86°41′E) is located at an altitude of 4475 m a.s.l. (Kong et al., 2011) about 18 km north of Tangra Yumco (Figure 1b). Its present day lake level is 70 m below the recent lake level of Tangra Yumco. Lacustrine deposits which are identified up to 4740 m a.s.l. and indicate that Tangqung Co and Tangra Yumco were formerly merged and formed a vast paleolake (Kong et al., 2011; Liu et al., 2013). This lake is at least 5 m deep, occupies an area of 63 km^2, and had a salinity of 100‰ in 2009.

Material and methods

Sedimentary facies and lake level context

Massive carbonate banks are exposed near Tangra Yumco, Tanqung Co, and Xuru Co. These carbonate banks consist of massive micritic calcite identified as lacustrine deposits and reflecting periods of deep water and environmental stability (Long et al., 2012). The underlying clastic sediments were consequently deposited while the lake level was rising, whereas the overlying clastic sediments were deposited while the lake level was falling. Nine sediment samples for OSL dating were collected during 2010, 2011, and 2012 field campaigns below, above, or in between these carbonate banks using opaque tubes to determine the timing of falling and rising lake levels (Table 1). The altitude above sea level was measured with a handheld GPS device (measured error: 6–10 m; Table 1).

The nine samples originate from five different sections near Tangra Yumco, Tanqung Co, and Xuru Co. According to field observations, all samples represent shallow lacustrine facies. Three of the samples, UIC3494, UIC3498, and UIC3499, were collected in a narrow valley connecting the catchments of Tangra Yumco and Tanqung Co (Figure 1c) which exposes a roughly 3-m-thick two-parted carbonate bank. Sample UIC3494 was collected 50 cm below the lower carbonate bank and consists of fine sand to gravel probably representing a fluvio-lacustrine facies prior to the initial lake level rise. Sample UIC3498 was obtained from up to 60-cm-thick cross-bedded sediments with medium sand to gravel intercalating the carbonate bank (Figure 1c). Modern day observations showed that cross-bedded sediment structures are deposited in very close proximity to the lake level. The described facies thus represents a very shallow fluvio-lacustrine environment. Sample UIC3499 is from 42 cm above the carbonate bank and overlies cross-bedded fan-like carbonate sands representing a shallow fluvio-lacustrine facies deposited during a falling lake level (Figure 1c). Sample UIC3495 was collected in a river valley near the western shore of central Tangra Yumco (Figure 1d). It was taken 5 cm below the approximately 1.5-m-thick carbonate bank in layered reddish sands that likely represent a shallow lacustrine facies deposited prior to a rising lake level. Sample UIC3496 was taken from a section in a river valley east of Tangra Yumco between two carbonate banks, 20 cm below the higher carbonate bank, and consists of brownish layered medium sands with fine gravels likely representing a fluvio-lacustrine facies. Sample UIC3497 was taken 10 cm below a 70-cm-thick carbonate bank of yellowish fine to medium grained laminated sands probably indicating a very shallow lake facies prior to a rising lake level. The outcrop is situated in a river valley at the northwestern shore of Tangra Yumco also exposing a section that was previously investigated by Long et al. (2012) but is located further upstream and 30 m higher in altitude (Figure 1b). Samples UIC3517–19 were collected in a wide river valley near the eastern shore of Xuru Co (Figure 1e). UIC3517 was collected 5 cm below the carbonate bank in fluvio-lacustrine layered fine sands with indistinct ripples and fine gravels reflecting a subsequent lake level rise. UIC3518 was obtained from a medium sandy calcareous layer of 4–6 cm thickness containing copious charophyte stems and oospores. The mass occurrence of charophytes indicates that the water depth was probably <10 m. This layer is intercalated in the two-parted carbonate bank reflecting littoral lacustrine conditions of a temporarily lower lake level. Sample UIC3519 was taken immediately above the carbonate bank in sandy marl with many snails representing a shallow and sheltered lake facies deposited while the lake level was falling.

OSL dating

Sample preparation. The sediments were dry sieved to extract the 100- to 150-µm-sized grains and the quartz fraction was

Downloaded from hol.sagepub.com by guest on September 2, 2015

isolated after settling in sodium metatungstate solutions of 2.55 and 2.7 g cc^{-1}. Immersion in 40% hydrofluoric acid for 40 min dissolved any feldspar grains remaining in the extract and etched the alpha-irradiated portion of quartz grains (Mejdahl and Christiansen, 1994). These grains were subsequently treated with 5 mL of 37% hydrochloric acid to remove insoluble precipitates. The purity of the quartz extracts was checked by petrographic inspection. A 2-mm area of quartz was bonded with a silicone adhesive to a set of 10-mm aluminum disks for experimentation. All OSL measurements were performed using an automated Risø TL/OSL-DA-20 reader stimulating the samples with blue light (470 ± 20 nm).

Prior to experimentation, grains extracted from each prepared sample were checked for possible feldspathic contamination using infrared stimulation. Although no feldspar grains were observed during the petrographic inspection, the infrared stimulation produced a significant luminescence emission emanating from samples UIC3494, UIC3496, and UIC3497. These emissions may result from feldspathic inclusions within the quartz grains. As a prior infrared stimulation could not sufficiently remove this contaminating signal, samples UIC3494, UIC3496, and UIC3497 were rejected from further analyses (Table 2).

D_e determination. Both the single-aliquot regeneration (SAR) protocol (Wintle and Murray, 2000) and the multiple-aliquot regeneration (MAR) protocol (Jain et al., 2003; Waters et al., 2011) were applied to quartz grain separates for equivalent dose (D_e) determination. In SAR, 30 disks were exposed to light from blue LEDs for 40 s at 125°C. The OSL signal for D_e estimates was integrated over the first 0.8 s of 40-s stimulation, with background from emissions of the last 10 s. A test dose of 6.26 Gy was applied. In turn, aliquots were rejected, if (1) the zero dose exceeded 5% of the natural dose, (2) the recycling ratio was beyond 1.0 ± 0.1, or (3) the error in determination of D_e exceeded 10%.

All samples were subjected to a preheat dose recovery test, to determine if the samples sufficiently recovered a given laboratory dose using the SAR protocol. The preheat was in 20°C increments at 180–220°C with a cut heat of 160°C for samples UIC3498, UIC3499, UIC3517, and UIC3519. Sample UIC3518 was preheated to 180–280°C to test if a dose can be recovered at higher temperatures. A preheat dose recovery test for sample UIC3495 was performed at 180–260°C and with a cut heat of 220 and 160°C. Samples UIC3498, UIC3499, UIC3517, UIC3518, and UIC3519 did not recover the given laboratory dose in any of the preheat dose recovery tests, invalidating the use of that SAR protocol to date those samples. As a result, these samples were dated using the MAR protocol. In contrast, sample UIC3495 sufficiently recovered the given laboratory dose when preheated to 220°C (Figure 4a) and was then dated using the SAR protocol. This sample was also dated using the MAR protocol as an internal check for D_e consistency.

In the MAR protocol, two sets of aliquots were prepared for D_e determination. The first set of 8 aliquots was used to define the natural luminescence emission. The second set of 20 aliquots was used to measure the regenerative luminescence emission and was treated with different regenerative doses to evaluate the growth reconstruction. The highest regenerative dose of up to 62 or 120 Gy exceeded the corresponding natural luminescence. Prior to adding a regenerative dose, the natural luminescence emission was reset with an 8-h exposure to a 275-W GE Mercury Vapor Sunlamp. D_e estimation by the MAR protocol integrates over 100 s of stimulation. Background values are based on dark counts of the Risø reader. A preheat treatment of 150°C (140°C for UIC3495) was applied after the laboratory irradiation for 1 h to remove the thermally unstable signal (Forman et al., 2014; Kang et al., 2012). The data are collected at an elevated temperature of 125°C during excitation by blue diodes at 10% power (Wintle and Murray, 2000). The efficaciousness of the preheat treatment used for the test dose was checked by comparing the reconstruction shape between the natural and the test dose (Bailey, 2003; Tripaldi and Forman, 2007). A preheat of 150°C for 1 h (140°C for UIC3495) produced a luminescence distribution most similar to the natural emissions.

The validity of the preheat choice and the existence of a residual component of sample UIC3495 was tested as a residual component could invalidate SAR. A linear modulation OSL (LM-OSL; UIC3495) which ramps the power of the diodes from 0% to 100% in order to separate the so called fast, medium, and slow components (Bulur et al., 2000) was performed to evaluate the varying sensitivity of the resolved components to heat and to light. All measurements were performed at an elevated temperature of 125°C with a test dose of 6.23 Gy. This procedure was applied to sediments that were light reset respective to the SAR and MAR protocols. To detect residual charge, the natural luminescence emission of all samples was compared with a fully reset laboratory-generated analog that was preheated and not preheated, respectively (1 h at 150°C; 140°C for UIC3495). These analogs were created by removing the remaining charge in the traps by an 8-h exposure to a sunlamp after the measurement of the natural luminescence emission and a subsequent charging with a test dose of 62 Gy.

Potential residual charge due to incomplete bleaching of the sediments was removed mathematically from the natural luminescence emission to produce a reassessed D_e. As it is the case with the other MAR data, the naturals were scaled using the component-specific dose normalization technique (Jain et al., 2003). Since the test dose data produced by the MAR protocol were generated from a fully reset analog and were therefore free of residual charge, any excess charge, potentially due to incomplete bleaching of the sediments, could be removed mathematically from the natural luminescence emission by comparing the scaled MAR results with the inverted test dose, both indexed by stimulation time. Subtracting the resultant charge from the natural luminescence emission yielded a modified natural luminescence emission potentially free of residual charge and a flattened natural L_x/T_x with a reassessed D_e. The L_x/T_x ratio is the standardized luminescence response to an absorbed dose.

Dose rate determination. Elemental concentrations of U, Th, and K were measured by inductively coupled plasma mass spectrometry (ICP-MS). The water content was estimated based on experience values using grain size and approximate estimated pore volume as the mass percentage averaged over the burial period. The dose rate was adjusted to compensate for the mass attenuation of the grains (Fain et al., 1999). The cosmic ray component was calculated after Prescott and Hutton (1994) by factoring in the overlying water column during burial time.

Cosmogenic nuclide dating

An updated ^{10}Be calibration data set (Heyman, 2014) enables the recalculation of previously reported cosmogenic nuclide dating results of Rades et al. (2015) from Tangra Yumco and Kong et al. (2011) from Tanqung Co. A modified version of the CRONUS-Earth online code (Balco et al., 2008), the updated ^{10}Be calibration data set (Heyman, 2014), and cosmogenic nuclide dating results (Kong et al., 2011; Rades et al., 2013) were used for the recalculation of the Holocene ages.

Lake level reconstruction and hydrological balance

OSL ages and recalculated cosmogenic nuclide ages of this study were combined with feldspar luminescence data (Rades et al.,

Downloaded from hol.sagepub.com by guest on September 2, 2015

Table 2. Optical ages on quartz fraction of exposed lacustrine sediments from the Tangra Yumco catchment.

OSL ages

Lab ID	IR signal	Protocol applied	D_e [Gy]	U [ppm][b]	Th [ppm][b]	K [%][b]	Cosmic dose rate [Gy/ka][c]	Water content [%]	Dose rate [Gy ka^{-1}]	SAR age [a]	MAR age [a]	remarks
UIC3497	yes	—	—	—	—	—	—	—	—	—	—	rejected due to IR signal
UIC3494	yes	—	—	—	—	—	—	—	—	—	—	rejected due to IR signal
UIC3498	no	MAR[d]	9.50 ± 1.02	5.9 ± 0.1	11.0 ± 0.1	2.22 ± 0.02	0.304 ± 0.030	5 ± 2	4.4623	—	2,130 ± 260	residual charge
UIC3499	no	MAR[d]	4.30 ± 0.11	6.7 ± 0.1	11.9 ± 0.1	2.52 ± 0.03	0.395 ± 0.040	15 ± 5	4.5548	—	940 ± 70	residual charge
UIC3495	no	SAR[a] / MAR[d]	21.10 ± 1.21 (SAR) / 44.079 ± 0.222 (MAR)	2.7 ± 0.1	15.5 ± 0.1	2.50 ± 0.03	0.186 ± 0.023	5 ± 2	4.1874	5,039 ± 390	10,530 ± 590	residual charge
UIC3496	yes	—	—	—	—	—	—	—	—	—	—	rejected due to IR signal
UIC3517	no	MAR[d]	37.55 ± 0.172	3.3 ± 0.1	15.6 ± 0.1	3.29 ± 0.03	0.181 ± 0.019	10 ± 3	4.7728	—	7,870 ± 490	residual charge
UIC3518	no	MAR[d]	5.748 ± 0.148	4.0 ± 0.1	12.9 ± 0.1	1.74 ± 0.02	0.198 ± 0.019	10 ± 3	3.4302	—	1,680 ± 110	residual charge
UIC3519	no	MAR[d]	2.24 ± 0.19	5.5 ± 0.1	18.9 ± 0.1	2.47 ± 0.02	0.338 ± 0.034	10 ± 3	4.9216	—	460 ± 50	residual charge

[a]SAR single-aliquot regeneration protocols according to Wintle and Murray (2000)
[b]U, Th, and K_2O determined by ICP-MS at Activation Laboratory Inc. Ontario, Canada
[c]Prescott and Hutton (1994)
[d]MAR multi-aliquot regeneration protocols according to Waters et al. (2011)

Downloaded from hol.sagepub.com by guest on September 2, 2015

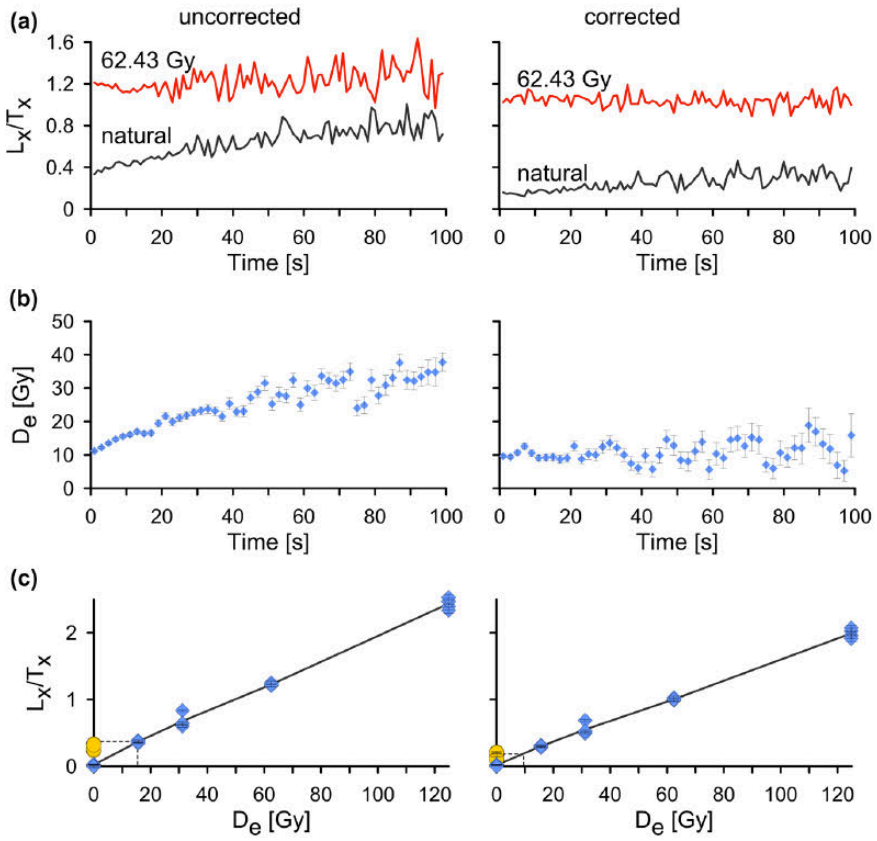

Figure 2. MAR data for sample UIC3498. Uncorrected data (left) and dose sensitivity and residual charge corrected data (right). (a) Normalized shine down curve for test dose of 62.43 Gy ≙ 600 s β-irradiation (red) and natural data (black). Uncorrected data (left) show a rise with increasing time representing the excess value which is equal to the residual signal. (b) D_e plateau with every second data point plotted. Uncorrected data (left) show residual signal. Corrected data (right) are markedly flattened. (c) Growth curve of data point 1 with uncorrected (left) and corrected (right) D_e.

2015), and lake surface monitoring by satellite altimetry data (Crétaux et al., 2011) to establish a Holocene lake level reconstruction for Tangra Yumco. All ages were plotted on the altitude above sea level (m a.s.l.). According to satellite altimetry data, the recent lake level is at 4536 m a.s.l. (in 2014; Crétaux et al., 2011) which is 9 m below the recent lake level of 4545 m a.s.l. (in 2011 and 2012; Rades et al., 2013) used in this study. Comparison of lake level computed from satellite altimetry data and measured by in situ gauges reveals an error of 3–80 cm (Crétaux et al., 2011). To ensure comparability, lake level information of Crétaux et al. (2011) was adjusted to 4545 m a.s.l. Lake level modeling was done using MATLAB and SRTM data with 90-m resolution (Jarvis et al., 2008). The lake area at each altitude and corresponding water volume was calculated based on the model. The size of the catchment when Tanqung Co and Tangra Yumco were merged was estimated based on Google™ Earth. We finally calculated the average rate of the lake level changes by using the duration and the height of the lake level change.

Dating results and discussion

OSL ages

The MAR results of all but one sample show a significant increase in the natural L_x/T_x ratios and resultant D_e values with stimulation time (Figure 2a and b) implying that quartz grains may contain some measurable residual charge and suffer from partially solar resetting. In the case of UIC3495, the amount of residual charge may be small and is indistinguishable from background counts. LM-OSL emissions for the natural luminescence emissions show an elevated slow component compared with fully light reset laboratory analogs (Figure 3a). The elevated slow component of the natural luminescence emissions indicates that the quartz grains contain a residual charge in the slow component that was not fully solar reset prior to deposition. This laboratory bleached level is the basis of a correction that identifies potential inherited charge particularly for medium and slow components. Applying this correction results in a decrease in dispersion of the natural L_x/T_x and a plateau in D_e values (Figure 2a and b) and thus we believe yields credible age estimates.

SAR and MAR results of UIC3495 are not consistent (Table 2). A D_e of 21.09 ± 1.21 Gy and a corresponding age of 5.0 ± 0.4 ka were calculated with the SAR protocol (Figure 4b–d) and a D_e of 44.08 ± 0.22 Gy with a corresponding age of 10.5 ± 0.6 ka with the MAR protocol (Table 2). The LM-OSL experiment, demonstrating the effect of the SAR and MAR bleaching treatments on the post-natural SAR test dose charge distribution of UIC3495, shows that all the components are diminished as a result of receiving the MAR bleach treatment (Figure 3b) but are not diminished when receiving the SAR bleach treatment. The inconsistency between the SAR and MAR results for UIC3495 is apparently attributable to procedural differences with the bleach treatment (Figure 3b). Since the MAR bleach treatment is a solar analog, it may be more suitable for bleaching this sample. Consequently, the D_e of 44.08 ± 0.22 Gy and the age of 10.5 ± 0.6 ka obtained with the MAR protocol are considered as more reliable and used for the lake level reconstruction.

Results based on the MAR protocol (Table 2 and Figure 5b) indicate that the rising lake level of Tangra Yumco passed the altitude of the sampling location at 10.5 ± 0.6 ka (UIC3495) and 2.1 ± 0.3 ka (UIC3498). A falling lake level passed the sampling location at 0.9 ± 0.1 ka (UIC3499). Likewise, the rising lake level of Xuru Co passed the altitude of the sampling location at 7.9 ± 0.5 ka (UIC3517) and 1.7 ± 0.1 ka (UIC3518), while a falling lake level passed the sampling location at 0.5 ± 0.1 ka (UIC3519).

Downloaded from hol.sagepub.com by guest on September 2, 2015

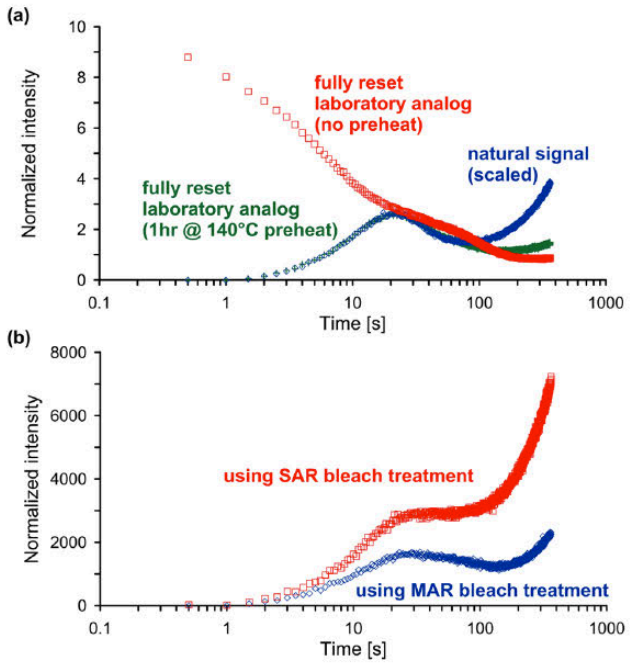

Figure 3. Results of internal checks, linear modulation OSL (LM-OSL) data. (a) LM-OSL data showing the distribution of charge among the fast, medium, and slow component. Natural luminescence emissions (blue diamonds), presented with its fully reset laboratory-generated analog, with (green pluses) and without (red boxes) preheat treatment, for comparison. Excess charge in the slow component of the natural luminescence emission (blue diamonds) compared with the fully reset laboratory analog (green pluses, red boxes) indicates residual charge and partially optical bleaching prior to burial. (b) LM-OSL data showing the effect of the SAR (red boxes) and MAR (blue diamonds) bleaching treatments on the post-natural SAR test dose charge distribution. All components are diminished as a result of receiving the MAR bleach treatment, suggesting that the lower natural L_x/T_x ratio observed in the SAR naturals is apparently attributable to procedural differences with the bleach treatment. As the choice of bleach treatment does not alter the results of the subsequent dose cycles, it provides an explanation for the observed difference in the SAR and MAR results. As the MAR bleach treatment is a solar analog, this suggests that the MAR bleach treatment is more suitable for bleaching this sample.

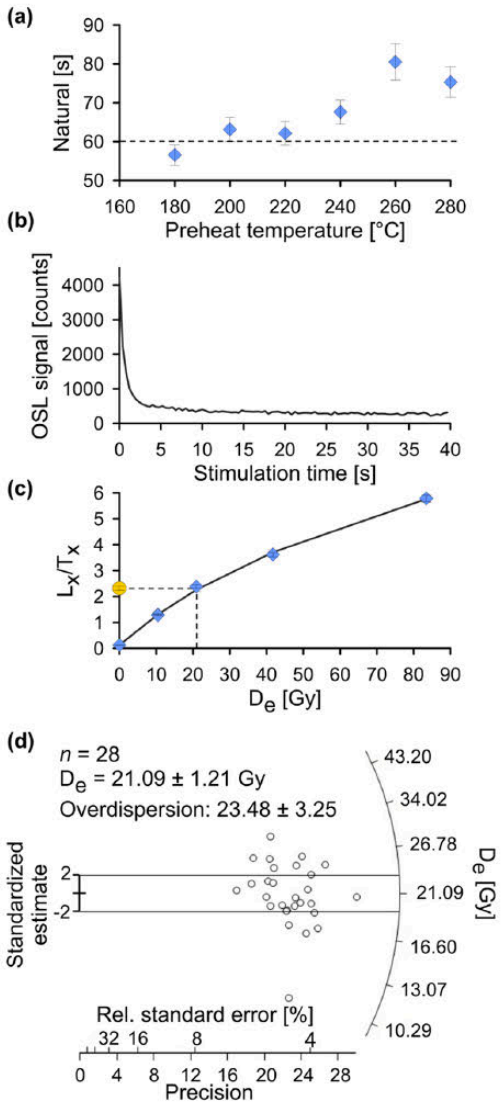

Figure 4. SAR data for sample UIC3495. (a) Results of preheat dose recovery test. The given laboratory dose (dashed line) is most sufficiently recovered using a preheat of 220°C. (b) Typical shine down curve showing a fast decay of the most light sensitive component. (c) Growth curve of data point 3 with $D_e = 21.09 \pm 1.21$ Gy. The reported D_e and its error matches the mean value of all 28 data points precisely. (d) Radial plot based on 28 aliquots (n). A total of 15 of the 28 data points depicted fall within the 2σ-region. The mean value of all 28 data points is $D_e = 21.09 \pm 1.21$ Gy as also reconstructed by the growth curve.

Cosmogenic nuclide ages

Use of the updated ^{10}Be calibration data set values (Heyman, 2014) has increased the ages reported in Rades et al. (2013) by 0.4–0.9 ka and in Kong et al. (2011) by 0.6–0.7 ka. According to the recalculated data of Kong et al. (2011), the lake level of Tanqung Co was at an altitude of 235 m arll (165 m arll of Tangra Yumco) at 9.4 ± 0.6 ka and at 1 m arll (69 m below the recent lake level of Tangra Yumco) at 3.7 ± 0.4 ka (Figure 5b and Table 3). Recalculation of the ages reported in Rades et al. (2013) indicates that the lake level reached an altitude of 181–183 m arll at 8.8–8.2 ± 0.5 ka and was at 140–145 m arll at 5.0–4.5 ± 0.3 ka. All ages are given with a 1σ error in Table 3 and were used hereafter with their mean values of 8.5 ± 0.5 and 4.8 ± 0.3 ka.

Discussion of environmental implications

Lake level reconstruction

A comparison of the OSL ages and the recalculated cosmogenic nuclide ages of this study with previously published feldspar luminescence ages of paleoshorelines (Rades et al., 2015) and satellite altimetry data of Crétaux et al. (2011) allows the establishment of a Holocene lake level reconstruction for Tangra Yumco (Figure 5b). A rising lake level was recorded at 10.5 ka (Figure 5b), and the lake level reached a highstand of 181–183 m arll prior to 8.5 ka (Rades et al., 2013). Since cosmogenic nuclide ages determine the time when the lake level retreated from the sampled material, the exact timing when the lake level reached 181–183 m arll remains unknown and cannot be resolved by our data. The progression of the lake level after 8.5 ka is not well defined because of a lack of concordance between recalculated cosmogenic nuclide and feldspar luminescence ages (Figure 5b). Recalculated cosmogenic nuclide ages imply that the lake level was at the altitude of 140–145 m arll at 4.8 ka, whereas feldspar luminescence data indicate a lake level at 137–142 m arll at 6.8–6.3 ka revealing a significant offset (Rades et al., 2015). Consequently, the lake level decline between 8.5 and 4.0 ka is roughly estimated (Figure 5b, dashed line). The pace of the lake level fall appears to decline between 4.0 and 2.8 ka, with a water level at 78 m arll at 2.8 ka (Rades et al., 2015). A significant lake level decline from 78 to 39 m arll (Rades et al., 2015) occurred after 2.8 ka (Figure 5b). A short-term lake level rise started prior to 2.1 ka and culminated in

Downloaded from hol.sagepub.com by guest on September 2, 2015

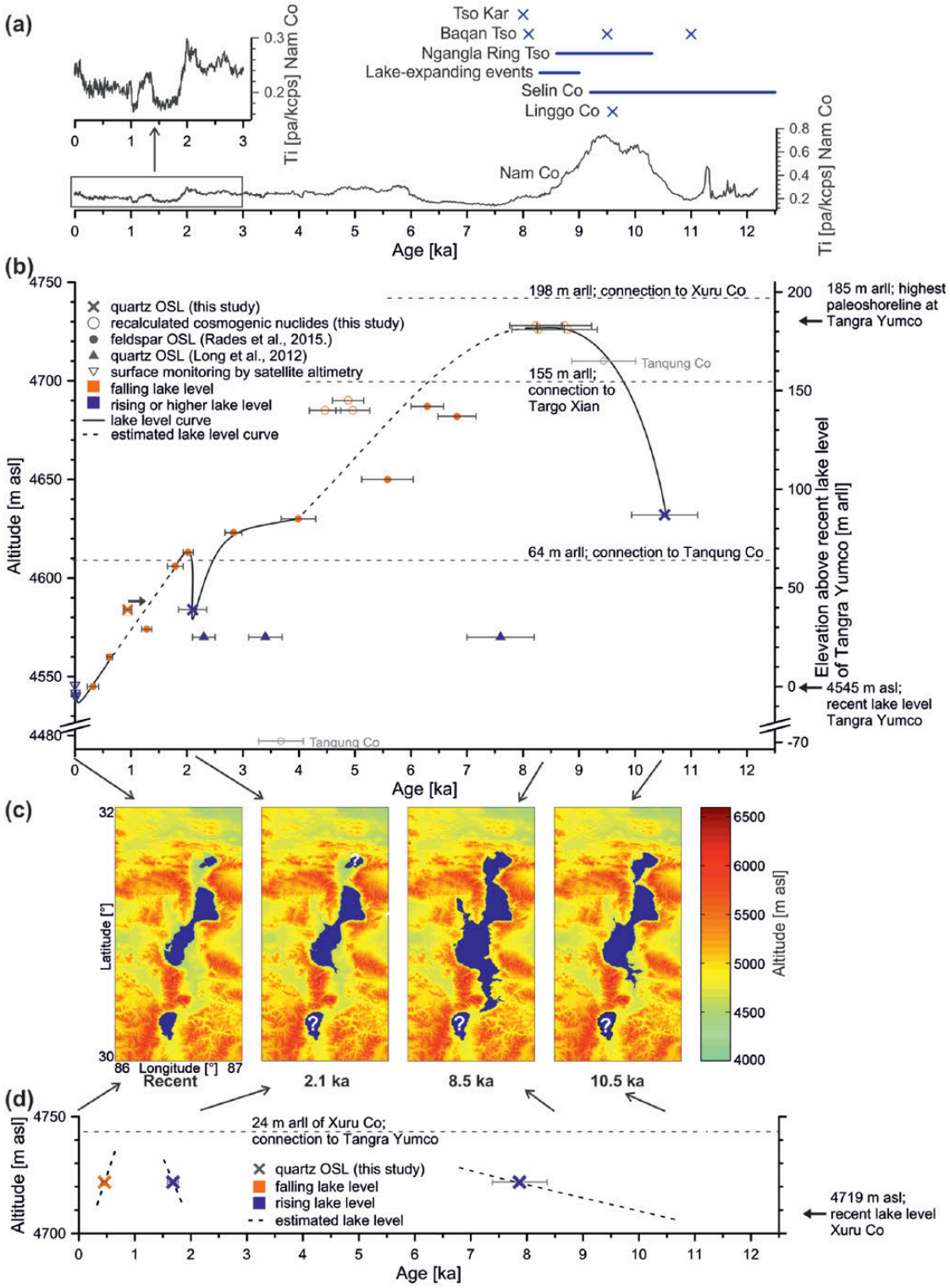

Figure 5. Lake level reconstructions, lake areas of Xuru Co, Tangra Yumco, and Tanqung Co, and comparison with other records. (a) Lake level highstands of Tso Kar (Demske et al., 2009), Baqan Tso (Huth et al., 2015), Ngangla Ring Tso (Hudson et al., 2015), Selin Co (Li et al., 2009), Linggo Co (Pan et al., 2012), and lake-expanding events on the southern and central Tibetan Plateau (Jia et al., 2001; blue crosses and lines). Ti of lake Nam Co indicates monsoonal precipitation showing moistest conditions and a lake level highstand at 9.5 cal. ka BP (Doberschütz et al., 2014). Detailed view of the past 3 ka (please note different scaling) showing a short-term wet spell at Nam Co at 1.5–1.3 cal. ka BP possibly corresponding to the lake level rise at 2.1 ka at Tangra Yumco. (b) Holocene lake level reconstruction of Tangra Yumco based on quartz OSL ages (this study), recalculated cosmogenic nuclide ages (this study; ages from Tanqung Co are labeled and gray because of possible inconsistencies with our reconstruction), feldspar luminescence data of beach ridges (Rades et al., 2015), and lake surface monitoring by satellite altimetry (Crétaux et al., 2011) compared with quartz OSL data (Long et al., 2012). Lake level is estimated between 8.5–4.0 and 1.8–0.6 ka (dashed line); the lake level decline might have been earlier than 0.9 ka because the sample was not taken directly above the lacustrine deposits (arrow). (c) Lake areas of Xuru Co, Tangra Yumco, and Tanqung Co at recent times, 2.1, 8.5, and 10.5 ka based on a digital elevation model from SRTM data covering 30°N–32°N and 86°E–87°E (Jarvis et al., 2008). Unknown lake level altitude at given time indicated with question mark. (d) Estimated lake level reconstruction (dashed line) of Xuru Co based on quartz OSL ages (this study). Both lake level reconstructions from Xuru Co and Tangra Yumco show a similar behavior with a lake level rise in the early and late Holocene.

Downloaded from hol.sagepub.com by guest on September 2, 2015

Table 3. Recalculated cosmogenic nuclide ages.

Cosmogenic nuclide ages										
Longitude E (°)	Latitude N (°)	Altitude (m)	Elevation above recent lake level of Tangra Yumco (m)	Sample thickness (cm)	Topographic shielding	^{10}Be concentration (10^3 atoms g^{-1})	Age (ka)	**Age (ka) *this study***	Internal 1σ error (ka) *this study*	External 1σ error (ka) *this study*
86.3601[a]	31.0478[a]	4726[a]	181[a]	1[a]	0.999[a]	566 ± 19[a]	7.87[ab]	**8.8[b]**	0.30[b]	0.54[b]
86.6263[a]	31.0437[a]	4685[a]	140[a]	1[a]	0.999[a]	269 ± 10[a]	4.04[ab]	**4.5[b]**	0.16[b]	0.28[b]
86.6698[a]	31.0975[a]	4728[a]	183[a]	3[a]	0.990[a]	550 ± 13[a]	7.82[ab]	**8.7[b]**	0.21[b]	0.49[b]
86.6698[a]	31.0975[a]	4728[a]	183[a]	5[a]	0.990[a]	511 ± 13[a]	7.39[ab]	**8.2[b]**	0.22[b]	0.47[b]
86.7863[a]	31.2563[a]	4690[a]	135[a]	3[a]	0.990[a]	294.3 ± 7.7[a]	4.42[ab]	**4.9[b]**	0.13[b]	0.28[b]
86.7863[a]	31.2609[a]	4726[a]	181[a]	4[a]	0.995[a]	525 ± 13[a]	7.44[ab]	**8.3[b]**	0.21[b]	0.47[b]
86.7858[a]	31.2564[a]	4685[a]	140[a]	4[a]	0.922[a]	295 ± 10[a]	4.50[ab]	**5.0[b]**	0.17[b]	0.30[b]
86.6500[c]	31.4167[c]	4476[c]	−69[c]	3.32[c]	1[c]	210 ± 20[c]	2.8[cd]	**3.7[d]**	0.34[d]	0.40[d]
86.7833[c]	31.6167[c]	4710[c]	165[c]	3.32[c]	1[c]	640 ± 20[c]	7.4[cd]	**9.4[d]**	0.31[d]	0.57[d]

[a]Rades et al. (2013).

[b]Time-dependent production rate scaling model of Lal (1991)/Stone (2000); zero erosion; rock density: 2.65 g cm^{-3}; standards KNI-6-2 with ^{10}Be/^{9}Be ratio of 5.349×10^{-13} and KNI-5-3 with ^{10}Be/^{9}Be ratio of 6.320×10^{-13} (Nishiizumi et al., 2007).

[c]Kong et al. (2011).

[d]Scaling method of Stone (2000); production rate of 5.1 atoms g^{-1} a^{-1}; erosion rate: 0.00015 cm a^{-1}; rock density: 2.65 g cm^{-3}; NIST standard SRM-4325 with ^{10}Be/^{9}Be ratio of 3.00×10^{-11}.

Figures in bold show the recalculated data from this study.

a less pronounced lake level highstand at 2.0 ka (Figure 5b). According to a quartz OSL age, the end of the lacustrine deposition at 39 m arll of Tangra Yumco with a falling lake level is indicated at 0.9 ka. Samples dated to 2.1 and 0.9 ka were obtained from a section with two carbonate banks that are intercalated by cross-bedded sediments (Figure 1c). Since the upper bank represents the less pronounced lake level rise (2.1–0.9 ka), the lower bank likely represents the preceding phase of higher lake level (10.5–2.8 ka). However, the falling lake level dated by quartz OSL to 0.9 ka is not consistent with a feldspar luminescence age of 1.3 ka (29 m arll) of Rades et al. (2015). Sediment samples dated to 2.1 and 0.9 ka were taken 0.30 m below and 0.42 m above the carbonate bank (Figure 1c) implying that the lake level fall or rise might not be exactly defined. Cross-bedded sediments of both sampling sites suggest the deposition of fan-like sediments with a high sedimentation rate. Therefore, the time elapsed between the deposition of the sampled sediments and onset or end of lacustrine deposition is probably short, but the end of the lacustrine deposition might have occurred a little earlier than 0.9 ka since the sample was taken 0.42 m above the carbonate bank. The difference in altitude of the ages at 1.3 ka (29 m arll) and 0.9 ka (39 m arll) might be caused by the significant vertical error of the GPS. Therefore, the lake level is estimated around 1.3 ka (Rades et al., 2015). Probably, the lake level continued falling as indicated by an ongoing survey of lake surface monitoring by satellite altimetry (Crétaux et al., 2011) that revealed a rising lake level at Tangra Yumco since AD 1997 (Figure 5b). Since AD 1997, the lake level has risen approximately 6 m at an average rate of 0.38 m a^{-1} (Crétaux et al., 2011).

At Xuru Co, the rising lake level passed the sampling location at 7.9 ka coinciding with the lake level highstand at Tangra Yumco at 8.5 ka as both ages overlap in the 1σ error and are statistically similar. Since the lake level highstand at Xuru Co is not recorded by any data, it probably occurred shortly after 7.9 ka. In the late Holocene, ages at 2.1 ka at Tangra Yumco and 1.7 ka at Xuru Co that mark a rising lake level are within the 2σ dating error so we assume that the lake level rose simultaneously. Although the morphology of the Xuru Co catchment is less steep probably producing a much slower lake level rise than the Tangra Yumco catchment, the similar lake level evolution indicates that lake levels of both lakes are controlled by the same supra-regional process and probably monsoonal variations.

There are no indications that the lake level of Tangra Yumco exceeded the highest well-preserved paleoshoreline of 185 m arll (Rades et al., 2013) and established a connection to Xuru Co (198 m arll) at least during the Holocene. Poorly preserved paleoshorelines with altitudes of >260 m arll were dated by Kong et al. (2011). Although ages reveal internal inconsistencies, ages of >120 ka suggest that a connection with Xuru Co may have occurred pre-Holocene. There is, however, the possibility that Xuru Co, in turn, drained into Tangra Yumco during a potential lake level highstand of 24 m arll and thus contributed to the hydrological budget of Tangra Yumco during the early Holocene. This scenario is indicated by an overflow channel coming from Xuru Co visible on Google™ Earth satellite imagery. The Targo Xian peat bog, located on a recessional lake terrace within the Tangra Yumco catchment, was integrated into Tangra Yumco between 9.5 and 7.0 ka. Tanqung Co was part of Tangra Yumco forming a paleolake system from the early Holocene until approximately 2.5 ka and briefly during the minor lake level highstand at 2.0 ka (Figure 5b and c). Thus, Tanqung Co cannot be considered as individual lake system until 2.5 ka, and recalculated cosmogenic nuclide ages of 9.4 and 3.7 ka are not consistent with our lake level reconstruction. The age of 9.4 ka at Tanqung Co indicates that its lake level had an altitude close to the lake level highstand of Tangra Yumco, but as it represents a falling lake level, it is not consistent with our reconstruction. The age of 3.7 ka defines a lake level 69 m below the recent lake level of Tangra Yumco which is in contradiction with our lake level reconstruction because both lakes were merged until 2.5 ka and the Tangra Yumco paleolake was at 82 m arll. However, if the catchments of Tangra Yumco and Tanqung Co would have been disconnected earlier than 2.5 ka, a much lower lake level of Tanqung Co could have been likely. The catchments of Tangra Yumco and Tanqung Co are separated by a swell that is incised by a deep and narrow valley setting the recent overflow threshold to 64 m arll. If the overflow threshold of Tangra Yumco would have been about 20 m higher because of sediment infill of the valley, Tangra Yumco and Tanqung Co would have been disconnected at 3.7 ka. Tangra Yumco would have drained via a river through the valley into Tanqung Co. Because of a much lower catchment-to-lake area ratio of Tanqung Co (3.2) than of Tangra Yumco (6.0), lake levels of Tanqung Co could fall much faster than lake levels of Tangra Yumco and could have been 69 m below the recent lake level of Tangra Yumco at 3.7 ka. Whether this scenario is applicable could only be revealed by an additional shoreline chronology study in the Tanqung Co catchment.

Hydrological balance

The hydrological balance of Tangra Yumco, controlled by precipitation, discharge, and evaporation, is positive in the early

Downloaded from hol.sagepub.com by guest on September 2, 2015

Holocene as indicated by the lake level rise. The lake level of Tangra Yumco rose 94 m between 10.5 ka and, at the latest, 8.5 ka, as the exact timing when the lake level highstand was reached cannot be resolved. Taking into account the time and the difference in altitude, the lake level of Tangra Yumco rose at an average rate of at least 0.05 m a^{-1}. This rate might have been higher, if the lake level reached the highstand significantly earlier than 8.5 ka. The additional water volume necessary to raise the lake level about 94 m amounts up to approximately 162 km^3. For comparison, the lake level rise ongoing since AD 1997 of about 6 m has an average rate of about 0.38 m a^{-1}, while the annual precipitation is about 200–250 mm a^{-1} (Miehe et al., 2014). The lake surface at the lake level highstand is about 2074 km^2 and thus about two and a half times the recent size.

Comparison with other records from the Tangra Yumco catchment

Besides Rades et al. (2013, 2015) and Kong et al. (2011), two other studies were conducted in the Tangra Yumco catchment. A Holocene climate reconstruction based on sedimentology, ostracod analyses, and palynology of a sediment record from Targo Xian (4700 m a.s.l.; 10 km east of Tangra Yumco, part of the Tangra Yumco catchment) indicated a moist early Holocene with a lake level of Tangra Yumco below Targo Xian and dryer conditions commencing roughly around 8 cal. ka BP (Miehe et al., 2014). This agrees perfectly with the lake level reconstruction presented here that shows a rising lake level in the early Holocene and a lake level highstand at 8.5 ka. The lake level reconstruction presented here confirms an incorporation of Targo Xian into Tangra Yumco until 7–6 ka but implies that Targo Xian was disconnected from Tangra Yumco afterwards, although Miehe et al. (2014) initially suggested that Targo Xian was incorporated in Tangra Yumco until 2.6 cal. ka BP. Moister and unstable conditions are indicated at 1.8–1.0 cal. ka BP (Miehe et al., 2014) and coincide roughly with a rising lake level at 2.1 ka. Findings of Miehe et al. (2014) generally correspond with the data presented here and support our lake level reconstruction and its climatic implications.

Long et al. (2012) defined a moist phase between 7.6 and 2.3 ka based on OSL data obtained from deep-lake sediments at about 25 m arll (Figure 5b). The sediments described as deep-lake sediments by Long et al. (2012) are identical to the sediments we broadly described as lacustrine deposits or carbonate bank. Despite some methodical uncertainties discussed by Rades et al. (2013), data of Long et al. (2012) are well in phase with our data. Since samples in the study of Long et al. (2012) were taken from within the lacustrine deposits, the ages of 7.6, 3.4, and 2.3 ka define a phase when the lake level was already significantly higher than the sampling location well corresponding to our reconstructed lake level in this period (Figure 5b). Methodical uncertainties as described by Rades et al. (2013) might result in an underestimation of the ages of Long et al. (2012). Especially the age of 7.6 ka might be considerably underestimated as the sample integrates over a sediment thickness of 10 cm and was recovered 10 cm above the base of the lacustrine deposits. However, the lake level decline shown by our data after 2.8 ka might probably be linked to the end of lacustrine deposition at around 2.3 ka that is indicated by Long et al. (2012).

Comparison with other lake level highstands on the Tibetan Plateau

Lake level highstands comparable (Figure 5a) to the one of Tangra Yumco at 8.5 ka were recorded, for example, at Nam Co (360 km east of Tangra Yumco) at 9.5 cal. ka BP (Doberschütz et al., 2014), at Linggo Co (340 km northeast) at 12.5–9.2 ka (Pan et al., 2012), at Selin Co (180 km northeast) at 9.6 ka (Li et al., 2009), at Ngangla Ring Tso (300 km west) at 10.0–8.6 ka (Hudson et al., 2015), and at Baqan Tso (35 km northwest of Ngangla Ring Tso) at 9.5 and 8.1 ka (Huth et al., 2015). A simultaneous lake level highstand occurred in the Himalayan mountains of northwestern India (Tso Kar) at 8.0 cal. ka BP (Demske et al., 2009; Figure 5a). Jia et al. (2001) defined a Holocene phase of lake-expanding events on the Tibetan Plateau at 9.0–5.0 ka based on a review of previously published studies. On the southern-central Tibetan Plateau, where Tangra Yumco is situated, lake-expanding events took place from 9.0 to 8.3 ka (Jia et al., 2001; Figure 5a). The review of these studies shows that lake levels on the Tibetan Plateau were highest in the early Holocene and almost synchronous with the lake level highstand at Tangra Yumco. The highest lake levels in the early Holocene in parts of the Tibetan Plateau and Himalayan mountains coincide with an increase of monsoonal strength at 10.0–9.0 ka (Overpeck et al., 1996). This implies that lake levels are monsoon controlled and the lake level highstand at Tangra Yumco can thus be ascribed to an increase of monsoonal precipitation in the early Holocene reflecting the monsoonal dominance on the southern-central Tibetan Plateau. However, the lake level rise at 2.1 ka is not recorded in other monsoonal records, but a short-term wet spell occurred at Nam Co at 1.5–1.3 cal. ka BP (Kasper et al., 2012) that probably might correspond to this less pronounced lake level rise at 2.1 ka (Figure 5a and b).

Conclusion

The MAR protocol after Waters et al. (2011) on quartz grains proved to be suitable for age determination on shallow lacustrine sediments from Tangra Yumco. The partial bleaching of the sediment samples can successfully be corrected by a mathematical model. Based on the obtained OSL ages, recalculated cosmogenic nuclide ages, and previously published OSL ages a lake level reconstruction for Tangra Yumco shows that the lake level is rising at least since 10.5 ka culminating in a lake level highstand of 181–183 m arll at 8.5 ka and falling thereafter intercalated by a less pronounced lake level rise at 2.1 ka. Our data demonstrate synchronicity of the lake level variations at Tangra Yumco and Xuru Co, which is also confirmed by the review of other Tibetan studies, indicating monsoonal control of the lake level. However, more data are needed to trace the lake level evolution in the earliest Holocene and especially during the late Pleistocene because only little is known about the lake level variations in these periods. The rate of recent lake level rise has been 0.38 m a^{-1} since AD 1997. This greatly exceeds the long-term average rate of 0.05 m a^{-1} that resulted in the about 94 m of lake level rise between 10.5 and 8.5 ka, suggesting rapid lake level changes in response to monsoon variability are possible for the Tangra Yumco system. This lake level reconstruction and the resultant calculated rate of lake level rise are unique for the southern-central Tibetan Plateau and provide valuable information about the monsoonal impact on lake level variations. Comparable data are desirable for longer time scales and from other sites.

Acknowledgements

Special thanks are given to Steven L Forman for enabling a research visit of M Ahlborn at the Luminescence Dating Research Laboratory of the University of Illinois at Chicago, for the constant support and teaching during the visit and afterwards, and for valuable comments on an earlier version of this manuscript. We further wish to thank two anonymous reviewers for comments helping to improve the manuscript, Whitney DiFoggio for help with sample preparation, Steffen Mischke for help with OSL sampling during the field campaign in 2012 and an outcrop photo, Eike F Rades for comments on an earlier version of this manuscript, Lailah Gifty Akita for providing a photo of the Xuru Co

Downloaded from hol.sagepub.com by guest on September 2, 2015

sampling location, and Jakob Heyman for the kind assistance with cosmogenic nuclide age recalculation.

Funding

The research visit of M Ahlborn at the Luminescence Dating Research Laboratory of the University of Illinois at Chicago was sponsored by the German Academic Exchange Service (DAAD) and the DFG priority program 1372 'TiP: Tibetan Plateau: Formation-Climate-Ecosystems'. This work is part of a Sino-German collaboration funded by DFG priority program 1372 (Grant No. MA1308/23-2) and the National Natural Science Foundation of China (Grant No. 41271225).

References

Aitken MJ (1998) *An Introduction to Optical Dating: The Dating of Quaternary Sediments by the Use of Photon-Stimulated Luminescence*. Oxford: Oxford University Press.

Armijo R, Tapponnier P, Mercier JL et al. (1986) Quaternary extension in southern Tibet: Field observations and tectonic implications. *Journal of Geophysical Research: Solid Earth (1978–2012)* 91: 13803–13872.

Bailey RM (2003) Paper I: The use of measurement-time dependent single-aliquot equivalent-dose estimates from quartz in the identification of incomplete signal resetting. *Radiation Measurements* 37: 673–683.

Balco G, Stone JO, Lifton NA et al. (2008) A complete and easily accessible means of calculating surface exposure ages or erosion rates from ^{10}Be and ^{26}Al measurements. *Quaternary Geochronology* 3: 174–195.

Berger GW, Pillans BJ, Bruce JG et al. (2002) Luminescence chronology of loess-paleosol sequences from southern South Island, New Zealand. *Quaternary Science Reviews* 21: 1899–1913.

Bulur E, Bøtter-Jensen L and Murray AS (2000) Optically stimulated luminescence from quartz measured using the linear modulation technique. *Radiation Measurements* 32: 407–411.

Chen Y, Zong Y, Li B et al. (2013) Shrinking lakes in Tibet linked to the weakening Asian monsoon in the past 8.2 ka. *Quaternary Research* 80: 189–198.

Crétaux J-F, Jelinski W, Calmant S et al. (2011) SOLS: A lake database to monitor in the Near Real Time water level and storage variations from remote sensing data. *Advances in Space Research* 47: 1497–1507.

Demske D, Tarasov PE, Wünnemann B et al. (2009) Late glacial and Holocene vegetation, Indian monsoon and westerly circulation in the Trans-Himalaya recorded in the lacustrine pollen sequence from Tso Kar, Ladakh, NW India. *Palaeogeography, Palaeoclimatology, Palaeoecology* 279: 172–185.

Dietze E, Hartmann K, Diekmann B et al. (2012) An end-member algorithm for deciphering modern detrital processes from lake sediments of Lake Donggi Cona, NE Tibetan Plateau, China. *Sedimentary Geology* 243–244: 169–180.

Dietze E, Wünnemann B, Hartmann K et al. (2013) Early to mid-Holocene lake high-stand sediments at Lake Donggi Cona, northeastern Tibetan Plateau, China. *Quaternary Research* 79: 325–336.

Doberschütz S, Frenzel P, Haberzettl T et al. (2014) Monsoonal forcing of Holocene paleoenvironmental change on the central Tibetan Plateau inferred using a sediment record from Lake Nam Co (Xizang, China). *Journal of Paleolimnology* 51: 253–266.

Fain J, Soumana S, Montret M et al. (1999) Luminescence and ESR dating Beta-dose attenuation for various grain shapes calculated by a Monte-Carlo method. *Quaternary Science Reviews* 18: 231–234.

Fan Q, Lai Z, Long H et al. (2010) OSL chronology for lacustrine sediments recording high stands of Gahai Lake in Qaidam Basin, northeastern Qinghai–Tibetan Plateau. *Quaternary Geochronology* 5: 223–227.

Forman SL, Wright DK and Bloszies C (2014) Variations in water level for Lake Turkana in the past 8500 years near Mt. Porr, Kenya and the transition from the African Humid Period to Holocene aridity. *Quaternary Science Reviews* 97: 84–101.

Forman SL, Spaeth M, Marín L et al. (2006) Episodic Late Holocene dune movements on the sand-sheet area, Great Sand Dunes National Park and Preserve, San Luis Valley, Colorado, USA. *Quaternary Research* 66: 97–108.

Haberzettl T, Henkel K, Kasper T et al. (2015) Independently dated paleomagnetic secular variation records from the Tibetan Plateau. *Earth and Planetary Science Letters* 416: 98–108.

Heyman J (2014) Paleoglaciation of the Tibetan Plateau and surrounding mountains based on exposure ages and ELA depression estimates. *Quaternary Science Reviews* 91: 30–41.

Hudson AM, Quade J, Huth TE et al. (2015) Lake level reconstruction for 12.8–2.3 ka of the Ngangla Ring Tso closed-basin lake system, southwest Tibetan Plateau. *Quaternary Research* 83: 66–79.

Huth T, Hudson AM, Quade J et al. (2015) Constraints on paleoclimate from 11.5 to 5.0 ka from shoreline dating and hydrologic budget modeling of Baqan Tso, southwestern Tibetan Plateau. *Quaternary Research* 83: 80–93.

Jain M, Bøtter-Jensen L and Singhvi AK (2003) Dose evaluation using multiple-aliquot quartz OSL: Test of methods and a new protocol for improved accuracy and precision. *Radiation Measurements* 37: 67–80.

Jarvis A, Reuter HI, Nelson A et al. (2008) Hole-filled seamless SRTM data V4, International Centre for Tropical Agriculture (CIAT). Available at: http://srtm.csi.cgiar.org.

Jia YL, Shi YF, Wang SM et al. (2001) Lake-expanding events in the Tibetan Plateau since 40 kaBP. *Science in China Series D: Earth Sciences* 44(1 suppl.): 301–315.

Kang SG, Wang XL and Lu YC (2012) The estimation of basic experimental parameters in the fine-grained quartz multiple-aliquot regenerative-dose OSL dating of Chinese loess. *Radiation Measurements* 47: 674–681.

Kasper T, Haberzettl T, Doberschütz S et al. (2012) Indian Ocean Summer Monsoon (IOSM)-dynamics within the past 4 ka recorded in the sediments of Lake Nam Co, central Tibetan Plateau (China). *Quaternary Science Reviews* 39: 73–85.

Kong P, Na C, Brown R et al. (2011) Cosmogenic ^{10}Be and ^{26}Al dating of paleolake shorelines in Tibet. *Journal of Asian Earth Sciences* 41: 263–273.

Lal D (1991) Cosmic ray labeling of erosion surfaces: *In situ* nuclide production rates and erosion models. *Earth and Planetary Science Letters* 104: 424–439.

Lee J, Li S-H and Aitchison JC (2009) OSL dating of paleoshorelines at Lagkor Tso, western Tibet. *Quaternary Geochronology* 4: 335–343.

Li D, Li Y, Ma B et al. (2009) Lake-level fluctuations since the Last Glaciation in Selin Co (lake), Central Tibet, investigated using optically stimulated luminescence dating of beach ridges. *Environmental Research Letters* 4: 045204.

Li S-H, Sun J-M and Zhao H (2002) Optical dating of dune sands in the northeastern deserts of China. *Palaeogeography, Palaeoclimatology, Palaeoecology* 181: 419–429.

Liu X-J, Lai Z, Madsen D et al. (2015) Last deglacial and Holocene lake level variations of Qinghai Lake, north-eastern Qinghai–Tibetan Plateau. *Journal of Quaternary Science* 30: 245–257.

Liu X-J, Lai Z-P, Zeng F-M et al. (2013) Holocene lake level variations on the Qinghai-Tibetan Plateau. *International Journal of Earth Sciences* 102: 2007–2016.

Downloaded from hol.sagepub.com by guest on September 2, 2015

Long H, Lai Z, Frenzel P et al. (2012) Holocene moist period recorded by the chronostratigraphy of a lake sedimentary sequence from Lake Tangra Yumco on the south Tibetan Plateau. *Quaternary Geochronology* 10: 136–142.

Mejdahl V and Christiansen HH (1994) Procedures used for luminescence dating of sediments. *Quaternary Science Reviews* 13: 403–406.

Miehe S, Miehe G, van Leeuwen JFN et al. (2014) Persistence of *Artemisia* steppe in the Tangra Yumco Basin, west-central Tibet, China: Despite or in consequence of Holocene lake-level changes? *Journal of Paleolimnology* 51: 267–285.

Mischke S, Aichner B, Diekmann B et al. (2010) Ostracods and stable isotopes of a late glacial and Holocene lake record from the NE Tibetan Plateau. *Chemical Geology* 276: 95–103.

Nishiizumi K, Imamura M, Caffee MW et al. (2007) Absolute calibration of 10Be AMS standards. *Nuclear Instruments and Methods in Physics Research Section B: Beam Interactions with Materials and Atoms* 258: 403–413.

Overpeck J, Anderson D, Trumbore S et al. (1996) The southwest Indian Monsoon over the last 18000 years. *Climate Dynamics* 12: 213–225.

Pan B, Yi C, Jiang T et al. (2012) Holocene lake-level changes of Linggo Co in central Tibet. *Quaternary Geochronology* 10: 117–122.

Prescott JR and Hutton JT (1994) Cosmic ray contributions to dose rates for luminescence and ESR dating: Large depths and long-term time variations. *Radiation Measurements* 23: 497–500.

Rades EF, Hetzel R, Xu Q et al. (2013) Constraining Holocene lake-level highstands on the Tibetan Plateau by ^{10}Be exposure dating: A case study at Tangra Yumco, southern Tibet. *Quaternary Science Reviews* 82: 68–77.

Rades EF, Tsukamoto S, Frechen M et al. (2015) A lake-level chronology based on feldspar luminescence dating of beach ridges at the Tangra Yum Co (southern Tibet). *Quaternary Research* 83: 469–478.

Shen J, Liu X, Wang S et al. (2005) Palaeoclimatic changes in the Qinghai Lake area during the last 18,000 years. *Quaternary International* 136: 131–140.

Stone JO (2000) Air pressure and cosmogenic isotope production. *Journal of Geophysical Research: Solid Earth* 105: 23753–23759.

Tripaldi A and Forman SL (2007) Geomorphology and chronology of Late Quaternary dune fields of western Argentina. *Palaeogeography, Palaeoclimatology, Palaeoecology* 251: 300–320.

Waters MR, Forman SL, Jennings TA et al. (2011) The Buttermilk Creek complex and the origins of Clovis at the Debra L. Friedkin site, Texas. *Science* 331: 1599–1603.

Wintle AG and Murray AS (2000) Quartz OSL: Effects of thermal treatment and their relevance to laboratory dating procedures. *Radiation Measurements* 32: 387–400.

Zhao Y, Yu Z, Chen F et al. (2007) Holocene vegetation and climate history at Hurleg Lake in the Qaidam Basin, northwest China. *Review of Palaeobotany and Palynology* 145: 275–288.

Downloaded from hol.sagepub.com by guest on September 2, 2015

CHAPTER 4 — Spatial and temporal variability of moisture availability on the southern Tibetan Plateau since 17.4 ka – the Tangra Yumco record

Ahlborn M, T Haberzettl, J Wang, K Henkel, T Kasper, G Daut, L Zhu, and R Mäusbacher (in review): Spatial and temporal variability of moisture availability on the southern Tibetan Plateau since 17.4 ka – the Tangra Yumco record. *Boreas.*

Submitted in the present form: 23 Oct 2015

Licensor: n.a.

Abstract

A possible heterogeneity of the spatial and temporal climate development on the Tibetan Plateau has controversially been discussed in recent years. Here we present the first attempt to systematically investigate possible spatial and temporal variations of moisture availability by examining two lakes, Nam Co and Tangra Yumco, on an east-west-transect on the southern-central Tibetan Plateau that is extended by Tso Moriri (northwestern Himalaya) and Naleng Co (south-eastern Tibetan Plateau). In this study, an independent record from Tangra Yumco was investigated with a multi-proxy approach to reconstruct moisture variations since the Lateglacial. Results were subsequently compared to Nam Co, Tso Moriri, and Naleng Co. As the precipitation regime on the Tibetan Plateau is significantly influenced by recycling and pre-monsoon precipitation, we compared our results to several records of monsoon intensity to investigate a possible impact of summer monsoon precipitation on the southern Tibetan Plateau.

Tangra Yumco was probably ice covered with only episodically thawing prior to 17.1 cal ka BP. A temperature rise after 17.1 cal ka BP resulted in seasonal ice coverage of the lake and probably thawing of the permafrost resulting in an increased input of organic material from the catchment. At 16.0 cal ka BP moisture availability initially increased, while it was highest at 10.1–9.4 cal ka BP coincident with highest temperatures. After 9.4 cal ka BP the moisture availability gradually decreased and showed only minor amplitude variations.

The comparison with Nam Co and Tso Moriri revealed a synchronous climate pattern on the southern Tibetan Plateau which is in phase with monsoon intensity in the Arabian Sea, the Bay of Bengal, and a Dole effect record. The synchronous pattern of moisture availability on

the southern Tibetan Plateau and monsoon intensity probably implies that moisture availability is predominantly controlled by monsoon-like processes.

Keywords

Monsoon, precipitation, lake sediments, Tangra Yumco, Nam Co, Tibetan Plateau

4.1 Introduction

Monsoon, by definition, is a seasonal change in wind direction and precipitation pattern *(Goswami 2005)*. It is widely accepted that precipitation regimes on the Tibetan Plateau are influenced by the summer monsoon systems *(e.g., Morrill et al. 2006, Jin et al. 2009, An et al. 2012b, Dallmeyer et al. 2012, Chen et al. 2013, Maussion et al. 2014)*. However, the precipitation regime on the Tibetan Plateau is generally dominated by convective precipitation not solely attributed to monsoon but also to recycling and pre-monsoon (spring) precipitation having regionally a significant effect on the hydrological cycle *(Dallmeyer et al. 2012, Maussion et al. 2014)*. In recent years, numerous studies have been conducted on the Tibetan Plateau in order to reveal past hydrological variations *(Shen et al. 2005, Wang et al. 2005, Morrill et al. 2006, Mischke et al. 2010a, Kasper et al. 2012, Doberschütz et al. 2014, Günther et al. 2015)*. In these studies moisture was equated to monsoon meaning that all changes in moisture availability were attributed to monsoonal dynamics. However, most proxies cannot define seasonal but rather annual to centennial changes in moisture availability and thus cannot provide information about seasonal changes in precipitation necessary for a summer monsoon reconstruction *(Dallmeyer et al. 2012)*.

Several studies suggested an asynchronous pattern of moisture availability of the Tibetan Plateau since the Last Glacial Maximum *(An et al. 2000, He et al. 2004, Herzschuh 2006, Mischke et al. 2008)*. In contrast, other studies rather indicate a synchronous pattern of moisture availability *(Feng et al. 2006, Chen et al. 2008, Dong et al. 2010, Mischke and Zhang 2010)*. However, as reliable, continuous records covering the Lateglacial and the Holocene are rare, a holistic picture of variability of moisture availability, including spatial and temporal

heterogeneities, and the impact on the environment is still missing *(Herzschuh 2006, Mischke and Zhang 2010)*.

To investigate past climate variability on the southern Tibetan Plateau, two lakes along an east-west-transect, including Nam Co and Tangra Yumco (Figure 4.1) were recently targeted for paleoenvironmental studies. Nam Co has thoroughly been investigated in recent years *(e.g., Daut et al. 2010, Mügler et al. 2010, Kasper et al. 2012, Kasper et al. 2013, Doberschütz et al. 2014, Günther et al. 2015, Kasper et al. 2015)* and several studies have been conducted in the Tangra Yumco catchment *(Kong et al. 2011, Long et al. 2012, Rades et al. 2013, Miehe et al. 2014, Ahlborn et al. 2015a, Ahlborn et al. 2015b, Akita et al. 2015, Long et al. 2015, Rades et al. 2015, Henkel et al. revised, Henkel et al. subm.)*. In this study we present results from an 11.2 m-long lacustrine sediment record from Tangra Yumco. The objectives of this study are fourfold: (1) we aim to deduce changes in moisture availability for the Tangra Yumco area since 17.4 cal ka BP. (2) We infer the temporal and spatial moisture availability on the southern Tibetan Plateau by comparison to Nam Co *(Kasper et al. 2015)* and, as they extend our transect, Tso Moriri *(*northwestern Himalaya; for reasons of simplification we refer to southern Tibetan Plateau; *Mishra et al. 2015)* and Naleng Co *(*south-eastern Tibetan Plateau; *Opitz et al. 2015)* (Figure 4.1). Plateau-wide inferences are based on a comparison to Lake Qinghai *(An et al. 2012b)* and Pumoyum Co *(Nishimura et al. 2014)*. (3) As nowadays the moisture gradually decreases from west to east *(Maussion et al. 2014)* we furthermore assess, if this moisture gradient has an impact on the temporal variability. (4) To reveal if the moisture availability on the southern Tibetan Plateau is influenced by monsoonal variations, the southern Tibetan Plateau will then be compared to

monsoon records from the Bay of Bengal *(Rashid et al. 2011)*, the Arabian Sea *(Schulz et al. 1998)*, and to a Dole effect record which reflects the deviation of the isotopic composition of air from seawater and is primarily governed by Asian and African monsoon variations *(Severinghaus et al. 2009)*.

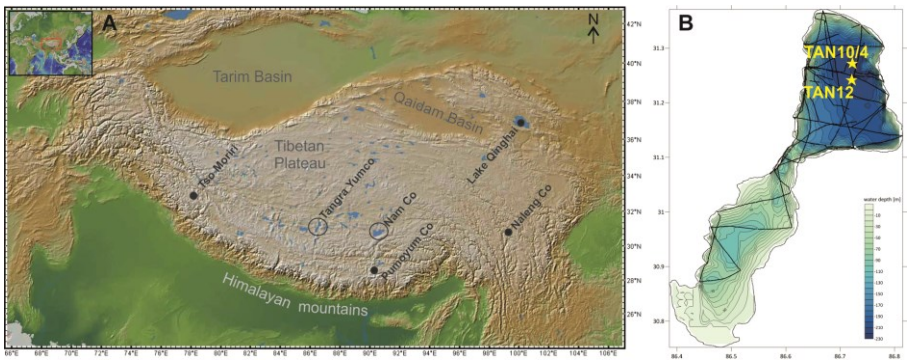

Figure 4.1: Study site. A: Map of China with Tibetan Plateau and Tangra Yumco (circle), Nam Co (circle), Naleng Co, Tso Moriri, Pumoyum Co, Lake Qinghai. B: Bathymetric map of Tangra Yumco with sampling location of cores TAN10/4 and TAN12 with tracks of hydro-acoustic survey (black lines). Source: http://www.geomapapp.org.

4.2 Regional setting

Tangra Yumco (30°45'–31°22'N, 86°23'–89°49'E; Figure 4.1) is located on the southern-central Tibetan Plateau at an elevation of 4545 m asl *(Rades et al. 2013)* with a catchment of 8219 km^2 *(Long et al. 2012)*. The Tangra Yumco basin belongs to a north-south-trending graben at the northern slope of the Transhimalaya *(Miehe et al. 2014)*. Well-preserved paleoshorelines are exposed up to ~185 m above the recent lake level (m arll) *(Rades et al. 2013)*, whereas poorly-preserved paleoshorelines are exposed up to >260 m arll indicating extensive lake level changes during the past *(Kong et al. 2011)*. Precipitation at Tangra Yumco is dominated by convective rainfall *(Maussion et al. 2014)* often attributed

to the Indian summer monsoon originating from the south *(Miehe et al. 2014)*. Westerly winds prevail during the winter months *(Maussion et al. 2014)*. The extrapolated mean annual precipitation is 200–250 mm, the mean temperature in January is -11.4°C, and the mean July temperature 10.9°C *(Miehe et al. 2014)*.

Tangra Yumco (Figure 4.1) is a brackish lake with a salinity of 8.3‰ *(Akita et al. 2015)* covering 818 km² *(Long et al. 2012)*. With a water depth of 230 m Tangra Yumco is the deepest lake recorded on the Tibetan Plateau so far *(Wang et al. 2010)*. The lake has a northern and a southern part connected by a bottleneck-like structure. Two large rivers drain into Tangra Yumco entering the southern part of the lake from the southeast and west. Tangra Yumco lacks an outflow and is currently a terminal lake. A connection to the nearby Tanqung Co (about 18 km north of Tangra Yumco) is possible when the lake level of Tangra Yumco reaches an elevation of ~64 m arll *(Ahlborn et al. 2015b)*. Due to its terminal character lake level variations of Tangra Yumco are mainly controlled by precipitation and temperature (evaporation), while the contribution of glaciers is negligible *(Rades et al. 2013)*. The population in the Tangra Yumco area is sparse and human impact is mainly restricted to pastoralism *(Miehe et al. 2014)*.

4.3 Material and methods

4.3.1 Field methods

Hydro-acoustic surveys (Innomar SES-96 light and Lowrance Echosounder HDS 5) were conducted in the northern part of Tangra Yumco in 2010 and 2011. Based on these results coring locations were selected for the field campaigns in 2010 and 2012, when the sediment cores TAN10/4 and TAN12 were recovered (Table 4.1).

4.3.2 Non-destructive laboratory methods

Until further processing all cores were stored in darkness at +4°C. The cores were split and subjected to an initial core description including high-resolution imaging and magnetic susceptibility logging. The split cores were XRF scanned and X-rayed *(*ITRAX Corescanner; *Croudace et al. 2006)*. XRF-scanning was conducted with 2 mm resolution for sections TAN12/1 to 7 and with 0.2 mm resolution for sections TAN12/8 to 11 and TAN10/4 using a molybdenum tube set to 55 kV and 40 mA. Exposure time was 10 s for all sections of core TAN12 and 4 s for TAN10/4. To compensate for different exposure times, element peak area [pa] values were normalized to the exposure time applied and subsequently to kilo counts per second [kcps]. For principle component analysis (PCA), normalized values were z-transformed. Since core TAN10/4 was obtained from a different location within Tangra Yumco, overlapping XRF data of core TAN10/4 were plotted on a separate x-axis and adjusted to the data of core TAN12. Elements with pa >100 were considered as reliable and used for interpretation *(Brunschön et al. 2010, Kasper et al. 2012)*. Core TAN10/4 was parallelized with the upper part of core TAN12 based on lithology and Ti.

Table 4.1: Metadata of cores TAN10/4 and TAN12.

Cores metadata		
	TAN10/4	**TAN12/2/1-11**
Longitude	E 86°43.369'	E 86°43.246'
Latitude	N 31°15.159'	N 31°13.926'
Water depth	220 m	213 m
Coring methods	modified ETH gravity corer	Uwitec piston corer
Year of coring	2010	2012
Number of sections	1	11
Total length	1.62 m	11.5 m
Diameter	63 mm	90 mm
Number of radiocarbon ages	6	22

4.3.3 Destructive laboratory methods

Double-L-channels *(Nakagawa 2007, Nakagawa et al. 2012)* were taken from all sections and continuously sub-sampled in 1 cm intervals for grain size and geochemical analyses. For grain size analysis, samples were pretreated with H_2O_2 10% p.a. and HCl 10% p.a. to dissolve organic compounds and carbonates. Dispersion of the grains was ensured using sodium pyrophosphate ($Na_4P_2O_7$•10 H_2O, 0.1 mol L^{-1}) and samples were shaken for 2 h. Grain size distribution was measured in seven cycles of 60 s each and the first reproducible signal was used for interpretation applying the Frauenhofer optical model and a modified version of Gradistat 4.2 *(Blott and Pye 2001)* for statistical calculations.

Samples for geochemical analysis were freeze-dried and ground (<40 µm). For core TAN10/4 and section TAN12/10 analyses were performed in a varying resolution of 1 to 10 cm depending on observed variations. All samples were subjected to analyses of total carbon (TC),

total sulfur (TS), and total nitrogen (TN) using an elemental analyzer (Vario El Cube). Carbonates were dissolved using HCl 30% p.a. prior to measurements of total organic carbon (TOC). Total inorganic carbon (TIC) was calculated as the difference of TC and TOC and atomic C/N ratios were calculated. The error was estimated based on two triplicate measurements for core TAN10/4 and sixteen for core TAN12. Mean relative errors are 0.6% for TC, 11.2% for TS, 9.3% for TN, and 4.6% for TOC.

4.3.4 Event corrected composite depth (ECCD)

Possible event-related deposits *(*ERD; *Ahlborn et al. 2015a)* resulting from deposition of relocated sediment material were identified based on lithology, radiographic images, Ti values, grain size data, and water content *(Henkel et al. revised)*. For final interpretation, event layers and corresponding data were excluded from the record. The event corrected record is presented on an artificial depth axis, the so-called event corrected composite depth (ECCD) that is used hereafter *(Henkel et al. revised)*. Sedimentological units were established to subdivide the ECCD record based on the patterns of K, TOC, and grain size. Due to coring artefacts (piston and core catcher) data gaps of 17 cm occur between the sections (Figure 4.3).

4.3.5 Chronology

The chronology of core TAN10/4 is based on four ^{14}C AMS ages and confirmed by magnetostratigraphy *(Haberzettl et al. 2015)*, while the chronology of core TAN12 is based on 14 ^{14}C AMS ages *(Henkel et al. revised)*. Dating measurements were generally made on bulk sediment samples except one piece of wood that was dated from core TAN10/4

(Beta Analytics Inc., USA). To estimate the reservoir effect the water-sediment-interface was dated as well as one recent water plant. The mean of these ages was calculated as the reservoir effect and was subtracted from all ^{14}C ages except the age obtained from wood presuming that the reservoir effect was constant over time *(Henkel et al. revised)*. To set up the chronology the ages were calibrated with Calib 7.0 *(Stuiver and Reimer 1993)* applying the IntCal13 dataset *(Reimer et al. 2013)* and linearly interpolated *(Henkel et al. revised)*. Ages that would considerably alter the sedimentation rate although the changes in the lithology can be observed, were considered as too old and excluded from the chronology. The chronologies of cores TAN10/4 and TAN12 are discussed in detail by *Haberzettl et al. (2015)* and *Henkel et al. (revised)*.

4.4 Results

4.4.1 Chronology and Lithology

The composite profile of the parallelized core sections has a total length of 11.2 m. The event-corrected ECCD of the sediment sequence comprises 849 cm covering 17.4 ka cal BP (Figure 4.2) *(Henkel et al. revised)*. K, TOC, and grain size data enabled a subdivision of the core into six units (849–736 cm, 17.4–17.1 cal ka BP; 736–625 cm, 17.1–16.0 cal ka BP; 625–558 cm, 16.0–12.8 cal ka BP; 558–456 cm, 12.4–11.4 cal ka BP; 456–355 cm, 11.4–7.6 cal ka BP; 355–0 cm, 7.6–0.0 cal ka BP; Figure 4.3).

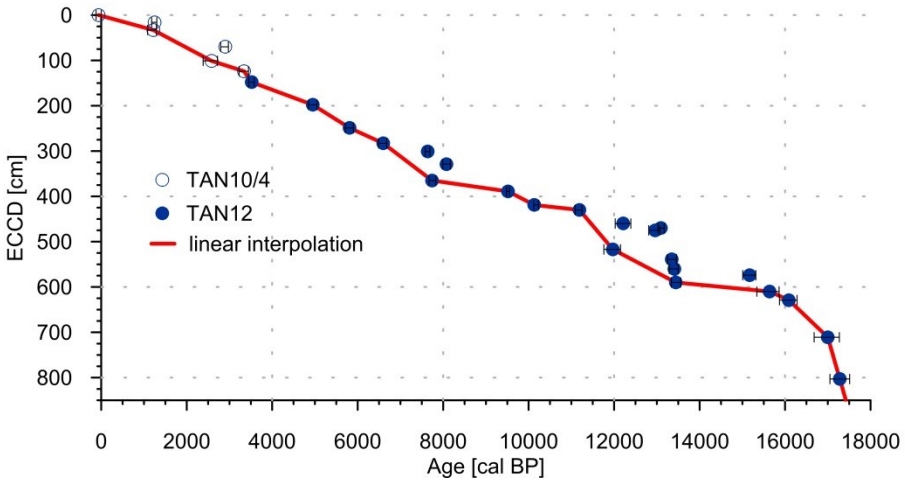

Figure 4.2: Chronology of record TAN12 as published in *Henkel et al. (revised)*. A change in sedimentation rate occurs around at 16.0 cal ka BP. The sedimentation rate is ~3.3 mm a^{-1} prior to 16.0 cal ka BP and mostly <0.6 mm a^{-1} thereafter.

Sediments are generally silty in the entire record and are disturbed by microfaults. Black sandy layers occur exclusively below 736 cm sediment depth. Colors are dark gray with faint lamination of millimeter-scale below 626 cm sediment depth. At 626-575 cm sediment depth, sediments are gray but overall lighter with clearly defined lamination of submillimeter scale. Above 575 cm sediment depth, sediments are brownish with light gray to gray laminae of subcentimeter to centimeter scale. Seventeen ERDs were identified *(Henkel et al. revised)* (Figure 4.3). The sedimentation rate is 0.9-3.3 mm a^{-1} prior to 16.0 cal ka BP and <0.6 mm a^{-1} after 16.0 cal ka BP.

4.4.2 Geochemical data

Ti is positively correlated with K, Fe, and Rb ($R_{Ti:K}$=0.69, $R_{Ti:Fe}$=0.69, and $R_{Ti:Rb}$=0.59) whereas the correlation to Ca is negative ($R_{Ca:K}$= -0.47, $R_{Ca:Ti}$= -0.47, $R_{Ca:Fe}$= -0.60, $R_{Ca:Rb}$= -0.73). Sr and Ca show a similar pattern although the correlation coefficient of $R_{Ca:Sr}$=0.40 is rather low. Results of the PCA show that the principle components 1 (PC1) and 2 (PC2) account for 77.48% of the total variance. PC1 yields high values for K, Ti, Fe, and Rb and accounts for 63.06% of the total variance while PC2 accounts for 14.43% and basically represents Sr (Figure 4.3). The remaining PCs have only low account on the total variance with <10% each. PC1 is rapidly increasing at 625 cm sediment depth showing a minor peak at 594–558 cm sediment depth. It is highly variable at 456–355 cm sediment depth and remains relatively stable above 355 cm. Between 456 and 297 cm sediment depth Ca is strongly negatively correlated with PC1 as the correlation coefficient is $R_{Ca:PC1}$= -0.83 (Figure 4.3).

TIC, TOC, TN, and C/N data generally show related patterns (Figure 4.3). TIC values range from 0.66–6.56 % and resemble the Ca pattern with a correlation coefficient of $R_{TIC:Ca}$=0.74. Due to the higher temporal resolution of Ca compared to TIC, Ca is used for further interpretations instead of TIC. Even though there are similar trends in the TOC and TIC patterns, the correlation coefficient of $R_{TOC:TIC}$=0.30 is low. TOC content is generally low, varies from 0.1–1.1 %, and is highly correlated to TN with $R_{TOC:TN}$=0.93. TOC and TN reveal lowest values in the entire core below 736 cm, highest values at 736–625 cm, lower but generally stable values at 625–594 cm, and a minor peak 594–558 cm sediment depth. Values are markedly reduced at 558–456 cm, increasing thereafter, and culminating in a broad maximum at 418–383

cm sediment depth. TOC and N are relatively stable above 297 cm with a maximum at 23–13 cm sediment depth. C/N ratios vary from 3.9–10.1 only exceeding 10 at 736–625 cm sediment depth (Figure 4.3).

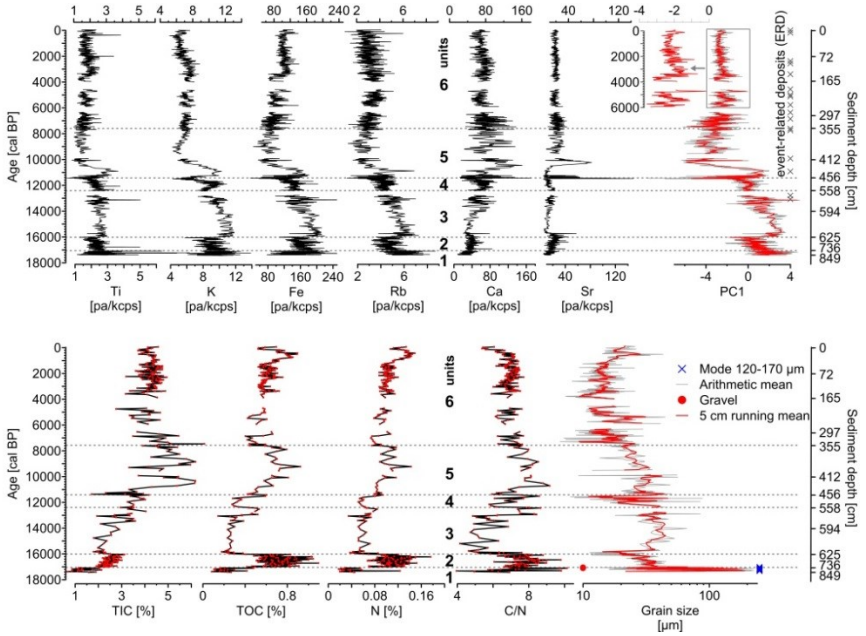

Figure 4.3: Results of XRF (4 mm resolution), PC1 representing the minerogenic input (gray) with 5 cm running mean (red) and event-related deposits (ERD), the past 6000 a on a different axis to reveal further details, CNS analyses (<10 cm resolution), and grain size analyses (1 cm resolution, gray) with 1 cm running mean (red) on a logarithmic scale. Discontinuity of the plots is due to data gaps between core sections.

TIC, TOC, TN, and C/N data generally show related patterns (Figure 4.3). TIC values range from 0.66-6.56 % and resemble the Ca pattern with a correlation coefficient of $R_{TIC:Ca}$=0.74. Due to the higher temporal resolution of Ca compared to TIC, Ca is used for further interpretations instead of TIC. Even though there are similar trends in the TOC and TIC patterns, the correlation coefficient of $R_{TOC:TIC}$=0.30 is low. TOC content is generally low, varies from 0.1-1.1 %, and is highly correlated to TN with $R_{TOC:TN}$=0.93. TOC and TN reveal lowest values in the entire core below 736 cm, highest values at 736-625 cm, lower but generally stable values at 625-594 cm, and a minor peak 594-558 cm

sediment depth. Values are markedly reduced at 558-456 cm, increasing thereafter, and culminating in a broad maximum at 418-383 cm sediment depth. TOC and N are relatively stable above 297 cm with a maximum at 23-13 cm sediment depth. C/N ratios vary from 3.9-10.1 only exceeding 10 at 736-625 cm sediment depth (Figure 4.3).

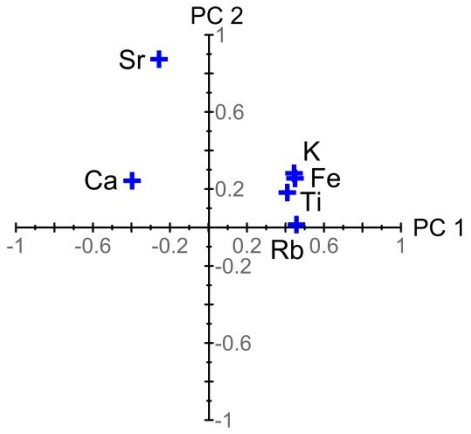

Figure 4.4: Results of the principle component analysis. The PC1 accounts for 63.06% while PC2 accounts for 14.43% of the total variance and basically represents Sr. PC1 is considered to reflect the allochthonous clastic input as it has high accounts of K, Ti, Fe, and Rb.

4.4.3 Grain size data

Arithmetic mean values of the grain size data vary between 7.3–225.1 µm and roughly resemble the PC1 pattern (Figure 4.3). Large modes between 120 and 220 µm only occur below 736 cm associated with an unimodal distribution and maximum mean values (220 µm). Gravel (>2 mm) is recorded at 768 and 750 cm sediment depth (Figure 4.3). Above 736 cm mean values decrease down to 12 µm followed by a sharp increase to 30 µm at 625 cm, and relatively stable values thereafter. A drop to 8 µm occurs at 558 cm sediment depth, followed by a maximum of 56 µm at 418–387 cm. Values decline down to 9 µm until 297 cm sediment depth and show minor variations thereafter

(Figure 4.3). A final coarsening is visible towards the top of the sequence within the uppermost 72 cm.

4.5 Interpretation

4.5.1 Geochemical data

As demonstrated in previous studies Ti can be considered as indicator for allochthonous clastic input into a lake system *(Haberzettl et al. 2009, Kasper et al. 2012, Doberschütz et al. 2014)*. Clastic material is often transported fluvially into the lake due to enhanced surface runoff *(Kasper et al. 2012)*. Surface runoff, in turn, is closely related to moisture availability in terms of precipitation *(Haberzettl et al. 2005)*. As observed in other studies before *(Brunschön et al. 2010)* high correlations of Ti with K, Fe, and Rb indicate that these elements represent the allochthonous clastic input into Tangra Yumco. As these elements have a high load on PC1, it reflects the allochthonous clastic input by runoff and is hence interpreted as indicator for precipitation (Figure 4.3).

Non-vascular aquatic plants contain high proportions of N-rich protein resulting in low C/N ratios that are typically between 4 and 10. Terrestrial vascular plants have a low protein content but are enriched in TOC due to their cellulose content resulting in higher C/N ratios of >10 *(Kemp et al. 1977, Krishnamurthy et al. 1986, Meyers and Ishiwatari 1993)*. As C/N ratios in this record are constantly <10, the TOC content mainly reflects changes in the lake-internal biogenic production. C/N values >10 can suggest enhanced input of terrestrial plant remains from the catchment. Despite the weak correlation of TIC and TOC, the similar pattern indicates a common long term controlling mechanism. Hence, it is assumed that on long time scales carbonate production is coupled to enhanced biological production. Sr is mainly associated with carbonates

(Wu et al. 2006) but strongly influenced by the carbonate phase dominating in the lake sediments as Sr can substitute Ca in the aragonite crystal lattice *(Jin et al. 2005)*. Since Sr closely resembles the Ca pattern, Sr, Ca (and TIC), and TOC are thus indicative for autochthonous biological production which has often been linked to temperature variations *(Zhu et al. 2008, Kasper et al. 2012)*.

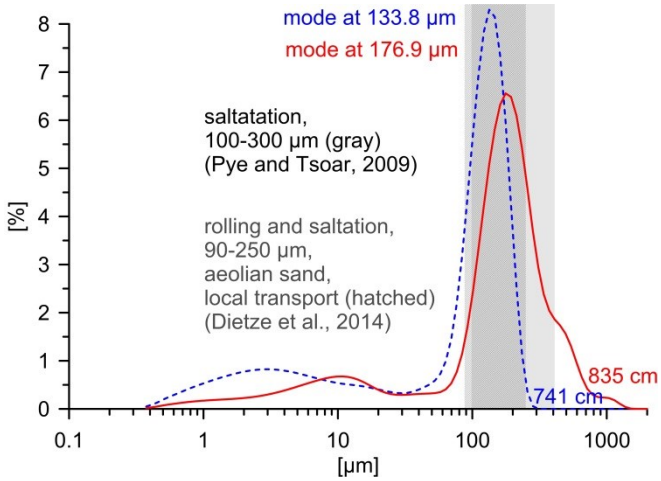

Figure 4.5: Grain size distribution of sand layers prior to 17.1 cal ka BP. Layer at 835 cm sediment depth (17.4 cal ka BP; red bold) has a mode at 176.9 µm. Layer at 741 cm sediment depth (17.1 cal ka BP; blue dashed) has a mode at 133.8 µm. Unimodal distribution indicates aeolian transport. Rolling and saltation happens to grains with a size of 90–250 µm *(*brown; *Dietze et al. 2014)* or 100–300 µm *(*gray; *Pye and Tsoar 2009)*.

4.5.2 Grain size data and sedimentation rate

Coarser grains are associated with enhanced surface runoff which is linked to moister conditions, whereas grain sizes are finer when runoff is reduced *(Håkanson and Jansson 2002)*. Unimodal and well sorted grain size distributions with modes between 120 and 170 µm are probably linked to aeolian processes such as saltation and associated with strong winds (Figure 4.5) *(Pye and Tsoar 2009, Dietze et al. 2014)*. The sedimentation rate can serve as indicator for lake level variations *(Kasper et al. 2015)*. As the sedimentation rate is controlled by the distance to the shore, the sedimentation rate is higher when the lake level is low, while the sedimentation rate is lower when the lake level is higher because less material is transported to the coring location *(Kasper et al. 2015)* and the catchment to lake surface (which is the area of potential deposition of transported sediment to the lake) becomes smaller.

4.6 Discussion

4.6.1 Paleohydrology of Tangra Yumco

Unit 1: 17.4-17.1 cal ka BP, 849-736 cm. A high sedimentation rate, low allochthonous clastic input, and low lake-internal biological production (Figure 4.6) suggest that Tangra Yumco probably has been a very shallow lake and environmental conditions were therefore generally dry. Sandy layers might reflect aeolian transport (Figure 4.5) which also points to a dry environment with sparse vegetation cover making sediments easily available for erosion and aeolian transport. As the climatic conditions on the Tibetan Plateau during this time have been interpreted to be also rather cold *(Kasper et al. 2015)*, this combination of cold and dry climate is favorable for the formation of clear lake ice

without a snow cover which would inhibit an aeolian transport by saltation. Hence, Tangra Yumco probably was ice covered during long periods of the year and sediments were moved by saltation on the ice. Deposition of the coarse aeolian sediments probably occurred during episodic thawing. Gravel might have been transported as ice-rafted debris to the center of the lake and deposited during these thawing episodes. The low internal biological production supports the idea of cooler temperatures.

Unit 2: 17.1-16.0 cal ka BP, 736-625 cm. During this time the highly variable, but in general enhanced carbonate precipitation and biological productivity as well as enhanced input of terrestrial organic matter suggest rising temperatures probably leading to a thawing of the permafrost. The thawing permafrost released large amounts of terrestrial TOC from the topsoil then available for erosion, transport, and deposition in the lake. Higher temperatures moreover could have enhanced autochthonous biological production resulting in higher carbonate production, while climatic conditions were persistently dry as indicated by low allochthonous clastic input.

Unit 3: 16.0-12.4 cal ka BP, 625-539 cm. The sudden rise of the allochthonous clastic input and the decrease in sedimentation rate at the beginning of this period (Figure 4.6) suggests the onset of moister conditions at 16.0 cal ka BP probably associated with a rising lake level (Figure 4.6). Tangra Yumco might have been a very shallow lake until this time and the rising lake levels might have increased the distance of the coring location to the shore consequently reducing the delivery and deposition of terrestrial TOC from the catchment. The increasing water

volume might have altered the water chemistry and decreased the carbonate production. Autochthonous biological production and moisture availability peak at 13.6–12.4 cal ka BP pointing to warmer and moister conditions, coinciding with the first occurrence of ERDs in this record (Figure 4.6). ERDs are generally caused by seismic events triggering landslides or subaquatic mass movements *(e.g., Karlin et al. 2004, Petersen et al. 2014)*, hydrologic events *(e.g., Brown et al. 2000, Nesje et al. 2001, Ahlborn et al. 2015a)*, or lake level variations causing instability of the slopes *(e.g., Schnellmann et al. 2006, Akita et al. 2015)*. Microfaults can be found within the sediment record, clearly proving seismic impacts. However, there is no evidence for a seismic trigger of ERDs or strong lake level variations leading to instability of the slopes at this time. Probably hydrologic events, associated with intensive precipitation (peak in PC 1), as described at the small TT Lake located within the Tangra Yumco catchment *(Ahlborn et al. 2015a)*, are more likely triggers for these ERDs and support the idea of a rising lake level.

Unit 4: 12.4-11.4 cal ka BP, 539-456 cm. Reduced allochthonous clastic input, lower biological productivity (Figure 4.6), and variable but in general finer grain sizes indicating variable sediment transport energy in the tributaries, point to generally reduced moisture availability. ERDs do not occur in unit 4 (Figure 4.6) possibly due to enhanced aridity and an apparent lack of intensive precipitation events. Reduced intra-lake and terrestrial biological productivity probably point to generally lower temperatures during this time. However, cooler conditions would also extend the ice covered winter season associated with calm water conditions, probably leading to the deposition of the finer particles.

Unit 5: 11.4-7.6 cal ka BP, 456-355 cm. The strong negative correlation of the allochthonous input and the carbonate precipitation (Figure 4.3) in this unit indicate a dilution effect of the clastic input by carbonate precipitation. Thus, between 11.4 and 7.6 cal ka BP moisture availability is reflected solely by the sediment transport energy (i.e., grain sizes) revealing an increasing tendency until 10.1 cal ka BP and a decreasing trend from 9.4 to 7.6 ka cal BP (Figure 4.6). A decoupling of biological productivity and carbonate precipitation seems to have occurred during this unit, probably due to a substantial change of the water chemistry (lowering of ion concentration) caused by input of large amounts of freshwater *(Kasper et al. 2015)*. The freshwater could have been provided by the nearby Xuru Co which would generate an overflow to Tangra Yumco at about 24 m above its recent lake level and might have discharged into Tangra Yumco at that time *(Ahlborn et al. 2015b)*. ERDs at 11.1 and 9.9 cal ka BP may coincide with enhanced moisture availability and related hydrologic events or slope instabilities due to a quick lake level rise. ERDs at 7.8 and 7.6 ka cal BP are likely related to reduced moisture availability and probably a falling lake level and hence exposed loose easily erodible sediments coupled with hydrologic events.

A Holocene lake level reconstruction from Tangra Yumco (Figure 4.6) based on optically stimulated luminescence (OSL) ages of exposed lacustrine sediments and recalculated cosmogenic nuclide ages of beach terraces indicate a rising lake level at 10.5 ka, a lake level highstand prior to 8.5 ka, and falling lake level thereafter *(Ahlborn et al. 2015b)*. These results are well in phase with increasing moisture availability until 10.1 cal ka BP and its maximum at 10.1–9.4 cal ka BP observed in this study. Comparison with the OSL derived lake level reconstruction also confirms a falling lake level after 9.2 cal ka BP

(Ahlborn et al. 2015b). Results from the Targo Xian peat bog, located about 16 km east of the southern shore of Tangra Yumco but within its catchment, are in phase with reconstructions from Tangra Yumco as they reveal an onset of wetter conditions at 11.5 cal ka BP and a further increase in moisture availability at 11.0 cal ka BP *(Miehe et al. 2014)*.

Unit 6: 7.6-0.0 cal ka BP, 355-0 cm. Environmental conditions during this period were rather stable with only minor variations in autochthonous biological production and moisture availability (Figure 4.6). Sediment transport energy is again decoupled from the allochthonous clastic input which is apparently still affected by dilution by Ca prior to 6.8 cal ka BP. As finer particles were deposited, the sediment transport energy further declined, suggesting a decrease in moisture availability at the onset of this period. Moisture availability constantly diminished with several short-term wet spells at 5.5–5.3, 2.4–2.1, and 1.5–1.3 cal ka BP. After 0.8 cal ka BP a trend towards moister conditions is visible Figure 4.6). Autochthonous biological productivity fluctuated slightly prior to 5.2 cal ka BP and remained stable afterwards except for a significant warm spell at about 0.8–0.4 cal ka BP. Eleven ERDs occurred in unit 6 (Figure 4.6) possibly due to a further falling lake level exposing large amounts of sediments making them prone to erosion.

Lake level reconstructions at Tangra Yumco *(Ahlborn et al. 2015b)* confirm the further falling lake level (Figure 4.6). An OSL dating derived short-term lake level rise at 2.1 ka *(Ahlborn et al. 2015b)* might be associated with wet spells shown by the allochthonous clastic input in this study. The increase in moisture availability revealed by allochthonous clastic input prior to 0.8 cal ka BP appears to be a little earlier in this study than the OSL dated lake level rise at 0.3 ka *(Ahlborn*

et al. 2015b). Probably the higher temperatures at 0.8–0.4 cal ka BP enhanced the evaporation maintaining a stable lake level of Tangra Yumco although the moisture supply was still high (Figure 4.6). Data from the Targo Xian peat bog imply drier condition after 7.5 cal ka BP *(Miehe et al. 2014)* being in phase with the climatic conditions reconstructed for Tangra Yumco *(*this study; *Ahlborn et al. 2015b)*. After 2.6 cal ka BP dry conditions prevailed at Targo Xian interrupted by a moist phase at 1.8–1.0 cal ka BP that might correspond to increased moisture at 1.5–1.3 cal ka BP at Tangra Yumco. Moist conditions at Targo Xian after 0.9 cal ka BP are in phase with the onset of enhanced moisture supply at Tangra Yumco at 0.8 cal ka BP.

4.6.2 Paleohydrology of the southern Tibetan Plateau

As unit 1 comprises only 300 years, it is not used for comparison to other records. At 17.1–16.0 cal ka BP (unit 2, Lateglacial) similar conditions as at Tangra Yumco are observed at Nam Co *(Kasper et al. 2015)*, Tso Moriri *(Mishra et al. 2015)*, and Pumoyum Co *(Nishimura et al. 2014)*. At Nam Co warming conditions (Figure 4.6) resulted in thawing permafrost promoting terrestrial vegetation and higher input of TOC as a consequence of now erodible topsoil, while melting glaciers contributed to rising lake levels during generally dry climatic conditions *(Kasper et al. 2015)*. At Tso Moriri (Figure 4.6) meltwater inflow increased at 16.4 cal ka BP causing rising lake levels *(Mishra et al. 2015)*, while at Pumoyum Co deglaciation started as early as 18.5 cal ka BP *(Nishimura et al. 2014)*. Conditions at Naleng Co have continuously been cold and dry which is not in phase with results from other records on the southern Tibetan Plateau *(Opitz et al. 2015)*.

From 16.0–12.4 cal ka BP (unit 3) the sharp increase in moisture availability at 16.0 cal ka BP at Tangra Yumco and warmer and moister conditions peaking at 13.6–12.4 cal ka BP have also been observed at Nam Co *(Kasper et al. 2015)*, whereas only the latter at Tso Moriri *(Mishra et al. 2015)* and Naleng Co *(Opitz et al. 2015)*. Moisture availability at Naleng Co increased significantly at 14.8 cal ka BP *(Opitz et al. 2015)* but because of this temporal shift of 1,200 years the correspondence to enhanced moisture availability at Tangra Yumco is vague. A comparison of the records from Tangra Yumco and Nam Co to those of Naleng Co *(Opitz et al. 2015)* and Tso Moriri *(Mishra et al. 2015)* might be hampered by the different resolution of the chronologies especially during the Lateglacial. At Nam Co climate started to get moister at 16.2 cal ka BP *(Kasper et al. 2015)*, while an increase in moisture availability is not clearly detectable at Tso Moriri *(Mishra et al. 2015)*. At Pumoyum Co *(Nishimura et al. 2014)* and Lake Qinghai *(An et al. 2012b)* climatic conditions became moister at 15.0 cal ka BP. At Naleng Co *(Opitz et al. 2015)* and Nam Co *(Kasper et al. 2015)* peaks in moisture availability at 13.4–12.3 and 14.0–13.0 ka cal BP, respectively, while at Lake Qinghai conditions were moister at 13.7–12.5 cal ka BP. These peaks were associated with the Bølling-Allerød chronozone (B/A) *(Kasper et al. 2015, Opitz et al. 2015)* and occurred simultaneously to minor peaks in moisture availability and temperature at Tangra Yumco at 13.6–12.4 cal ka BP and a significant peak in moisture availability at 13.1–11.7 cal ka BP in Tso Moriri *(Mishra et al. 2015)*.

Similar cold and dry conditions as recorded at Tangra Yumco at 12.4–11.4 cal ka BP (unit 4) occurred at Naleng Co at 12.3–11.6 cal ka BP and at Nam Co (Figure 4.6) at 13.0–11.8 cal ka BP *(Kasper et al. 2015)*. Cold and dry conditions prevailed at Tso Moriri at

11.7–11.4 cal ka BP *(Mishra et al. 2015)* and at Lake Qinghai at 12.5–11.5 cal ka BP, while the Pumoyum Co record revealed only a minor reduction of moisture at 12.2–11.6 ka BP *(Nishimura et al. 2014)*. Aside of the co-occurrence in all considered archives on the southern Tibetan Plateau this climatic event has been discovered on the entire Northern Hemisphere denoted as the Younger Dryas chronozone *(Bard et al. 2000)*.

After 11.4 cal ka BP (unit 5) rapidly rising moisture availability at Tangra Yumco culminating in the highest lake level at 10.1–9.4 cal ka BP coincides with increasing moisture availability and temperature at Naleng Co at 11.5 cal ka BP reaching their maxima prior to 8.3 cal ka BP *(Opitz et al. 2015)*. The highest lake levels since the Last Glacial Maximum at Nam were recorded Co at 9.5 cal ka BP *(Kasper et al. 2015)* and highest available moisture appeared at Tso Moriri at 11.2–8.5 cal ka BP *(Mishra et al. 2015; Figure 6)*. Contemporaneously, wettest conditions occurred at Pumoyum Co at 10.8–10.0 cal ka BP *(Nishimura et al. 2014)*. At Lake Qinghai an abrupt increase in moisture availability at 11.5 cal ka BP marks the transition to the Holocene *(An et al. 2012b; Figure 4.6)*. All archives discussed here reveal a rapid increase in moisture availability at the transition from the Late Glacial to the Holocene. Further, they show their individual highest lake levels during the early Holocene suggesting a homogenous evolution of moisture availability on the southern Tibetan Plateau.

Nam Co shows a generally similar pattern as Tangra Yumco during the mid- and Late Holocene (after 7.6 cal ka BP, unit 6) with gradually decreasing moisture availability but reveals higher amplitude variations in moisture availability probably representing local peculiarities. However, a warm period at 0.8–0.4 cal ka BP and a lake level increase after

0.3 cal ka BP occurred concurrently with Tangra Yumco (Figure 4.7) *(Kasper et al. 2015)*. At Naleng Co *(Opitz et al. 2015)*, Tso Moriri *(Mishra et al. 2015)*, and at Lake Qinghai *(An et al. 2012b)* the moisture availability also gradually decreased or showed only minor variations (Figure 4.6) suggesting a homogeneous aridification on the Tibetan Plateau during the mid- and Late Holocene. Like at other lakes, aridification prevailed at Pumoyum Co but was interrupted by higher moisture availability at 4.5–2.5 cal ka BP attributed to local convective precipitation *(Nishimura et al. 2014)*.

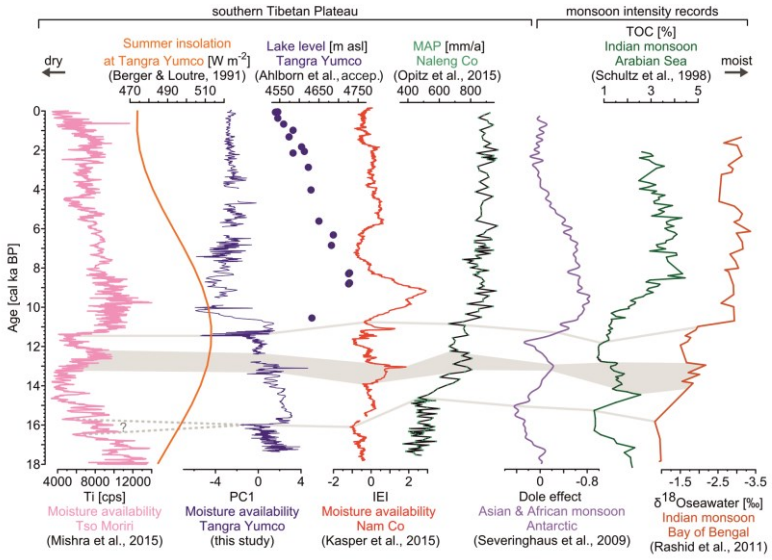

Figure 4.6: Comparison of clastic input of Tso Moriri *(Mishra et al. 2015)*, summer insolation at Tangra Yumco *(Berger and Loutre 1991)*, PC1 of Tangra Yumco with lake level curve *(*blue dots; *Ahlborn et al. 2015b)*, inflow–evaporation index *(*IEI; *Kasper et al. 2015)*, mean annual precipitation (MAP) of Naleng Co *(Opitz et al. 2015)*, Asian and African monsoon record *(Severinghaus et al. 2009)*, Indian monsoon record from the Arabian Sea *(Schulz et al. 1998)*, Indian monsoon record from the bay of Bengal *(Rashid et al. 2011)*. Increase in moisture availability around 16.0 cal ka BP; moisture and temperature peak at around 13.6-12.4 cal ka BP on the southern Tibetan Plateau; cold and dry conditions prior to Holocene transition at around 13.6-12.4 cal ka BP on the southern Tibetan Plateau; increase in moisture availability around 11.4 cal ka BP on the southern Tibetan Plateau (see text).

As shown by the comparison of Tangra Yumco, Naleng Co, Nam Co, and Tso Moriri (Figure 4.6) the evolution of the precipitation pattern shows no temporal or spatial variability but a generally homogenous evolution on the southern Tibetan Plateau superimposed by local peculiarities. However, the onset of moister conditions recorded at Tangra Yumco and Nam Co at around 16.0 cal ka BP are either less pronounced (Tso Moriri) or a little later (Naleng Co and Pumoyum Co). These effects might be due to dating uncertainties in the cases of Naleng Co and Pumoyum Co.

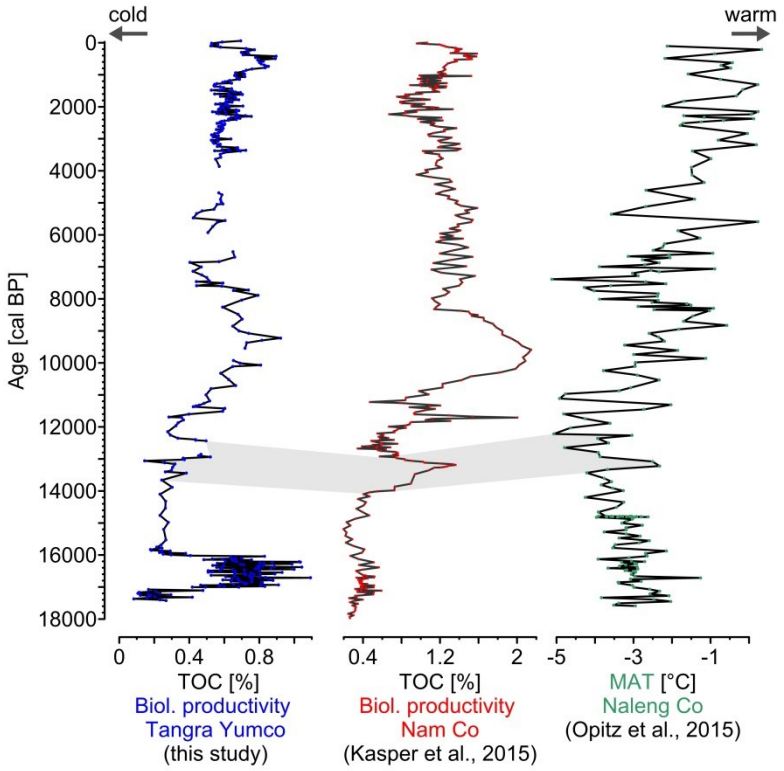

Figure 4.7: Indicators for temperature variations from the southern Tibetan Plateau. TOC as indicator for biological productivity of Tangra Yumco (this study), TOC as indicator for biological productivity of Nam Co *(Kasper et al. 2015)*, and mean annual temperature (MAT) of Naleng Co *(Opitz et al. 2015)*.

The nowadays documented east-west-gradient of available moisture (Maussion et al. 2014, Biskop et al. 2015) does not influence the temporally synchronous evolution of moisture availability. However, the methods used in this study cannot determine quantitative moisture availability and a potential moisture gradient may have existed in the past. The precipitation pattern on the southern Tibetan Plateau is generally consistent with results from Pumoyum Co (Nishimura et al. 2014) and Lake Qinghai (An et al. 2012b) probably suggesting a plateau-wide synchronous climate pattern (Figure 4.6).

4.6.3 Implications for precipitation regimes on the Tibetan Plateau

To assess a possible monsoonal influence on the precipitation regime on the southern Tibetan Plateau, records of monsoon intensity from the Arabian Sea *(Schulz et al. 1998)*, the Bay of Bengal *(Rashid et al. 2011)*, and a Dole effect record from an ice core from Antarctica that is primarily governed by the African and Asian monsoon intensity *(Severinghaus et al. 2009; Figure 6)* were compared to our data. The onset of higher moisture availability on the southern Tibetan Plateau at 16.0 cal ka BP (unit 3) occurs almost synchronous with an increase in monsoon intensity recorded in the Bay of Bengal after 15.6 cal ka BP *(Rashid et al. 2011)* and in the Arabian Sea at 15.3 cal ka BP *(Schulz et al. 1998)*, while a strengthening of the African and Asian monsoon was recorded in the Dole effect record at 15.1 cal ka BP *(Severinghaus et al. 2009)*. A moister and warmer period at 13.6–12.4 cal ka BP (unit 3) on the southern Tibetan Plateau matches a peak in monsoon intensity in the records from the Bay of Bengal at 14.6–12.7 cal ka BP *(Rashid et al. 2011)*, the Arabian Sea at 14.4–12.9 cal ka BP *(Schulz et al. 1998)*, and the Dole effect record around 13.0 cal ka BP *(Severinghaus et al. 2009)*,

which has been denoted as the B/A chronozone (Figure 6). This phase is followed by distinct colder and drier conditions on the southern Tibetan Plateau at 12.4–11.4 cal ka BP (unit 4). Contemporaneous reduced monsoon intensities are reported from the Bay of Bengal at 12.8–11.4 cal ka BP *(Rashid et al. 2011)*, in the Arabian Sea at 12.8–11.8 cal ka BP *(Schulz et al. 1998)*, and in the Dole effect record around 12.0 cal ka BP *(Severinghaus et al. 2009)* and identified as the YD chronozone. The subsequent rapid and significant increase in moisture availability on the southern Tibetan Plateau around 11.4 cal ka BP (unit 5) coincides with a monsoonal strengthening as shown in the Bay of Bengal at 11.0 cal ka BP *(Rashid et al. 2011)*, the Arabian Sea at 11.7 cal ka BP *(Schulz et al. 1998)*, and in the Dole effect record around 11.4 cal ka BP *(Severinghaus et al. 2009)*. Monsoon intensity recorded by the Dole effect record reaches its maximum at 9.8–9.4 cal ka BP *(Severinghaus et al. 2009)* matching the moistest conditions on the southern Tibetan Plateau. During the Mid- and Late Holocene, monsoon intensity records suggest stable or decreasing monsoon intensity with only minor amplitude variations *(Schulz et al. 1998, Severinghaus et al. 2009, Rashid et al. 2011; Figure 6)* similar to the conditions on the southern Tibetan Plateau.

Moisture availability on the southern Tibetan Plateau appears to be mainly synchronous to monsoon intensity as recorded in the Arabian Sea *(Schulz et al. 1998)*, the Bay of Bengal *(Rashid et al. 2011)*, and in the Dole effect record *(Severinghaus et al. 2009)*. Even though synchronicity of climatic events and shifts does not prove causality, a causal link between moisture availability on the southern Tibetan Plateau and the Asian summer monsoon is suggested based on the presented data. This implies that moisture availability on the southern Tibetan Plateau and

monsoon intensity in the Arabian Sea and the Bay of Bengal are likely governed by the same processes. As the increase of moisture availability on the southern Tibetan Plateau at around 16.0 cal ka BP coincides with increased monsoon intensity *(Schulz et al. 1998, Severinghaus et al. 2009, Rashid et al. 2011; Figure 6)*, it might probably reflect an initial influence of monsoonal precipitation on the southern Tibetan Plateau possibly caused by a rising summer insolation *(Berger and Loutre 1991)* (Figure 6). The rapid increase in moisture availability at around 11.4 cal ka BP corresponds to a maximum in summer insolation at Tangra Yumco *(Berger and Loutre 1991)*. The mid- to Late Holocene gradual decrease in precipitation also follows the declining summer insolation pattern *(Berger and Loutre 1991)* (Figure 6) implying that precipitation is probably controlled by changes in summer insolation as previously assumed for the monsoon domain *(Kutzbach 1981)*. As the evolution of moisture availability at Pumoyum Co *(Nishimura et al. 2014)* and Lake Qinghai *(An et al. 2012b)* is synchronous to the transect of Tangra Yumco, Nam Co, Tso Moriri, and Naleng Co, a homogenous monsoon pattern on the Tibetan Plateau is suggested. As indicated by climatic models and reanalysis data locally occurring peculiarities may probably be attributed to spatial differences in the annual cycle of precipitation, i.e. the amount of pre-monsoon or winter precipitation in different region of the Tibetan Plateau *(Dallmeyer et al. 2012, Maussion et al. 2014)*. Significant influences of pre-monsoon precipitation are nowadays occurring, for example, at Tso Moriri *(Mishra et al. 2015)* but cannot be assessed by our study. However, as all reviewed records generally show a similar pattern corresponding to monsoon intensity records a monsoon-like precipitation regime is suggested.

4.7 Conclusions

The initial onset of moist conditions at Tangra Yumco occurs at 16.0 cal ka BP, while maximum moisture is reached in the early Holocene and following a decreasing trend thereafter. A comparison to results from Naleng Co, Nam Co, and Tso Moriri suggest a generally synchronous precipitation pattern on the southern Tibetan Plateau. A nowadays observed east-west-moisture-gradient did apparently not result in a temporal shift of moisture variability. However, a spatial moisture gradient referring to the amount of moisture might be likely and could probably be revealed in future studies based on transfer functions utilizing pollen or microfossils. A homogenous precipitation regime on the entire Tibetan Plateau is indicated by a supraregional comparison to records in the southernmost (Pumoyum Co) and northernmost (Lake Qinghai) regions on the Tibetan Plateau. However, more systematical studies are urgently needed to investigate spatial and temporal climate evolution on the Tibetan Plateau and adjacent areas. Further, as implied by the synchronicity of moisture evolution on the southern Tibetan Plateau and monsoon intensity recorded in the source area of the monsoon, the precipitation regime on the southern Tibetan Plateau is primarily governed by monsoon-like processes.

CHAPTER 5 — Synthesis

5.1 Synthesis

Changes in moisture availability and the sedimentary response to catchment processes was thoroughly investigated by three studies conducted in the Tangra Yumco area. The initial study of a sediment core from the small TT Lake *(chapter 2)* assessed sedimentary dynamics, its controlling mechanisms, and catchment processes and thereby revealed that probably hydrologic events related to intense precipitation triggered event-related deposits (ERD). The deposition of ERD was apparently independent from the prevailing climatic conditions showing that hydrologic events could appear in all climatic settings arising in the Tangra Yumco region during the past.

The findings from TT Lake enabled the deciphering of sedimentary modes during the past 17.4 cal ka BP which are covered by the sediment record from Tangra Yumco *(chapter 4)*. The validated methods and criteria for ERD identification from TT Lake were employed at Tangra Yumco identifying eleven ERDs in the record that are probably also mostly triggered by hydrologic events. These ERDs including all associated data were removed from the Tangra Yumco record allowing the establishment of an event-corrected record. The multi-proxy approach *(chapter 4)* applied on the sedimentary record from Tangra Yumco proved to be useful to determine changes in moisture availability and allowed the establishment of a well-dated record going far back in time, which is generally scarce on the Tibetan Plateau. The different

analytical methods applied allowed a more comprehensive assessment of processes controlling proxies in the Tangra Yumco record. This was shown for example in the early Holocene when allochthonous clastic input loses correlation to grain size data indicating a dilution of the allochthonous clastic input by biologically induced carbonates complicating a straightforward interpretation and assessment of the prevailing conditions. Striking climatic features in the Tangra Yumco record are the aeolian input limited to the period prior to 17.1 cal ka BP, an increase in moisture availability at 16.0 cal ka BP, a rapid increase in moisture availability at the transition to the Holocene at 11.4 cal ka BP, and moistest conditions at 10.1-9.4 cal ka BP.

The comparison of these results to the quantitative reconstruction of lake level variations, based on OSL dating of currently exposed lacustrine sediments, recalculated cosmogenic nuclide ages, and previously published data, allowed a detailed assessment of lake level variations and revealed magnitude, timing, and pace of lake level changes as response to variations of moisture availability *(chapters 3 and 4)*. A rising lake level was recorded at 10.5 ka and a lake level highstand occurred prior to 8.5 ka. The lake level continuously dropped after 8.5 ka intercalated by a minor lake level rise starting at 2.1 ka. A recent ongoing lake level rise started at 0.3 ka. During the early Holocene, the lake level decline at 8.5 ka is indicated by recalculated cosmogenic nuclide ages but the onset of the lake level highstand prior to 8.5 ka could not be resolved by OSL and cosmogenic nuclide data. A refining of the lake level reconstruction in the early Holocene became possible by the combination of both Tangra Yumco data sets. The moistest conditions were recorded in the sedimentary record at 10.1-9.4 cal ka BP, while recalculated cosmogenic nuclide ages indicate

a falling lake level after 8.5 cal ka BP. The lake level apparently rose more quickly than suggested by the OSL based lake level reconstruction and reached a highstand of 181-183 m arll probably during moistest conditions at 10.1-9.4 cal ka BP (Figure 5.1).

5.2 Discussion

5.2.1 Tangra Yumco

Two previously published studies on lacustrine sediments from the Tangra Yumco catchment *(Long et al. 2012, Miehe et al. 2014)* are available for comparison with the Tangra Yumco sediment core and the lake level history. Results of these studies from the Tangra Yumco catchment *(Long et al. 2012, Miehe et al. 2014)* are generally in phase with Tangra Yumco records presented in this thesis. As successfully demonstrated by the OSL based lake level history and a study published by *Long et al. (2012)* facies identification based on bedding, grains size, and/or microfossils of exposed sedimentary profiles combined with dating of the respective facies can provide valuable information about lake levels changes. *Long et al. (2012)* found moist conditions at 7.6-2.3 ka in the Tangra Yumco catchment by dating exposed lacustrine sediments that are generally consistent with the Holocene lake level reconstruction in this study. Due to methodical uncertainties the ages of *Long et al. (2012)* may underestimate the true age and do not define the onset of moister conditions at Tangra Yumco *(Rades et al. 2013)*. Considering this underestimation, the onset of moister conditions of *Long et al. (2012)* might be synchronous with the onset of lacustrine deposition defined by the lake level reconstruction at 10.5 ka. The Targo Xian peat bog, located within the Tangra Yumco catchment, revealed climatic conditions similar to the pattern derived from the Tangra Yumco record in

this study. Moisture availability rapidly increases around 11.5 cal ka BP, is highest during the early Holocene, and declines around 8.0 cal ka BP *(Miehe et al. 2014)*. The established lake level history of Tangra Yumco allowed a refining of the lake level of Tangra Yumco changes previously proposed by *Miehe et al. (2014)*. According to their data the Targo Xian peat bog was flooded by Tangra Yumco at 11.1 cal ka BP until at least 2.6 cal ka BP. However, the reconstructed lake level history of Tangra Yumco suggests that the lake level of Tangra Yumco reached the Targo Xian peat bog initially around 10.0 cal ka BP and retreated from this site as early as approximately 7-6 cal ka BP. Probably a small pond or lake persisted at the peat bog site indicating prolonged lacustrine conditions *(Rades et al. 2013)*.

5.2.2 The southern Tibetan Plateau

This thesis evaluates and compares the results from the easternmost lake of the east-west-transect Nam Co *(Kasper et al. 2012, Kasper et al. 2013, Doberschütz et al. 2014, Kasper et al. 2015)* and the central lake Tangra Yumco *(chapter 4)* for the first time and provides implications for the variability of moisture availability on the southern Tibetan Plateau. As investigations on Taro Co, the westernmost lake on the east-west-transect, are currently in progress, the east-west-transect was extended by recently published data from lake Tso Moriri further to the west *(Mishra et al. 2015)* and Naleng Co further to the east *(Opitz et al. 2015)*.

All four records, Tangra Yumco, Nam Co *(Kasper et al. 2015)*, Tso Moriri *(Mishra et al. 2015)*, and Naleng Co *(Opitz et al. 2015)* generally show a similar climatic pattern, whereas Tangra Yumco, Nam Co, and Tso Moriri also record a synchronous rise in temperature at around 17.1 cal ka BP (Figure 5.1). All records reveal a moisture and

temperature peak at around 13.6-12.4 cal ka BP, drier and colder conditions at around 12.4-11.4 cal ka BP, sharply increasing moisture availability at the transition to the Holocene around 11.4 cal ka BP, and moistest conditions during the early Holocene followed by a gradual decrease in moisture availability thereafter *(Kasper et al. 2015, Mishra et al. 2015, Opitz et al. 2015)*. Lake level of Tangra Yumco and Nam Co are both constantly rising since 0.3 cal ka BP *(Kasper et al. 2015)*. More moisture became available around 16.0 cal ka BP at Tangra Yumco and Nam Co, whereas this signal is indistinct and fuzzy at Tso Moriri and occurs later at Naleng Co (Figure 5.1). The chronologies of Tso Moriri and Naleng Co have a different resolution than chronologies of Tangra Yumco and Nam Co especially in the Late Glacial what might complicate the comparison of the records during that time. Hence, inconsistencies between the records from Naleng Co and Tso Moriri with those from Tangra Yumco and Nam Co at around 16.0 cal ka BP might be attributed to the differences in the chronological resolution.

Despite the apparent similarities of the records on the southern Tibetan Plateau, reanalysis data *(Maussion et al. 2014)* and the ECHAM5/JSBACH climate model *(Dallmeyer et al. 2012)* revealed differences in the past availability of moisture and the annual cycle of precipitation. Reanalysis data covering the period AD 2000–2011 indicate that the decadal seasonal mean of precipitation shows a strong east-west-gradient in summer rainfall (JJA) with more precipitation in west than is the east *(Maussion et al. 2014, Biskop et al. 2015)*. This gradient in moisture availability was also observed during field campaigns showing a decrease in moisture availability from Nam Co in the east to Taro Co in the west as indicated by sparser vegetation and dune formation closer to Taro Co *(T. Haberzettl, personal*

communication). As all records shown here only provide data that indicate a relative change in moisture availability over time (except for Naleng Co), it cannot be assessed if a similar gradient existed in the past. Moreover, all sites are currently affected by summer precipitation, but Tso Moriri additionally receives a significant amount of winter precipitation *(Maussion et al. 2014)*. This winter precipitation regime cannot be traced further back in time as an impact on the hydrological budget cannot be assessed with the parameters used in this study *(Mishra et al. 2015)*. The data of the ECHAM5/JSBACH climate model showed differences in moisture availability in the regions of the Tangra Yumco, Nam Co, Tso Moriri, and Naleng Co regions during mid- to Late Holocene *(Dallmeyer et al. 2012)*. While Tangra Yumco and Nam Co received more moisture during the mid-Holocene than today, regions of Tso Moriri and Naleng Co were drier than today *(Dallmeyer et al. 2012)*. These results agree with sedimentary records from Tangra Yumco and Nam Co *(Kasper et al. 2015)* but do not agree with records from Tso Moriri *(Mishra et al. 2015)* and Naleng Co *(Opitz et al. 2015)*.

While the long-term trend appears to be similar on the southern Tibetan Plateau, minor short-term differences between the records could possibly represent local peculiarities attributed to temporary differences in the annual cycle of precipitation. While the moisture availability in the Tangra Yumco record gradually decreases during the mid- to Late Holocene *(chapters 3 and 4)*, the variability of moisture availability was markedly higher in Nam Co during this period *(Kasper et al. 2015)*. Pumoyum Co shows an increase in moisture availability at 4.5-2.5 cal ka BP that was not recorded elsewhere *(Nishimura et al. 2014)*. These differences might result from local differences in the precipitation regime *(Nishimura et al. 2014)* and probably represent

deviations from the synchronous long-term trend of the records.

5.2.3 The precipitation regime on the Tibetan Plateau

As the impact of water recycling and pre-monsoon (spring) precipitation was recently under discussion *(Dallmeyer et al. 2012, Maussion et al. 2014)*, a thorough assessment of the monsoonal impact on the study sites is of crucial importance because a significant amount of pre-monsoon precipitation or water recycling may alter the pattern of moisture availability and lead to misinterpretations concerning the climatic development. Most studies equal moisture availability on the Tibetan Plateau with monsoonal precipitation without defining the prevailing precipitation process but lack a seasonal resolution to actually determine season-related climate events such as monsoonal precipitation *(e.g., Morrill et al. 2006, Daut et al. 2010, Dietze et al. 2013, Miehe et al. 2014)*. As the data presented here also lack a seasonal resolution and cannot reveal the annual cycle of precipitation, a comparison of the records from the southern Tibetan Plateau to records of monsoon intensity from the Indian Ocean *(Schulz et al. 1998, Rashid et al. 2011)* as well as a Dole effect record *(Severinghaus et al. 2009)* systematically assessed the monsoonal impact on past variations of moisture availability on the southern Tibetan Plateau. The Dole effect describes the different isotopic composition of sea water and the atmospheric water and is primarily governed by the African and Asian monsoonal strength *(Severinghaus et al. 2009)*.

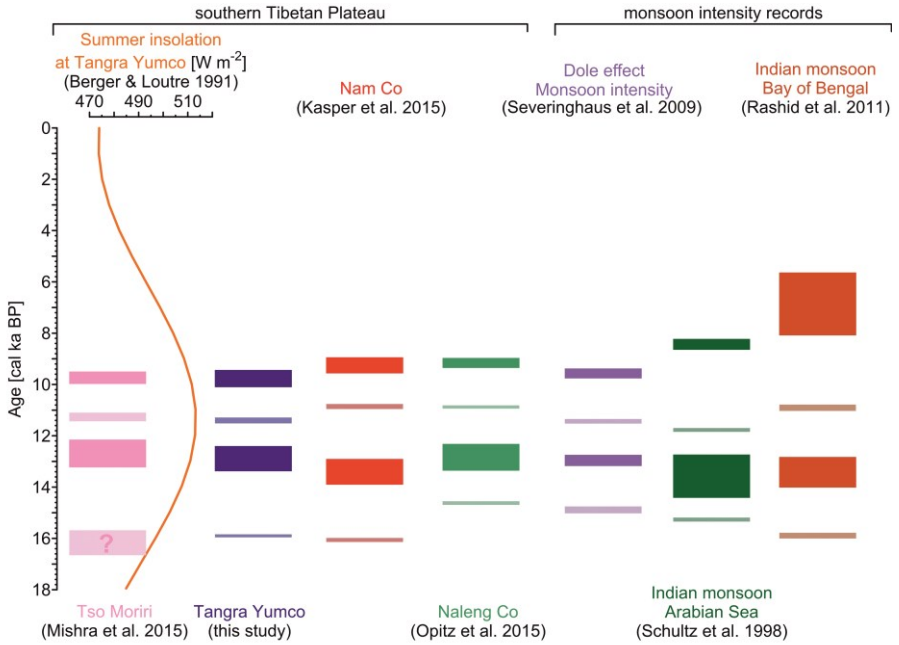

Figure 5.1: Comparison of moisture availability on the southern Tibetan Plateau with monsoon intensity records from the source area of the monsoon and summer insolation. Indicated is high or highest moisture availability (darker bars) and increasing moisture availability (light bars). The comparison reveals a generally synchronous pattern of moisture availability. An increase in moisture availability around 16 cal ka BP at Tso Moriri is not clearly defined (question mark).

The comparison revealed that the most pronounced features of the records from the southern east-west-transect occur synchronous with the monsoon intensity records. The moisture availability rose synchronously around 16.0 cal ka BP (indistinct at Tso Moriri and delayed in Naleng Co). Moisture availability and temperature were higher at around 13.6-12.4 cal ka BP followed by drier and colder condition until 11.4 cal ka BP, and a sharp increase in moisture availability thereafter *(chapter 4; Schulz et al. 1998, Severinghaus et al. 2009, Rashid et al. 2011, Kasper et al. 2015, Mishra et al. 2015, Opitz et al. 2015)*. The rapid increase in moisture availability on the southern Tibetan Plateau coincides with highest summer insolation, and the general pattern of both through time match *(Berger and Loutre 1991)*. This is in accordance with

observations of *Maussion et al. (2014)* who showed that the southern-central Tibetan Plateau, where Tangra Yumco and Nam Co are located, is controlled by a summer precipitation regime, i.e., monsoon today.

The increase in moisture availability at around 16.0 cal ka BP probably represents a first pulse of monsoonal influence on the southern Tibetan Plateau. Similar inferences are also indicated by palynological analysis on the Nam Co record. A significant change in the pollen assemblage at 16.5 cal ka BP suggests a shift in the prevailing wind direction *(L. Zhu, personal communication)*. This change in wind direction is interpreted as a modification of the controlling atmospheric circulation and a change from westerly to monsoonal influence *(L. Zhu, personal communication)*.

A comparison of the southern (Tangra Yumco, Nam Co, Tso Moriri, and Naleng Co) east-west-transect with the northern (Donggi Cona and Lake Heihai) east-west-transect was supposed to reveal implications for the precipitation regime on the entire Tibetan Plateau and has been one of the major aims of the *TiP* research projects. However, until now, this comparison does not allow a final conclusion about a synchronicity of moisture development on the northern and southern Tibetan Plateau as results from Donggi Cona, the eastern lake of the northern east-west-transect, are not straightforward. Results from a multi-proxy record indicate deglaciation after around 19.0 cal ka BP, cold and dry condition during the Younger Dryas chronozone, a moist early to mid-Holocene, and an aridification thereafter *(Opitz et al. 2012)*. These results are well in phase with the southern east-west-transect suggesting that moisture availability evolved synchronously on the northern and southern Tibetan Plateau and that this moisture availability is governed by the same precipitation processes, most likely linked to monsoon. In contrast,

results from ostracod analyses from Donggi Cona indicate drier condition in the early Holocene and wettest condition after 6.8 cal ka BP *(Mischke et al. 2010a)* and do not correspond to the southern east-west-transect. This would imply a rather asynchronous development of moisture availability or that moisture availability on the northern Tibetan Plateau is probably not controlled by the same precipitation processes as on the southern Tibetan Plateau. However, as suggested by a climate model and reanalysis data influences of different monsoon regimes such as the Indian and the East Asian monsoon or significant amounts of water recycling and pre-monsoon precipitation may probably alter the hydrological budget of a specific study site and complicate climatic reconstructions *(Dallmeyer et al. 2012, Maussion et al. 2014)*. Donggi Cona, for instance, is located in a region where the climate model of *Dallmeyer et al. (2012)* assessed drier conditions in the mid-Holocene (6 ka) compared to the present-day situation due to an East Asian monsoon influence matching the results of the ostracod analysis *(Mischke et al. 2010a)*. This is in contrast to the findings presented in this thesis, as on the southern Tibetan Plateau the mid-Holocene was apparently moister than present-day conditions and an exclusive control of the Indian monsoon is indicated *(Dallmeyer et al. 2012)*.

Lake Heihai, the western lake of the northern east-west-transect, shows moist conditions during the early Holocene synchronous to the southern east-west-transect. The rising lake levels after 3 cal ka BP are not observed on the southern Tibetan Plateau suggesting a rather different controlling mechanism of moisture availability *(G. Lockot, personal communication)*. Rising lake levels after 3 cal ka BP at Lake Heihai could possibly either represent a local peculiarity resulting from a site-specific annual cycle of precipitation or a distinct different

precipitation regime after 3 cal ka BP. Wet conditions in the late Holocene were also observed at the lakes Bosten and Balikun, north of Lake Heihai, and were attributed to westerly wind influence *(Huang et al. 2009, An et al. 2012a)*. This is possibly suggesting that a distinct different precipitation regime from the southern Tibetan Plateau, particularly westerly circulation, is prevailing in this region after 3 cal ka BP. As monsoonal and westerly winds are in anti-phase relationship dependent on their individual strength *(An et al. 2012b)*, Lake Heihai might have been under monsoonal influence during the early Holocene when monsoonal influence was strongest and its northward extension maximal. In the late Holocene, on the contrary, the lake might have been under reinforced westerly dominance as a result of the weakened monsoon with a reduced extension due to a decreased summer insolation *(Berger and Loutre 1991)*. These mechanisms controlling the moisture availability in the Lake Heihai region might explain the differences to the climate pattern on the southern Tibetan Plateau during the mid- to Late Holocene.

5.3 Conclusions

5.3.1 Tangra Yumco

This thesis is part of the southern east-west-transect of *TiP* investigating lake Tangra Yumco and its catchment processes in three individual studies. The synthesis of these three studies allowed a better understanding of climatic processes prevailing in the Tangra Yumco area and of the variations of moisture availability during the past 17.4 cal ka BP and its impact on the lake levels changes. Results from the sediments from TT Lake were transferable to the record from Tangra Yumco and helped to decipher sedimentary dynamics in the Tangra

Yumco long core during the past 17.4 cal ka BP. The combination of sediment records with shoreline investigations allowed a detailed assessment of the lake level history of Tangra Yumco. The long core study further refined the early Holocene lake level highstand that was determined based on recalculated cosmogenic nuclide ages highlighting the value of this multi-proxy and multi-dating approach. This record is suitable for comparison to other records along the east-west-transect on the southern Tibetan Plateau.

5.3.2 The southern Tibetan Plateau

The results of the comparison of the records from the east-west-transect on the southern Tibetan Plateau indicate a synchronous pattern of moisture availability on the southern Tibetan Plateau. These results contribute to the controversial discussions about the spatial and temporal variability of moisture availability. Presented results support a synchronous spatial pattern of moisture availability on the southern Tibetan Plateau that was suggested previously. If the observed modern east-west-gradient in available moisture prevailed also during the past, it has apparently had no impact on the synchronicity of the records. Even though the magnitude of changes in moisture availability might have been different, their timing was not. The systematic study of several lacustrine systems along the east-west-transect on the southern Tibetan Plateau proved to be a target-aimed and reasonable research approach.

5.3.3 The precipitation regimes on the Tibetan Plateau

The major climatic features appear synchronous on the southern Tibetan Plateau and in the monsoon intensity records. This correspondence of the records suggests a similar dominating precipitation process.

Therefore, it can be assumed that monsoonal or monsoon-related precipitation contributed the major amount to the total annual precipitation on the Tibetan Plateau. Water recycling as well as pre-monsoon precipitation seem to be negligible in the hydrological budget of the studied sites. The comparison of the records from the east-west-transect to the monsoon intensity records demonstrates an easy approach to assess the influence of monsoonal precipitation on the annual cycle of precipitation on a certain study site. The coincidence of the pattern of moisture availability and the summer insolation probably indicates that summer insolation is the main controlling factor on the precipitation regime.

The comparison to the northern east-west-transect is complicated. Inconsistencies between studies from Donggi Cona demonstrate the necessity to carefully assess the prevailing precipitation regime and the impact of recycling and pre-monsoon precipitation. A comparison of Lake Heihai and the southern Tibetan Plateau suggests that the same precipitation process, most likely monsoon-related, prevailed before approximately 3 cal ka BP at both sites. After 3 cal ka BP, however, monsoon-related processed prevailed on the southern Tibetan Plateau, while the area of Lake Heihai was possibly controlled by the westerly winds. The comparison of the southern and northern Tibetan Plateau reveals valuable information about the spatial limit of the monsoon-related precipitation regime. However, a straightforward association to a specific precipitation regime seems to be more difficult in the marginal regions of the Tibetan Plateau than in the core regions such as the Tangra Yumco and Nam Co areas.

5.4 Outlook and future research

5.4.1 Extension of the multi-proxy data set for Tangra Yumco

Biomarker analyses were successfully applied on the sedimentary records from Nam Co *(e.g., Günther et al. 2011, Günther et al. 2015)* showing that compound-specific δD values of sedimentary *n*-alkanes primarily record evapotranspiration and relative humidity *(Günther et al. 2011)*. Evapotranspiration cannot be assessed with methods used in this thesis. However, as biomarker analyses on the sedimentary record from Tangra Yumco are currently in progress, these data will provide valuable additional information about the environmental response to temperature and solar radiation.

A change in moisture availability at Tangra Yumco at around 16.0 cal ka BP may probably represent a change in the atmospheric circulation as observed at Nam Co *(L. Zhu, personal communication)*. This hypothesis is supported by the presented data, and further research needs to assess this change in moisture availability more precisely. For this purpose a high-resolution palynological analysis on the Tangra Yumco long record is currently in progress performed by Qingfeng Ma (Key Laboratory of Tibetan Environment Changes and Land Surface Processes, Institute of Tibetan Plateau Research, Chinese Academy of Sciences, China). It is aimed to reveal a potential change in the wind direction indicated by a change in the pollen assemblage as it occurs at Nam Co at 16.5 cal ka BP *(L. Zhu, personal communication)* which is in the same timeframe as at Tangra Yumco.

5.4.2 Quantitative reconstructions of moisture availability on the southern Tibetan Plateau

To distinguish a possible spatial east-west-gradient in moisture availability in the past, quantitative estimates of precipitation or other environmental parameters are necessary. Transfer functions based on pollen *(e.g., Herzschuh et al. 2014)* or ostracods *(e.g., Frenzel et al. 2010)* or multi-proxy data sets *(e.g., Giralt et al. 2011)* should be applied to quantitatively assess the differences in moisture availability in future works. Although climate reconstructions based on pollen can be biased, if anthropogenic activity modified the past vegetation pattern, pollen-based transfer functions of suitable records provide a good estimation of quantitative amounts of precipitation *(Herzschuh et al. 2014)*. Quantitative reconstruction of lake level or precipitation can assess the magnitude of the monsoonal impact and absolute changes in precipitation as recently demonstrated with a pollen transfer function applied on pollen from Naleng Co by *Opitz et al. (2015)*.

5.4.3 Spatial and temporal extension of the southern east-west-transect

Efforts should be undertaken to complete the east-west-transect and to extent it temporally and spatially. Preliminary results from Taro Co show a decrease in moisture availability after 7.4 cal ka BP *(unpublished data)* which is in phase with recently published palynological data *(Ma et al. 2014)*. In 2014 colleagues from the Key Laboratory of Tibetan Environment Changes and Land Surface Processes, Institute of Tibetan Plateau Research, Chinese Academy of Sciences, China retrieved two paired parallel cores from the profundal zone of Taro Co. The composite record is about 12 m long and a basal radiocarbon age of this sediment

core is 27 cal ka BP *(J. Wang, personal communication)*. This record is a promising basis for completing the east-west-transect and will further contribute to a detailed picture of spatial changes of moisture availability on the southern Tibetan Plateau.

A spatial extension of the east-west-transect into arid central Asia in the west and the Chinese or Southeast Asian lowlands would allow to further investigate the monsoon-westerly interaction and the relationship and variability of the Indian and the East Asian monsoon systems. This would be helpful for unraveling which climatic records may have been influenced by the East Asian monsoon or by both monsoon domains in the past.

A temporal extension of the records from the southern Tibetan Plateau would allow valuable insights of monsoonal development during a glacial-interglacial cycle. A recently conducted seismic survey on Nam Co suggests that this lake is filled with more than 800 m of sediments as no acoustic basement was detected down to this depth *(Haberzettl 2015)*. These sediments could possibly represent the past 460 to 1.900 ka as indicated by an extrapolation of the known sediment accumulation rates of the past 24 cal ka BP *(Haberzettl 2015)*. As these first results suggest Nam Co is a suitable archive for an International Continental Drilling Program (ICDP) campaign a workshop proposal was submitted to the ICDP in January, 2015.

5.4.4 Comparison of southern and northern east-west-transect

A more detailed comparison of the northern and southern east-west-transect should be pursued in future. The preliminary comparison conducted in this thesis provides first promising results that imply a change in the precipitation in the Lake Heihai area, whereas the

southern Tibetan Plateau is constantly controlled by the same precipitation regime. A more detailed investigation about a potential movement of the monsoonal limit on the northern Tibetan Plateau would allow for a more detailed understanding of the forcing mechanisms of the monsoon extension and intensity.

5.4.5 Understanding of the annual cycle of precipitation

A higher temporal resolution of the data sets would allow for a more detailed assessment of short-term climatic fluctuations superimposed by the long-term trend as well as an improved understanding of the annual cycle of precipitation. Until now the knowledge about the impact of recycling and pre-monsoon precipitation on the hydrological budget on the Tibetan Plateau is very limited. There are only few archives that can provide a subseasonal resolution to allow insights in the annual cycle of precipitation on the Tibetan Plateau but there are efforts to access archives with subseasonal resolution such as varved lake sediments *(e.g., Zhang et al. 2010, Chu et al. 2011)*, tree-rings *(e.g., Bräuning 2006, Shao et al. 2010)*, and skeletal remains of animals *(Wang et al. 2008, Taft et al. 2012)*. However, the complexity of the annual cycle of precipitation and its spatial extent highlights the necessity to include the pre-monsoon season into climate reconstructions *(Dallmeyer et al. 2012)* that is difficult to realize in studies using the common archives as the temporal resolution is too low. While XRF data from Tangra Yumco partly provide annual resolution, CNS data, for example, have a rather bicentennial resolution. However, since CNS samples integrate over at least 1 cm sediment thickness in this study, the potential resolution has also been limited by methodical constrains. The complexity might be, most properly assessed by climate models and reanalysis data. More

climate models and reanalysis data sets are needed to better understand cause and effect of variability on the annual cycle of precipitation and improve the reliability of climatic predictions. Models such as an atmosphere-only general circulation model (ECHAM5) have been used to simulate the Indian monsoon through time on a interannual to multi-decadal timescale *(Polanski et al. 2013)*. The validity of this model is monitored by a comparison to paleoclimate reconstructions based on various proxies obtained from sedimentary records highlighting the importance of establishing well-dated long-term climate records like the Tangra Yumco record.

5.4.6 Moisture transport

Unlike previously assumed *(e.g., Tian et al. 2001, Herzschuh et al. 2014)* reanalysis data show that the moisture transport from the Bay of Bengal is blocked by the Himalayan mountains and redirected northeastwards and not directly transported to the Tibetan Plateau *(Maussion et al. 2014)*. Thus, the sources of monsoonal air masses and the transport route are unknown and to further understand monsoonal dynamics a determination and tracking of the transport pathways of monsoonal air masses is obligatory by e.g., climate models.

5.4.7 Improvement of understanding of the proxies

Uncertain chronologies and a poor understanding of the proxies *(Mischke et al. 2010b, Opitz et al. 2015)* may result in misinterpretation. In this manner, the multi-dating approach of Tangra Yumco and Nam Co proved to be a suitable method. As valid chronologies are a crucial precondition for climate reconstruction *(Mischke et al. 2013, Haberzettl 2015)* more effort should be spent on this. Studies like the recently published

assessment of controlling mechanisms on sediment distribution pattern of Nam Co *(Wang et al. 2015)* provide an understanding of the proxies used for climatic reconstruction and should be applied more often prior to data interpretation to avoid misinterpretation. This study was conducted within the project "Central Asian Climate Dynamics – *CADY*", funded by the Federal Ministry of Education and Research of Germany (BMBF). *CADY* is the first step towards a systematic monitoring of Tibetan lakes to reveal sedimentary processes helping to facilitate proxy interpretation. Supported by the recovery of additional sediment surface samples two morings equipped with sequential sediment traps, thermistors, and two multiprobes at the top and bottom were installed at Nam Co in order to follow seasonal climatic variations affecting the water column and sediment deposition.

References

Ahlborn M, Haberzettl T, Wang J, Alivernini M, Schlütz F, Schwarz A, Su Y, Frenzel P, Daut G, Zhu L, and Mäusbacher R, 2015a: Sediment dynamics and hydrologic events affecting small lacustrine systems on the southern-central Tibetan Plateau – the example of TT Lake. *The Holocene,* 25: 508-522.

Ahlborn M, Haberzettl T, Wang J, Fürstenberg S, Mäusbacher R, Mazzocco J, Pierson J, Zhu L, and Frenzel P, 2015b: Holocene lake level history of the Tangra Yumco lake system, southern-central Tibetan Plateau. *The Holocene*.

Ahmad N, 1974: *Ground water Resources of Pakistan.* Lahore.

Akita LG, Frenzel P, Haberzettl T, Kasper T, Wang J, and Reicherter K, 2015: Ostracoda (Crustacea) as indicators of subaqueous mass movements: An example from the large brackish lake Tangra Yumco on the southern Tibetan Plateau, China. *Palaeogeography, Palaeoclimatology, Palaeoecology,* 419: 60-74.

An C-B, Lu Y, Zhao J, Tao S, Dong W, Li H, Jin M, and Wang Z, 2012a: A high-resolution record of Holocene environmental and climatic changes from Lake Balikun (Xinjiang, China): Implications for central Asia. *The Holocene,* 22: 43-52.

An Z, Porter SC, Kutzbach JE, Wu X, Wang S, Liu X, Li X, and Zhou W, 2000: Asynchronous Holocene optimum of the East Asian monsoon. *Quaternary Science Reviews,* 19: 743-762.

An Z, Kutzbach JE, Prell WL, and Porter SC, 2001: Evolution of Asian monsoons and phased uplift of the Himalaya-Tibetan plateau since Late Miocene times. *Nature,* 411: 62-66.

An Z, Colman SM, Zhou W, Li X, Brown ET, Jull AJT, Cai Y, Huang Y, Lu X, Chang H, Song Y, Sun Y, Xu H, Liu W, Jin Z, Liu X, Cheng P, Liu Y, Ai L, Li X, Liu X, Yan L, Shi Z, Wang X, Wu F, Qiang X, Dong J, Lu F, and Xu X, 2012b: Interplay between the Westerlies and Asian monsoon recorded in Lake Qinghai sediments since 32 ka. *Scientific Reports,* 2: 1-7.

Bard E, Rostek F, Turon J-L, and Gendreau S, 2000: Hydrological impact of Heinrich events in the subtropical northeast Atlantic. *Science,* 289: 1321-1324.

Berger A, and Loutre MF, 1991: Insolation values for the climate of the last 10 million years. *Quaternary Science Reviews,* 10: 297-317.

Biskop S, Maussion F, Krause P, and Fink M, 2015: What are the key drivers of regional differences in the water balance on the Tibetan Plateau? *Hydrology & Earth System Sciences Discussions,* 12: 4271–4314.

Blott SJ, and Pye K, 2001: GRADISTAT: A grain size distribution and statistics package for the analysis of unconsolidated sediments. *Earth surface processes and Landforms,* 26: 1237-1248.

Bräuning A, 2006: Tree-ring evidence of 'Little Ice Age' glacier advances in southern Tibet. *The Holocene,* 16: 369-380.

Broccoli AJ, and Manabe S, 1992: The Effects of Orography on Midlatitude Nortern Hemisphere Dry Climates. *Journal of Climate,* 5: 1181-1201.

Brown SL, Bierman PR, Lini A, and Southon J, 2000: 10 000 yr record of extreme hydrologic events. *Geology,* 28: 335-338.

Brunschön C, Haberzettl T, and Behling H, 2010: High-resolution studies on vegetation succession, hydrological variations, anthropogenic impact and genesis of a subrecent lake in southern Ecuador. *Vegetation History and Archaeobotany,* 19: 191-206.

Chen F, Yu Z, Yang M, Ito E, Wang S, Madsen DB, Huang X, Zhao Y, Sato T, Birks HJB, Boomer I, Chen J, An C, and Wünnemann B, 2008: Holocene moisture evolution in arid central Asia and its out-of-phase relationship with Asian monsoon history. *Quaternary Science Reviews,* 27: 351-364.

Chen Y, Zong Y, Li B, Li S, and Aitchison JC, 2013: Shrinking lakes in Tibet linked to the weakening Asian monsoon in the past 8.2 ka. *Quaternary Research,* 80: 189-198.

Chu G, Sun Q, Yang K, Li A, Yu X, Xu T, Yan F, Wang H, Liu M, Wang X, Xie M, Lin Y, and Liu Q, 2011: Evidence for decreasing South Asian summer monsoon in the past 160 years from varved sediment in Lake Xinluhai, Tibetan Plateau. *Journal of Geophysical Research: Atmospheres,* 116: 1-11.

Croudace IW, Rindby A, and Rothwell RG, 2006: ITRAX: description and evaluation of a new multi-function X-ray core scanner. In: Rothwell RG (ed) *New Techniques in Sediment Core Analysis.* Geological Society, London, Special Publications, 51-63.

Dallmeyer A, Claussen M, Wang Y, and Herzschuh U, 2012: Spatial variability of Holocene changes in the annual precipitation pattern: a model-data synthesis for the Asian monsoon region. *Climate Dynamics,* 40: 2919-2936.

Daut G, Mäusbacher R, Baade J, Gleixner G, Kroemer E, Mügler I, Wallner J, Wang J, and Zhu L, 2010: Late Quaternary hydrological changes inferred from lake level fluctuations of Nam Co (Tibetan Plateau, China). *Quaternary International,* 218: 86–93.

Dietze E, Hartmann K, Diekmann B, IJmker J, Lehmkuhl F, Opitz S, Stauch G, Wünnemann B, and Borchers A, 2012: An end-member algorithm for deciphering modern detrital processes from lake sediments of Lake Donggi Cona, NE Tibetan Plateau, China. *Sedimentary Geology,* 243–244: 169-180.

Dietze E, Wünnemann B, Hartmann K, Diekmann B, Jin H, Stauch G, Yang S, and Lehmkuhl F, 2013: Early to mid-Holocene lake high-stand sediments at Lake Donggi Cona, northeastern Tibetan Plateau, China. *Quaternary Research,* 79: 325-336.

Dietze E, Maussion F, Ahlborn M, Diekmann B, Hartmann K, Henkel K, Kasper T, Lockot G, Opitz S, and Haberzettl T, 2014: Sediment transport processes across the Tibetan Plateau inferred from robust grain-size end members in lake sediments. *Climate of the Past,* 10: 91-106.

Ding Y, 2007: The Variability of the Asian Summer Monsoon. *Journal of the Meteorological Society of Japan,* 85B: 21-54.

Doberschütz S, Frenzel P, Haberzettl T, Kasper T, Wang J, Zhu L, Daut G, Schwalb A, and Mäusbacher R, 2014: Monsoonal forcing of Holocene paleoenvironmental change on the central Tibetan Plateau inferred using a sediment record from Lake Nam Co (Xizang, China). *Journal of Paleolimnology,* 51: 253-266.

Dong J, Wang Y, Cheng H, Hardt B, Edwards RL, Kong X, Wu J, Chen S, Liu D, Jiang X, and Zhao K, 2010: A high-resolution stalagmite record of the Holocene East Asian monsoon from Mt Shennongjia, central China. *The Holocene,* 20: 257-264.

Feng Z-D, An CB, and Wang HB, 2006: Holocene climatic and environmental changes in the arid and semi-arid areas of China: a review. *The Holocene,* 16: 119-130.

Frenzel P, Wrozyna C, Xie M, Zhu L, and Schwalb A, 2010: Palaeo-water depth estimation for a 600-year record from Nam Co (Tibet) using an ostracod-based transfer function. *Quaternary International,* 218: 157-165.

Gadgil S, Vinayachandran PN, Francis PA, and Gadgil S, 2004: Extremes of the Indian summer monsoon rainfall, ENSO and equatorial Indian Ocean oscillation. *Geophysical Research Letters,* 31: 1-4.

Gain AK, and Giupponi C, 2015: A dynamic assessment of water scarcity risk in the Lower Brahmaputra River Basin: An integrated approach. *Ecological Indicators,* 48: 120-131.

Gasse F, Arnold M, Fontes JC, Fort M, Gibert E, Huc A, Li B, Li Y, Liu Q, Mélières F, Van Campo E, Wang F, and Zhang Q, 1991: A 13,000-year climate record from western Tibet. *Nature,* 353: 742-745.

Giralt S, Rico-Herrero MT, Vega JC, and Valero-Garcés BL, 2011: Quantitative climate reconstruction linking meteorological, limnological and XRF core scanner datasets: the Lake Sanabria case study, NW Spain. *Journal of Paleolimnology,* 46: 487-502.

Goswami BN, 2005: South Asian monsoon. In: Lau WKM and Waliser DE (eds) *Intraseasonal Variability in the Atmosphere-Ocean Climate System.* Springer, Berlin Heidelberg, 19-61.

Günther F, Mügler I, Mäusbacher R, Daut G, Leopold K, Gerstmann UC, Xu B, Yao T, and Gleixner G, 2011: Response of δD values of sedimentary *n*-alkanes to variations in source water isotope signals and climate proxies at lake Nam Co, Tibetan Plateau. *Quaternary International,* 236: 82-90.

Günther F, Witt R, Schouten S, Mäusbacher R, Daut G, Zhu L, Xu B, Yao T, and Gleixner G, 2015: Quaternary ecological responses and impacts of the Indian Ocean Summer Monsoon at Nam Co, Southern Tibetan Plateau. *Quaternary Science Reviews,* 112: 66-77.

Gupta AK, Anderson DM, and Overpeck JT, 2003: Abrupt changes in the Asian southwest monsoon during the Holocene and their links to the North Atlantic Ocean. *Nature,* 421: 354-357.

Haberzettl T, Fey M, Lücke A, Maidana N, Mayr C, Ohlendorf C, Schäbitz F, Schleser GH, Wille M, and Zolitschka B, 2005: Climatically induced lake level changes during the last two millennia as reflected in sediments of Laguna Potrok Aike, southern Patagonia (Santa Cruz, Argentina). *Journal of Paleolimnology,* 33: 283-302.

Haberzettl T, Anselmetti FS, Bowen SW, Fey M, Mayr C, Zolitschka B, Ariztegui D, Mauz B, Ohlendorf C, Kastner S, Lücke A, Schäbitz F, and Wille M, 2009: Late Pleistocene dust deposition in the Patagonian steppe - extending and refining the paleoenvironmental and tephrochronological record from Laguna Potrok Aike back to 55 ka. *Quaternary Science Reviews,* 28: 2927-2939.

Haberzettl T, 2015: *Advances in Limnogeology and Paleolimnology with a special focus on corroborated chronologies using paleomagnetic secular variations*. Habilitation thesis, Friedrich Schiller University Jena.

Haberzettl T, Henkel K, Kasper T, Ahlborn M, Su Y, Wang J, Appel E, St-Onge G, Stoner J, Daut G, Zhu L, and Mäusbacher R, 2015: Independently dated paleomagnetic secular variation records from the Tibetan Plateau. *Earth and Planetary Science Letters,* 416: 98-108.

Håkanson L, and Jansson M, 2002: *Principles of Lake Sedimentology.* The Blackburn Press, New Jersey.

He Y, Theakstone WH, Zhang Z, Zhang D, Yao T, Chen T, Shen Y, and Pang H, 2004: Asynchronous Holocene climatic change across China. *Quaternary Research,* 61: 52– 63.

Henkel K, Haberzettl T, St-Onge G, Ahlborn M, Daut G, Wang J, Mäusbacher R, and Zhu L, revised: High-resolution paleomagnetic and sedimentological investigations on the Tibetan Plateau for the past 15.8 ka cal BP - the Tangra Yumco record. *Geochemistry, Geophysics, Geosystems*.

Henkel K, Haberzettl T, Miehe S, Ahlborn M, Dietze E, Daut G, and Mäusbacher R, subm.: An early Holocene monsoon driven lake level high stand inferred from a sediment core in the Tangra Yumco basin, central Tibetan Plateau. *Journal of Paleolimnology*.

Herzschuh U, 2006: Palaeo-moisture evolution in monsoonal Central Asia during the last 50,000 years. *Quaternary Science Reviews,* 25: 163–178.

Herzschuh U, Borkowski J, Schewe J, Mischke S, and Tian F, 2014: Moisture-advection feedback supports strong early-to-mid Holocene monsoon climate on the eastern Tibetan Plateau as inferred from a pollen-based reconstruction. *Palaeogeography, Palaeoclimatology, Palaeoecology,* 402: 44-54.

Holmes JA, Cook ER, and Yang B, 2009: Climate change over the past 2000 years in Western China. *Quaternary International,* 194: 91–107.

Huang XZ, Chen FH, Fan YX, and Yang ML, 2009: Dry late-glacial and early Holocene climate in arid central Asia indicated by lithological and palynological evidence from Bosten Lake, China. *Quaternary International,* 194: 19-27.

IJmker J, Stauch G, Hartmann K, Diekmann B, Dietze E, Opitz S, Wünnemann B, and Lehmkuhl F, 2012: Environmental conditions in the Donggi Cona lake catchment, NE Tibetan Plateau, based on factor analysis of geochemical data. *Journal of Asian Earth Sciences,* 44: 176–188.

Immerzeel WW, van Beek LPH, and Bierkens MFP, 2010: Climate Change Will Affect the Asian Water Towers. *Science,* 328: 1382-1385.

Immerzeel WW, and Bierkens MFP, 2012: Asia's water balance. *Nature Geoscience,* 5: 841-842.

Jian J, Webster PJ, and Hoyos CD, 2009: Large-scale controls on Ganges and Brahmaputra river discharge on intraseasonal and seasonal time-scales. *Quarterly Journal of the Royal Meteorological Society,* 135: 353-370.

Jin Z-D, Wu Y, Zhang X, and Wang S, 2005: Role of late glacial to mid-Holocene climate in catchment weathering in the central Tibetan Plateau. *Quaternary Research,* 63: 161-170.

Jin Z, Bickle MJ, Chapman HJ, Yu J, Wang S, and Chen S, 2009: Early to mid-Pleistocene ostracod $\delta^{18}O$ and $\delta^{13}C$ in the central Tibetan Plateau: Implication for Indian monsoon change. *Palaeogeography, Palaeoclimatology, Palaeoecology,* 280: 406-414.

Karlin RE, Holmes M, Abella SEB, and Sylwester R, 2004: Holocene landslides and a 3500-year record of Pacific Northwest earthquakes from sediments in Lake Washington. *Geological Society of America Bulletin,* 116: 94-108.

Kasper T, Haberzettl T, Doberschütz S, Daut G, Wang J, Zhu L, Nowaczyk N, and Mäusbacher R, 2012: Indian Ocean Summer Monsoon (IOSM)-dynamics within the past 4 ka recorded in the sediments of Lake Nam Co, central Tibetan Plateau (China). *Quaternary Science Reviews,* 39: 73-85.

Kasper T, Frenzel P, Haberzettl T, Schwarz A, Daut G, Meschner S, Wang J, Zhu L, and Mäusbacher R, 2013: Interplay between redox conditions and hydrological changes in sediments from Lake Nam Co (Tibetan Plateau) during the past 4000 cal BP inferred from geochemical and micropaleontological analyses. *Palaeogeography, Palaeoclimatology, Palaeoecology,* 392: 261-271.

Kasper T, 2014: *Tracking Monsoon variability and climatic change on the central Tibetan Plateau since the Last Glacial Maximum - A 24,000 year record from Lake Nam Co -*. PhD thesis, Friedrich Schiller University Jena.

Kasper T, Haberzettl T, Wang J, Daut G, Doberschütz S, Zhu L, and Mäusbacher R, 2015: Hydrological variations on the Central Tibetan Plateau since the Last Glacial Maximum and their teleconnection to inter-regional and hemispheric climate variations. *Journal of Quaternary Science,* 30: 70-78.

Kemp ALW, Thomas RL, Wong HKT, and Johnston LM, 1977: Nitrogen and C/N ratios in the sediments of Lakes Superior, Huron, St. Clair, Erie, and Ontario. *Canadian Journal of Earth Sciences,* 14: 2402-2413.

Kong P, Na C, Brown R, Fabel D, Freeman S, Xiao W, and Wang Y, 2011: Cosmogenic ^{10}Be and ^{26}Al dating of paleolake shorelines in Tibet. *Journal of Asian Earth Sciences,* 41: 263-273.

Krishnamurthy RV, Bhattacharya SK, and Kusumgar S, 1986: Palaeoclimatic changes deduced from $^{13}C/^{12}C$ and C/N ratios of Karewa lake sediments, India. *Nature,* 323: 150-152.

Krishnamurti TN, 1971a: Tropical East-West Circulations During the Northern Summer. *Journal of the Atmospheric Sciences,* 28: 1342-1347.

Krishnamurti TN, 1971b: Observational Study of the Tropical Upper Tropospheric Motion Field during the Northern Hemisphere Summer. *Journal of Applied Meteorology,* 10: 1066-1096.

Kutzbach JE, 1981: Monsoon Climate of the Early Holocene: Climate Experiment with the Earth's Orbital Parameters for 9000 Years Ago. *Science,* 214: 59-61.

Lal D, 1991: Cosmic ray labeling of erosion surfaces: *in situ* nuclide production rates and erosion models. *Earth and Planetary Science Letters,* 104: 424-439.

Lehmkuhl F, and Haselein F, 2000: Quaternary paleoenvironmental change on the Tibetan Plateau and adjacent areas (Western China and Western Mongolia). *Quaternary International,* 65/66: 121-145.

Li D, Li Y, Ma B, Dong G, Wang L, and Zhao J, 2009: Lake-level fluctuations since the Last Glaciation in Selin Co (lake), Central Tibet, investigated using optically stimulated luminescence dating of beach ridges. *Environmental Research Letters,* 4: 1-10.

Liniger H, Weingartner R, Grosjean M, Kull C, MacMillan L, Messerli B, Bisaz A, and Lutz U, 1998: *Mountains of the World: Water Towers for the 21st Century: a Contribution to Global Freshwater Management Mountain Agenda*. Mountain Agenda, Berne.

Liu X, Dong H, Yang X, Herzschuh U, Zhang E, Stuut J-BW, and Wang Y, 2009: Late Holocene forcing of the Asian winter and summer monsoon as evidenced by proxy records from the northern Qinghai–Tibetan Plateau. *Earth and Planetary Science Letters,* 280: 276–284.

Long H, Lai Z, Frenzel P, Fuchs M, and Haberzettl T, 2012: Holocene moist period recorded by the chronostratigraphy of a lake sedimentary sequence from Lake Tangra Yumco on the south Tibetan Plateau. *Quaternary Geochronology,* 10: 136-142.

Long H, Haberzettl T, Tsukamoto S, Shen J, Kasper T, Daut G, Zhu L, Mäusbacher R, and Frechen M, 2015: Luminescence dating of lacustrine sediments from Tangra Yumco (southern Tibetan Plateau) using post-IR IRSL signals from polymineral grains. *Boreas,* 44: 139-152.

Ma Q, Zhu L, Lü X, Guo Y, Ju J, Wang J, Wang Y, and Tang L, 2014: Pollen-inferred Holocene vegetation and climate histories in Taro Co, southwestern Tibetan Plateau. *Chinese Science Bulletin,* 59: 4101-4114.

Maussion F, Scherer D, Mölg T, Collier E, Curio J, and Finkelnburg R, 2014: Precipitation Seasonality and Variability over the Tibetan Plateau as Resolved by the High Asia Reanalysis. *Journal of Climate,* 27: 1910–1927.

Meadows A, and Meadows PS, 1999: *The Indus River: Biodiversity, Resources, Humankind.* Oxford University Press, Oxford.

Meyers PA, and Ishiwatari R, 1993: Lacustrine organic geochemistry—an overview of indicators of organic matter sources and diagenesis in lake sediments. *Organic Geochemistry,* 20: 867-900.

Miao C, Ni J, Borthwick AGL, and Yang L, 2011: A preliminary estimate of human and natural contributions to the changes in water discharge and sediment load in the Yellow River. *Global and Planetary Change,* 76: 196-205.

Miehe S, Miehe G, van Leeuwen JFN, Wrozyna C, van der Knaap WO, Duo L, and Haberzettl T, 2014: Persistence of *Artemisia* steppe in the Tangra Yumco Basin, west-central Tibet, China: despite or in consequence of Holocene lake-level changes? *Journal of Paleolimnology,* 51: 267-285.

Mischke S, Kramer M, Zhang C, Shang H, Herzschuh U, and Erzinger J, 2008: Reduced early Holocene moisture availability in the Bayan Har Mountains, northeastern Tibetan Plateau, inferred from a multi-proxy lake record. *Palaeogeography, Palaeoclimatology, Palaeoecology,* 267: 59-76.

Mischke S, Aichner B, Diekmann B, Herzschuh U, Plessen B, Wünnemann B, and Zhang C, 2010a: Ostracods and stable isotopes of a late glacial and Holocene lake record from the NE Tibetan Plateau. *Chemical Geology,* 276: 95-103.

Mischke S, and Zhang C, 2010: Holocene cold events on the Tibetan Plateau. *Global and Planetary Change,* 72: 155-163.

Mischke S, Zhang C, Börner A, and Herzschuh U, 2010b: Lateglacial and Holocene variation in aeolian sediment flux over the northeastern Tibetan Plateau recorded by laminated sediments of a saline meromictic lake. *Journal of Quaternary Science,* 25: 162-177.

Mischke S, Weynell M, Zhang C, and Wiechert U, 2013: Spatial variability of ^{14}C reservoir effects in Tibetan Plateau lakes. *Quaternary International,* 313–314: 147-155.

Mischke S, Zhang C, and Fan R, 2015: Early to mid-Holocene lake high-stand sediments at Lake Donggi Cona, northeastern Tibetan Plateau, China — Comment to the paper published by Dietze et al., Quaternary Research 79 (2013), 325-336. *Quaternary Research,* 83: 256-258.

Mishra PK, Anoop A, Schettler G, Prasad S, Jehangir A, Menzel P, Naumann R, Yousuf AR, Basavaiah N, Deenadayalan K, Wiesner MG, and Gaye B, 2015: Reconstructed late Quaternary hydrological changes from Lake Tso Moriri, NW Himalaya. *Quaternary International,* 371: 76-86.

Morrill C, Overpeck JT, and Cole JE, 2003: A synthesis of abrupt changes in the Asian summer monsoon since the last deglaciation. *The Holocene,* 13: 465–476.

Morrill C, Overpeck JT, Cole JE, Liu K-b, Shen C, and Tang L, 2006: Holocene variations in the Asian monsoon inferred from the geochemistry of lake sediments in central Tibet. *Quaternary Research,* 65: 232-243.

Mügler I, Sachse D, Werner M, Xu B, Wu G, Yao T, and Gleixner G, 2008: Effect of lake evaporation on δD values of lacustrine *n*-alkanes: A comparison of Nam Co (Tibetan Plateau) and Holzmaar (Germany). *Organic Geochemistry,* 39: 711–729.

Mügler I, Gleixner G, Günther F, Mäusbacher R, Daut G, Schütt B, Berking J, Schwalb A, Schwark L, Xu B, Yao T, Zhu L, and Yi C, 2010: A multi-proxy approach to reconstruct hydrological changes and Holocene climate development of Nam Co, Central Tibet. *Journal of Paleolimnology,* 43: 625-648.

Mukhopadhyay B, and Khan A, 2014: A quantitative assessment of the genetic sources of the hydrologic flow regimes in Upper Indus Basin and its significance in a changing climate. *Journal of Hydrology,* 509: 549-572.

Nakagawa T, 2007: Double-L channel: an amazingly non-destructive method of continuous sub-sampling from sediment cores. *Quaternary International Supplementary,* 298: 167-168.

Nakagawa T, Gotanda K, Haraguchi T, Danhara T, Yonenobu H, Brauer A, Yokoyama Y, Tada R, Takemura K, Staff RA, Payne R, Bronk Ramsey C, Bryant C, Brock F, Schlolaut G, Marshall M, Tarasov P, and Lamb H, 2012: SG06, a fully continuous and varved sediment core from Lake Suigetsu, Japan: stratigraphy and potential for improving the radiocarbon calibration model and understanding of late Quaternary climate changes. *Quaternary Science Reviews,* 36: 164-176.

Nesje A, Dahl SO, Matthews JA, and Berrisford MS, 2001: A ~4500-yr record of river floods obtained from a sediment core in Lake Atnsjøen, eastern Norway. *Journal of Paleolimnology,* 25: 329-342.

Nishimura M, Matsunaka T, Morita Y, Watanabe T, Nakamura T, Zhu L, Nara FW, Imai A, Izutsu Y, and Hasuike K, 2014: Paleoclimatic changes on the southern Tibetan Plateau over the past 19,000 years recorded in Lake Pumoyum Co, and their implications for the southwest monsoon evolution. *Palaeogeography, Palaeoclimatology, Palaeoecology,* 396: 75-92.

Opitz S, Wünnemann B, Aichner B, Dietze E, Hartmann K, Herzschuh U, lJmker J, Lehmkuhl F, Li S, Mischke S, Plotzki A, Stauch G, and Diekmann B, 2012: Late Glacial and Holocene development of Lake Donggi Cona, north-eastern Tibetan Plateau, inferred from sedimentological analysis. *Palaeogeography, Palaeoclimatology, Palaeoecology,* 337–338: 159-176.

Opitz S, Zhang C, Herzschuh U, and Mischke S, 2015: Climate variability on the south-eastern Tibetan Plateau since the Lateglacial based on a multiproxy approach from Lake Naleng – comparing pollen and non-pollen signals. *Quaternary Science Reviews,* 115: 112-122.

Overpeck J, Anderson D, Trumbore S, and Prell W, 1996: The southwest Indian Monsoon over the last 18 000 years. *Climate Dynamics,* 12: 213-225.

Petersen J, Wilhelm B, Revel M, Rolland Y, Crouzet C, Arnaud F, Brisset E, Chaumillon E, and Magand O, 2014: Sediments of Lake Vens (SW European Alps, France) record large-magnitude earthquake events. *Journal of Paleolimnology,* 51: 343-355.

Polanski S, Fallah B, Prasad S, and Cubasch U, 2013: Simulation of the Indian monsoon and its variability during the last millennium. *Climate of the Past Discussions,* 9: 703-740.

Pye K, and Tsoar H, 2009: *Aeolian sand and sand dunes.* Springer, Berlin Heidelberg.

Rades EF, Hetzel R, Xu Q, and Ding L, 2013: Constraining Holocene lake-level highstands on the Tibetan Plateau by ^{10}Be exposure dating: a case study at Tangra Yumco, southern Tibet. *Quaternary Science Reviews,* 82: 68-77.

Rades EF, Tsukamoto S, Frechen M, Qiang X, and Lin D, 2015: A lake-level chronology based on feldspar luminescence dating of beach ridges at the Tangra Yum Co (southern Tibet). *Quaternary Research,* 83: 469-478.

Ramage CS, 1971: *Monsoon Meteorology.* Academic Press, New York and London.

Rashid H, England E, Thompson L, and Polyak L, 2011: Late Glacial to Holocene Indian Summer Monsoon Variability Based upon Sediment Records Taken from the Bay of Bengal. *Terrestrial, Atmospheric and Oceanic Sciences,* 22: 215-228.

Reimer PJ, Bard E, Bayliss A, Beck JW, Blackwell PG, Ramsey CB, Buck CE, Cheng H, Edwards RL, and Friedrich M, 2013: IntCal13 and Marine13 radiocarbon age calibration curves 0–50,000 years cal BP. *Radiocarbon,* 55: 1869-1887.

Schneider U, Becker A, Finger P, Meyer-Christoffer A, Ziese M, and Rudolf B, 2014: GPCC's new land surface precipitation climatology based on quality-controlled in situ data and its role in quantifying the global water cycle. *Theoretical and Applied Climatology,* 115: 15-40.

Schnellmann M, Anselmetti FS, Giardini D, and Mckenzie JA, 2006: 15,000 Years of mass-movement history in Lake Lucerne: Implications for seismic and tsunami hazards. *Eclogae Geologicae Helvetiae,* 99: 409-428.

Schulz H, von Rad U, and Erlenkeuser H, 1998: Correlation between Arabian Sea and Greenland climate oscillations of the past 110,000 years. *Nature,* 393: 54-57.

Severinghaus JP, Beaudette R, Headly MA, Taylor K, and Brook EJ, 2009: Oxygen-18 of O_2 Records the Impact of Abrupt Climate Change on the Terrestrial Biosphere. *Science,* 324: 1431-1434.

Shao X, Xu Y, Yin Z-Y, Liang E, Zhu H, and Wang S, 2010: Climatic implications of a 3585-year tree-ring width chronology from the northeastern Qinghai-Tibetan Plateau. *Quaternary Science Reviews,* 29: 2111-2122.

Shen J, Liu X, Wang S, and Matsumoto R, 2005: Palaeoclimatic changes in the Qinghai Lake area during the last 18,000 years. *Quaternary International,* 136: 131-140.

Stone JO, 2000: Air pressure and cosmogenic isotope production. *Journal of Geophysical Research: Solid Earth,* 105: 753-759.

Stuiver M, and Reimer PJ, 1993: Radiocarbon Calibration Program, Calib Rev 6.0.0. *Radiocarbon,* 35: 215-230.

Taft L, Wiechert U, Riedel F, Weynell M, and Zhang H, 2012: Sub-seasonal oxygen and carbon isotope variations in shells of modern *Radix* sp. (Gastropoda) from the Tibetan Plateau: potential of a new archive for palaeoclimatic studies. *Quaternary Science Reviews,* 34: 44-56.

Taylor R, 2009: Rethinking Water Scarcity: The Role of Storage. *EOS,* 90: 237-238.

Tian L, Masson-Delmotte V, Stievenard M, Yao T, and Jouzel J, 2001: Tibetan Plateau summer monsoon northward extent revealed by measurements of water stable isotopes. *Journal of Geophysical Research: Atmospheres*: 28,081-028,088.

Viviroli D, Dürr HH, Messerli B, Meybeck M, and Weingartner R, 2007: Mountains of the world, water towers for humanity: Typology, mapping, and global significance. *Water Resources Research,* 43: 1-13.

Vörösmarty CJ, Green P, Salisbury J, and Lammers RB, 2000: Global Water Resources: Vulnerability from Climate Change and Population Growth. *Science,* 289: 284-288.

Wang H, Yang Z, Saito Y, Liu JP, and Sun X, 2006: Interannual and seasonal variation of the Huanghe (Yellow River) water discharge over the past 50 years: connections to impacts from ENSO events and dams. *Global and Planetary Change,* 50: 212-225.

Wang J, Peng P, Ma Q, and Zhu L, 2010: Modern limnological features of Tangra Yumco and Zhari Namco, Tibetan Plateau. *Journal of Lake Sciences,* 22: 629-632.

Wang J, Zhu L, Wang Y, Ju J, Daut G, and Li M, 2015: Spatial variability and the controlling mechanisms of surface sediments from Nam Co, central Tibetan Plateau, China. *Sedimentary Geology,* 319: 69-77.

Wang Y, Cheng H, Edwards RL, He Y, Kong X, An Z, Wu J, Kelly MJ, Dykoski CA, and Li X, 2005: The Holocene Asian Monsoon: Links to Solar Changes and North Atlantic Climate. *Science,* 308: 854-857.

Wang Y, Kromhout E, Zhang C, Xu Y, Parker W, Deng T, and Qiu Z, 2008: Stable isotopic variations in modern herbivore tooth enamel, plants and water on the Tibetan Plateau: Implications for paleoclimate and paleoelevation reconstructions. *Palaeogeography, Palaeoclimatology, Palaeoecology,* 260: 359-374.

Webster PJ, Magaña VO, Palmer TN, Shukla J, Tomas RA, Yanai M, and Yasunari T, 1998: Monsoons: Processes, predictability, and the prospects for prediction. *Journal of Geophysical Research: Oceans,* 103: 14,451-414,510.

Wu Y, Lücke A, Jin Z, Wang S, Schleser GH, Battarbee RW, and Xia W, 2006: Holocene climate development on the central Tibetan Plateau: A sedimentary record from Cuoe Lake. *Palaeogeography, Palaeoclimatology, Palaeoecology,* 234: 328–340.

Yang ZS, Milliman JD, Galler J, Liu JP, and Sun XG, 1998: Yellow River's Water and Sediment Discharge Decreasing Steadily. *EOS,* 79: 589-592.

Yu JQ, and Kelts KR, 2002: Abrupt changes in climatic conditions across the late-glacial/Holocene transition on the N. E. Tibet-Qinghai Plateau: evidence from Lake Qinghai, China. *Journal of Paleolimnology,* 28: 195-206.

Zhang K, Zhao Y, Yu Z, and Zhou A, 2010: A 2700-year high resolution pollen record of climate change from varved Sugan Lake in the Qaidam Basin, northeastern Tibetan Plateau. *Palaeogeography, Palaeoclimatology, Palaeoecology,* 297: 290-298.

Zhou W, Song S, Burr G, Jull AJT, Lu X, Yu H, and Cheng P, 2007: Is there a time-transgressive Holocene Optimum in the East Asian monsoon area? *Radiocarbon,* 49: 865-876.

Zhu L, Wu Y, Wang J, Lin X, Ju J, Xie M, Li M, Mäusbacher R, Schwalb A, and Daut G, 2008: Environmental changes since 8.4 ka reflected in the lacustrine core sediments from Nam Co, central Tibetan Plateau, China. *The Holocene,* 18: 831-839.

Acknowledgements

For advising my thesis, their support and encouragement I would like to thank Roland Mäusbacher, Torsten Haberzettl, as well as Peter Frenzel.

The studies of this thesis are part of the Sino-German collaboration within the DFG priority program 1372 "*TiP*" jointly financed by the National Natural Science Foundation of China and the German Academic Exchange Service (DAAD).

I am thankful to all co-authors and my colleagues Nadine Bräutigam, Gerhard Daut, Stefan Doberschütz, Brunhilde "Bruni" Dressler, Antje Ehrle, Karoline Henkel, Thomas Kasper, Carmen Kirchner, Beate Michalzik, Kerstin Näthe, Bastian Reinwarth, and Michael Wündsch. I furthermore appreciate the help of Willi Ackermann, Martina Ahlborn, Lailah Gifty Akita, Bipin Attavane, Nico Blaubach, Nicole Börner, Nora Bosse, Semi Ceylan-Ahlborn, Petra Enderlein, Whitney DiFoggio, Steven L. Forman, Heidrun Garlipp, Kati Hartwig, Jakob Heyman, Dana Höfer, Jianting Ju, Kim Jasmin Krahn, Carmen Kirchner, Jacques Labrie, Martin Lederer, Qingfeng Ma, Jeaneth Mazzocco, Stephanie Meschner, Steffen Mischke, Stephan Opitz, Isabell Pätz, James Pierson, Sushma Prasad, Eike F. Rades, Harunur Rashid, Thomas Reuss, Sascha Schröter, Hartmut Schulz, Jeffrey P. Severinghaus Reshma Shah, Sabine Stahl, Hilde Stute, Tina Trautmann, Lena Twardowski, Junbo Wang, Frank Wiese, Erika and Bogdan "Bob" Zalewski, and Liping Zhu.

Statement of authorship / Selbständigkeitserklärung

I hereby certify that this thesis has been composed by me and is based on my own work, unless stated otherwise. No other person's work has been used without due acknowledgement in this thesis. All references have been quoted and all sources of information have been specifically acknowledged.

Ich erkläre, dass ich die vorliegende Arbeit selbständig und unter Verwendung der angegebenen Hilfsmittel, persönlichen Mitteilungen und Quellen angefertigt habe.

December 4, 2015 Marieke Ahlborn